WAVE-SOIL TANK CALIBRATION AND GEOTECHNICAL STUDIES OF SEAFLOOR INSTABILITY

CENTRE FOR NEWFOUNDLAND STUDIES

TOTAL OF 10 PAGES ONLY
MAY BE XEROXED

(Without Author's Permission)

C. ROY DAWE

WAVE-SOIL TANK CALIBRATION
AND
GEOTECHNICAL STUDIES
OF
SEAFLOOR INSTABILITY

by

© C. Roy Dawe, B.Eng.

A thesis submitted in partial fulfillment
of the requirements for the degree of
Master of Engineering

Faculty of Engineering and Applied Science
Memorial University of Newfoundland

August 1984

St. John's Newfoundland Canada

WAVE-SOIL TANK CALIBRATION

AND

GEOTECHNICAL STUDIES

OF

SEAFLOOR INSTABILITY

To Doreen

Andrew and Graham

ABSTRACT

The general scope of this research is to understand the problem of seafloor instability due to ocean surface waves with particular reference to the offshore activities on the Canadian east coast. An evaluation of the wave effects on seabed stability is necessary in the determination of the long term stability of bottom-founded offshore production platforms and transportation systems for the Grand Banks and Sable Island regions.

A wave tank was designed and built for the purpose of conducting laboratory tests with sediments similar to those found on the east coast. The tank is 8.5 m long, 0.76 m wide and 1.0 m deep, with a capability of generating regular waves of maximum heights of about 0.12 m. The wave length can be varied from 0.5 m to 4 m. The representative seafloor was a bed of sand about 0.4 m deep, underlying a water column up to 0.5 m deep. The tank can be tilted so that slopes of up to 1:10 may be formed at the water-soil interface to represent seabed slopes. A beach was designed and built to absorb the wave energy and to minimize the effect of reflected waves. Reflection coefficients of less than 10% were obtained for the frequently used wave types. Reflection coefficients as low as 5% can be obtained for some specific sets of wave characteristics.

Waves with a steepness between 0.04 and 0.1 caused failure of the test bed of fine sand when it was in a loose state. Porewater pressure was measured by embedding pressure transducers inside the soil. Soil failure by liquefaction was confirmed by the measured pressures. However, the sand always stabilized again after about 10 to 20 cycles, resulting in a denser soil. The soil failure appears to be the result of transient wave effects rather than porewater pressure buildup. This is more pronounced when the soil is sloped.

In a parallel theoretical research of the same problem, solutions have been reported using Biot's equations. Comparison of the measured wave induced porewater pressures with the reported theoretical values show a good correlation in some cases.

The present studies show that the seabed will be subjected to mass movement under specific wave conditions. This failure depends on the seafloor sediment type and its initial insitu state. In combination with the bottom currents, the effect of the waves on the seabed could be quite severe.

ACKNOWLEDGEMENTS

This thesis was completed at the Faculty of Engineering and Applied Science, Memorial University of Newfoundland. The project was supported by a research fellowship from the university's Centre for Cold Oceans Research Engineering, for which the author is grateful.

Dr. T.R. Chari, Professor and Associate Dean of Engineering has acted as supervisor; his advice and guidance is much appreciated. The advice from many other faculty members and staff is also appreciated. The staff of Technical Services have been especially considerate and helpful. Many thanks to Terry Dyer for his care and attention in drafting the figures.

The manuscript has been typed by Mrs. Marilyn Warren, to whom the author is grateful.

TABLE OF CONTENTS

		PAGE
ABSTRACT		ii
ACKNOWLEDGEMENTS		iv
LIST OF TABLES		vii
LIST OF FIGURES		viii
NOTATIONS		xiv
CHAPTER		
I	INTRODUCTION	1
II	LITERATURE REVIEW	4
	2.1 Slope Stability Analysis	4
	2.2 Wave-Soil Interactions	12
	2.2.1 Analysis of Cohesive Sediments	12
	2.2.2 Instability of Cohesionless Soils	24
III	EXPERIMENTAL FACILITIES AND PROCEDURES	35
	3.1 Wave-Soil Tank	35
	3.1.1 Design Considerations	35
	3.2 Experimental Set-up	48
	3.2.1 Instrumentation	48
	3.2.2 Soil Sample	50
	3.2.3 Preparation of Sand Bed	51
IV	EXPERIMENTAL RESULTS AND DISCUSSION	59
	4.1 Wave Tank Performance Tests	59
	4.1.1 Wave Characteristics	60
	4.1.2 Wave Height and Wavemaker Stroke Correlation	60

		PAGE
4.1.3	Wave Length and Frequency Correlation	63
4.1.4	Wave Form	70
4.1.5	Beating	72
4.1.6	Build-up and Decay Time	79
4.1.7	Maximum Wave Heights	80
4.1.8	Reflection	86
4.2	Influence of Waves on a Bed of Fine Sand	97
4.2.1	Wave Pressure at the Mudline	99
4.2.2	Effects of Wave Pressure on a Flat Bed of Sand	103
4.2.3	Additional Triggering Forces Causing Soil Failure	143
4.2.4	Effects of Waves on a Sloping Bed of Sand	144
V	SUMMARY AND CONCLUSIONS	169
REFERENCES		174
APPENDIX		180

LIST OF TABLES

		Page
TABLE 1	Properties of the soil used	58
TABLE 2	Typical wave characteristics used in this research	61
TABLE 3	Reflection coefficients for different beach types and slope angles	92
TABLE 4	Measured and computed bottom pressures	100
TABLE 5	Phase lag of the pressure fluctuation below the mudline	118
TABLE 6	Measured and computed failure depths and corresponding porewater pressures	140

LIST OF FIGURES

Figure	Title	Page
1	A typical free body and force polygon from an infinite slope analysis (from Dunn et al, 1980)	8
2	Method of slices (from Dunn et al, 1980)	8
3	Geometry of assumed surface of sliding (from Henkel, 1970)	15
4	Wave shearing stress superimposed over soil shear strength profile (from Doyle, 1973)	23
5	Wave-soil tank	39
6	Waveboard (top view)	40
7	Wavemaker drive	41
8	Schematic of wave-soil tank	44
9	Schematic of beaches tested	45
10	Schematic of beaches tested	46
11	Beach end of tank	52
12	Wave probe	53
13	Instrumentation	54
14	Pressure transducer arrangement	55
15	Grain size distribution	56
16	Soil permeability at various void ratios	57
17	Regions of validity for various wave theories (from Shore Protection Manual, 1977)	64
18	Test of wavemaker theory for small wave-steepness (from Ursell et al, 1960)	65

Figure	Title	Page
19	Piston generator performance for regular waves (from Muggeridge and Murray, 1981)	65
20	Wavemaker performance	66
21	Frequency vs wavelength (d = 300 mm)	67
22	Frequency vs wavelength (d = 360 mm)	68
23	Frequency vs wavelength (d = 500 mm)	69
24	Wave profile at different stations in a wave flume (from Hansen and Svendsen, 1974)	73
25	Superposition of second order Stoke's main wave and free second harmonic wave (from Hansen and Svendsen, 1974)	74
26	Record of total wave motion and total second harmonic motion (from Hansen and Svendson, 1974)	74
27	Typical surface waves in the wave-soil tank	75
28	A typical record of meandering	76
29	An example of beating (from Flugge, 1962)	77
30	An example of beating. Period is 8 seconds for 1 Hz waves	81
31	An example of beating. Period is 9 seconds for 1.19 Hz waves	81
32	An example of beating. Period is 15 seconds for 1.03 Hz waves	82
33	An example of beating with periods of 8 seconds and approximately 80 seconds for 1.03 Hz waves	82
34	An example of beating. Approximate period of beats is 16 seconds	83

Figure	Title	Page
35	Typical wave record	84
36	Performance envelope of the wave generator	85
37	Change in wave height along the tank due to the summation of incident and reflected waves	89
38	A typical example showing the calculation of the reflection coefficient	90
39	Parabolic beach performance (15 deg.)	95
40	Parabolic beach performance (12 deg.)	96
41	Beach performance at different slopes	101
42	Typical surface wave and resulting bottom pressure	102
43	Porewater pressure change due to seepage induced liquefaction	106
44	Theoretical and measured porewater pressures at liquefaction	107
45	Excess porewater pressure during shock induced liquefaction	108
46	Variation of excess porewater after shock induced liquefaction	109
47	Pressure response to 0.71 Hz waves	113
48	Pressure response to 1.03 Hz and 1.27 Hz waves	114
49	Pressure response to 1.35 Hz waves	115
50	Pressure response to 1.35 Hz waves showing how the pressure response changes with time	116
51	Phase lag between pressure at mudline and pressure at z = -30 cm	120

Figure	Title	Page
52	Porewater pressure response (ρ_d = 1500 kg/m^3, no failure)	121
53	Normalized porewater pressure response - comparison of theory and experiments (ρ_d = 1500 kg/m^3, no failure)	122
54	Porewater pressure response (ρ_d = 1300 kg/m^3, no failure)	123
55	Normalized porewater pressure response comparison of theory and experiments (ρ_d = 1300 kg/m^3, no failure)	124
56	Porewater pressure response (ρ_d = 1250 kg/m^3, no visible failure)	127
57	Porewater pressure response (ρ_d = 1250 kg/m^3, no visible failure)	128
58	Porewater pressure response (ρ_d = 1250 kg/m^3, no visible failure)	129
59	Porewater pressure response (ρ_d = 1250 kg/m^3, no visible failure)	130
60	Porewater pressure response (ρ_d = 1250 kg/m^3, visible failure to 1.5 cm depth)	131
61	Porewater pressure response (ρ_d = 1250 kg/m^3, visible failure to 2 cm depth)	132
62	Porewater pressure response (ρ_d = 1250 kg/m^3, visible failure to 3 cm depth)	133

Figure	Title	Page
63	Porewater pressure response (ρ_d = 1250 kg/m^3, visible failure to 5 cm depth)	134
64	Porewater pressure response (ρ_d = 1250 kg/m^3, visible failure to 5 cm depth)	135
65	Porewater pressure response (ρ_d = 1250 kg/m^3, visible failure to 5 cm depth)	136
66	Porewater pressure response (ρ_d = 1250 kg/m^3, visible failure to 7 cm depth)	137
67	Porewater pressure response (ρ_d = 1250 kg/m^3, visible failure to 10 cm depth)	138
68	Computed and measured depths of wave induced failure for a flat bed of loose sand	146
69	Soil densification after liquefaction	148
70	Porewater pressure response to combined waves and shock loading	149
71	Excess porewater pressure during wave induced slope failure	150
72	Excess porewater pressure during wave induced slope failure	151
73	Excess porewater pressure during wave induced slope failure	152
74	Excess porewater pressure during wave induced slope failure	153
75	Excess porewater pressure during wave induced slope failure	154
76	Wave induced slope failure	155

Figure	Title	Page
77	Wave induced slope failure	156
78	Wave induced slope failure	157
79	Wave induced slope failure	158
80	Wave induced slope failure	159
81	Typical excavated trench	164
82	Porewater pressure response as waves trigger failure of a finite slope	165
83	Excavated trench acting as a damper	166
84	Porewater pressure response as soil failure is triggered by combined waves and shock	167

Symbols

The following symbols used in this thesis are generally in accordance with the recommendations of the Canadian Geotechnical Society (Barsvary et al, 1980). They are also defined when they first appear in the text of the thesis.

c	cohesion
c'	effective cohesion
C_R	reflection coefficient
c_u	undrained shear strength
d	water depth
D_r	relative density of soil
F.S.	factor of safety, $\frac{\text{ultimate shear strength}}{\text{working shear stress}}$
H	wave height measured from trough to peak
k_z	coefficient of permeability in the vertical direction
k_o	$2\pi/L$
L	wavelength
ℓ_n	total length of shearing surface
M_d	disturbing moment
m_v	coefficient of volume compressibility
N	number of stress cycles during a storm
N	normal force
N_ℓ	number of cycles to cause liquefaction
p	wave induced pressure below the surface of a fluid, relative to still conditions
p'_m	vertical effective stress at depth of failure

p_z	porewater pressure at depth z below the mudline
Δp_c	excess bottom pressure required to initiate mass movement of sediment
Δp_o	maximum wave induced pressure at the mudline
R	percent reduction in soil shearing resistance
r_u	pore pressure ratio, u/σ'_{v_o}
S_n	sum of cohesive and frictional strength
S_r	reserve strength
S_t	soil sensitivity
SWL	still water level
t	time axis
T	wave period
T	shearing force
T_n	tangential force
u	pore pressure
W_t	weight of soil wedge
x	horizontal axis in the direction of wave propagation
z	depth in soil, -ve down
z_s	depth of sliding surface
α_f	angle of slope at failure
β	angle of slope to the horizontal
ψ	rate of pore pressure generation
Δ	increment
γ	unit weight
γ'	submerged unit weight of soil

γ_w	unit weight of water
ϕ	angle of internal friction
σ	total normal stress
σ'	effective normal stress
σ'_{vo}	static effective vertical stress
τ	shearing stress
τ_c	cyclic shear stress
τ_R	ultimate or residual shear strength

CHAPTER I

INTRODUCTION

The stability and strength of sea bottom soil has become an important geotechnical research topic as a result of the increase in oil-related construction activity in the continental shelf and slope areas. Terzaghi (1956), Morgenstern (1967), Sheppard (1955), and Andresen and Bjerrum (1967) have documented submarine slope failures over a wide range of slope angles from less than 0.5 degrees up to about 30 degrees.

The complex topography of the Mississippi Delta, between the 10 m and the 64 m contours, is suggested to be the result of underwater landslides, even though the average slope of the seabed is only about 0.5 degrees or 1:125 (Sheppard 1955). At the other extreme, slumping in fine micaceous sands has occurred in inclinations of approximately 30 degrees (Morgenstern 1967).

Soil failure often has serious consequences. Slides in soft underconsolidated clays of the Mississippi Delta have been initiated by storm waves and have caused offshore platforms to overturn; also flare piles have buckled and moved laterally when forced by moving soil (Kraft and Watkins 1976).

A 3 m steel pipeline in Lake Ontario has failed several times, apparently because of liquefaction of sand due to storm waves (Christian et al 1974). Soil failure in this case caused the pipe to float to the surface of the soil.

Other consequences of submarine soil failure reported in the literature include broken communications cables, broken pipelines and destroyed harbour facilities (Terzaghi, 1956), (Kraft and Watkins, 1976).

Much theoretical and experimental work has been done to predict the behavior of cohesive sediments under wave action. However, similar research data for cohesionless soils are sparse. The research reported in this thesis is an attempt to fill that gap. This thesis includes a summary of the literature related to the stability of the sea bottom under wave loading. The results reported here are primarily experimental, with a correlation of theoretical results wherever appropriate.

The experimental facility consists of a glass sided tank, 8.5 m long, 0.76 m wide and 1.0 m deep. Waves up to 0.12 m high with periods between 0.6 sec. and 1.8 sec. can be generated in the tank. The wave tank was calibrated and was used to examine the effects of waves on a bed of fine sand which was placed to a thickness of 40 cm. Failure of both flat and sloped bottoms due to waves was examined by recording failure depth and excess porewater pressures in the sand bed. The porewater response inside the soil was measured at different depths and its effects in causing soil failure are discussed.

The research reported here is part of an ongoing project on seabed stability studies recently started at Memorial University of Newfoundland. A brief summary of the areas of further investigation is given at the end of the dissertation.

CHAPTER II

LITERATURE REVIEW

2.1 Slope Stability Analysis

The primary factors leading to the instability of soil slopes can be classified as (1) those causing increased applied stress and (2) those causing a reduction in soil strength. Factors causing increased stress on land include increased unit weight of soil by wetting, added external loads such as buildings, steepened slopes either by natural erosion or by excavation, and applied shock loads (Dunn et al 1980). An additional factor for marine environments causing increased stress, is wave loading (Henkel 1970).

Loss of strength may occur by absorption of water, increased porewater pressure, shock or cyclic loads, freezing and thawing action, loss of cementing materials, weathering processes, and excessive strains.

The rate of slide movement in a slope failure may vary from a few millimeters per hour to very rapid slides in which large movements take place in a few seconds. Slow slides occur in soils having a plastic stress-strain characteristic where there is no loss of strength with increasing strain. Rapid slides occur in situations where there is an abrupt loss of strength, as in liquefaction of fine sand or a sensitive clay.

Many slopes exhibit creep movements (a few millimeters per year) on a more or less continuous basis as a result of seasonal changes in moisture and temperature. Such movements are not to be confused with shear failure (Dunn et al 1980).

Some slopes cannot be readily analyzed. Examples include slopes of complex geology or badly weathered slopes where the varied materials and their strengths cannot be readily identified. Slopes involving heavily overconsolidated clays and shales or stiff fissured clays are difficult to analyse (Dunn et al 1980).

The most common methods of slope stability analyses are based on limit equilibrium. In this type of analysis, the factor of safety is estimated by examining the conditions of equilibrium when incipient failure is postulated along a predefined failure plane, and then comparing the strength necessary to maintain equilibrium with the available strength of the soil (Dunn et al 1980).

A second method of slope analysis is based on the use of the theory of elasticity or plasticity to determine the shearing stresses at critical places within a slope for comparison with the soil shearing strength. Finite element computer techniques are examples of this type of analysis. For example, the finite element method can be used to predict the distribution of shearing stresses in a sediment under a

given pressure distribution from assumed deformation characteristics for the sediment. Under this analysis it is possible to predict the form of the horizontal displacements and the maximum ratio of applied stress to available strength at all depths in the soil profile. Effects produced by gravity loads on the soil and a sloping seafloor can also be included (Wright 1976).

A third and recent method of analytical model that has been developed to assist in evaluating seafloor stability is the Layered Continua analysis (Bea and Aurora 1981). An example of this method has been published by Sharpery and Dunlap (1978). It is based on a rigorous viscoelastic analysis and a generalization of the method of equivalent linearization. The procedure accounts for the effects of soil inertia, nonlinear material damping, rate-dependence of the soil properties, and down-slope movement induced by wave action.

The following summary of slope stability analysis is based on limit equilibrium.

The safety factor, F.S., for a soil slope is usually defined as

$$F.S. = \frac{\text{ultimate shear strength}}{\text{working shear stress}} \qquad (1)$$

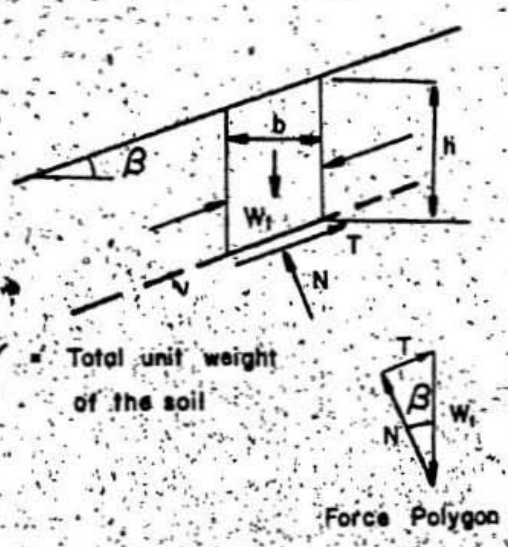


FIGURE 1 A TYPICAL FREE BODY AND FORCE POLYGON FROM AN INFINITE SLOPE ANALYSIS (FROM DUNN ET AL, 1980)

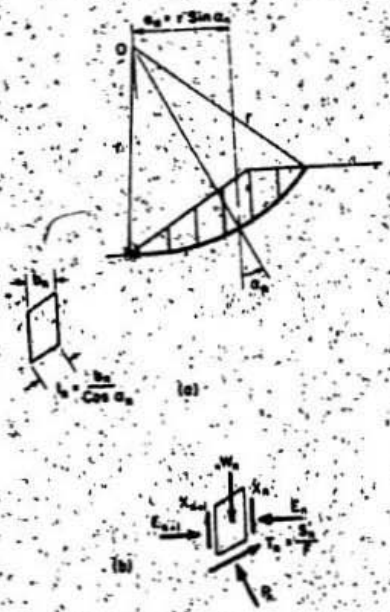


FIGURE 2 METHOD OF SLICES (FROM DUNN ET AL, 1980)

along the most likely failure surface (Lambe and Whitman, 1969). The ultimate or residual shear strength, τ_R, along the plane of failure can be expressed as

$$\tau_R = c' + (\sigma - u) \tan \phi' \qquad (2)$$

where: c' = apparent cohesion

ϕ' = angle of shearing resistance

σ = total stress normal to the failure plane

u = pore pressure

c' and ϕ' are in terms of effective stress.

The shear strength required for equilibrium is simply the shear stress along the failure plane being considered, to fulfill the requirements of static equilibrium.

Consider the free body diagram for a wedge of soil one unit thick, as shown in Figure 1. The weight of the wedge, W_t, is balanced by the normal force, N, and shearing force, T, on the bottom of the wedge; β is the angle of the slope to the horizontal. The normal and shearing forces are

$$N = W_t \cos \beta$$

$$T = W_t \sin \beta$$

Dividing these forces by the base dimensions of the wedge gives the normal stress, σ, and the shear stress, τ, required for equilibrium, in terms of unit weight, γ, thickness of wedge, h, and angle, β.

$$\sigma = \frac{N}{b/\cos\beta} = \gamma h \cos^2 \beta \qquad (3)$$

$$\tau = \frac{T}{b/\cos\beta} = \gamma h \sin \beta \cos \beta \qquad (4)$$

When c=0, and u=0, the strength, τ_R, can be expressed by

$$\tau_R = \sigma' \tan \phi'$$

where σ' is the effective normal stress.

The safety factor becomes

$$F.S. = \frac{\tau_R}{\tau} = \frac{\sigma' \tan \phi'}{h \gamma \sin \beta \cos \beta}$$

$$\therefore F.S. = \frac{\tan \phi'}{\tan \beta}$$

with F.S. = 1, the maximum slope β is equal to the angle of friction, ϕ'.

This simple condition can be expanded and generalized to include slopes of finite height and also the effects of excess pore water pressure and non-homogeneous soils.

Several methods of slices have long been in common use to evaluate slope stability (Bishop 1955), (Fellenius 1936), (Janbu 1973), and (Whitman and Bailey 1967). In these general methods, a trial failure arc is divided into a number of slices as shown in Figure 2.

The overturning moment is determined by summing the moment of the weight of each slice about the trial centre 0. The overturning moment, OM, is:

$$OM = \Sigma W_n a_n = r \Sigma W_n \sin \alpha_n \qquad (5)$$

where W_n is the weight of the n^{th} slice, a_n, r, and α_n are defined in Figure 2.

The side forces on each slice are not included in the moment equations, since, when all the slices are considered, the net moment of the side forces will be zero. The moment required for equilibrium is provided by the tangential force, $T_n = S_n'/F.S.$ on the base of each slice. The force S_n' is the sum of the cohesive and frictional strength at the base of each slice. For stability:

$$r \Sigma W_n \sin \alpha_n = r \Sigma T_n = r \Sigma \frac{S'_n}{F.S.}$$

$$= \frac{r\Sigma(c_n \ell_n + P_n \tan\phi_n)}{F.S.} \qquad (6)$$

The safety factor F.S. is

$$F.S. = \frac{\text{Resisting Moment}}{\text{Overturning Moment}} = \frac{\Sigma(c_n \ell_n + P_n \tan\phi_n)}{\Sigma W_n \sin \alpha_n} \qquad (7)$$

where analysis is based on total stress parameters c and ϕ.

Although the side forces cancel out of the overall moment equation, they do influence the magnitude of the normal reaction, P_n, on the base of the slice and thus the frictional shear strength at the base of the slice.

The side forces are actually indeterminate but can be approximated in various ways. One commonly used method of

analysis, Bishop's simplified method, is described below.

Methods of analysis that satisfy all the conditions of static equilibrium are necessarily more complicated and difficult to apply. Bishop (1955) found that by including horizontal side forces to compute P_n and also satisfying the overall moment equilibrium the resulting safety factor was only slightly less than that found by more rigorous methods.

The force P_n, and in turn the strength on the bottom of the slice will differ from the case where side forces are neglected. Each slice is assumed to have the same factor of safety, F.S., and a required strength, T_n, equal to the available strength at the bottom of the slice divided by F.S.

$$T_n = \frac{S_n'}{F.S.} = \frac{c_n' \ell_n}{F.S.} + \frac{P_n - u_n \ell_n}{F.S.} \tan \phi_n' \qquad (8)$$

Bishop assumed that the sum of the vertical side forces on each side ($X_n + X_{n+1}$) equalled zero. Then from a summation of vertical forces:

$$\Sigma F_v = P_n \cos\alpha_n + T_n \sin \alpha_n - W_n = 0$$

By substitution and simplification, the equation for the factor of safety using Bishop's simplified method can be shown as:

$$F.S. = \frac{\Sigma\{[c_n b_n + (W_n - u_n b_n)\tan\phi_n'] \frac{\text{Sec } \alpha_n}{1+\tan\phi_n' \cdot \tan\alpha_n / F.S.)}\}}{\Sigma W_n \text{ Sin } \alpha_n} \qquad (9)$$

Since the safety factor, F.S., appears on both sides, F.S. is calculated from successive trials starting with an initial estimate. If the then calculated F.S. is used in succeeding trials, convergence is quite rapid. The failure arc predicted by Bishop's simplified method has been found to compare well with the actual failure surface.

The method of slices was further developed by Morgenstern and Price (1965) so that all the equilibrium conditions were satisfied. Standard computer program packages are available for slope stability analysis of terrestrial slopes using the method of slices.

Although the basic principles of analysis are similar for terrestrial and seabed slopes, wave-induced pressures at the mudline is an additional factor to be considered for the seabed.

2.2 Wave-Soil Interactions

2.2.1 Analysis of Cohesive Sediments

One of the effects of ocean waves is the change of pressure within the water below the wave and the consequent pressure pulses generated at the mudline. Under a wave crest the pressure change is $+\Delta p$, under a trough the pressure change is $-\Delta p$. The magnitude of Δp depends on wavelength, L, wave height, H, and water depth, d (Wiegel 1964). From linear wave theory (Wiegel 1964), the maximum wave induced pressure at the mudline is given by:

$$\Delta p_o = \pm \frac{H \gamma_w}{2 \cosh (\frac{2\pi d}{L})} \qquad (10)$$

The pressure, $\Delta p(x,t)$, under one wave cycle is in phase with the surface wave and is given as:

$$\Delta p(x,t) = \Delta p_o \sin 2\pi(x/L - t/T) \qquad (11)$$

where:

$$L = \frac{gT^2}{2\pi} \tanh (2\pi d/L) \qquad (12)$$

Because of the difference in pressure under the crest and trough, the passage of a wave induces shear stresses within the soil. As a wave passes over an element of soil, that element experiences a cyclic fluctuation in magnitude and direction of these induced stresses. Stability analysis of the seabed under the influence of surface ocean waves is a relatively recent practice (Henkel 1970), (Doyle 1973), (Bea 1971).

It was first thought that submarine slides could be explained in terms of gravity forces and low sediment strengths (Terzaghi 1956). A slip-circle method of analysis later indicated that waves must play a direct role in causing some submarine landslides in soft underconsolidated soils, since soil strengths found to exist in failure areas indicate that gravity forces alone were insufficient to cause failure (Henkel, 1970).

It has been reported (Henkel 1970) that the pressure changes on the sea floor, associated with the passage of a wave, are able to cause failure in soft sediments in water depths up to about 120 m. It has also been noted that waves cause soft sediments to oscillate which, on sloping ground, leads to a mass transfer of soil down slope. Repeated reversals of shear strain in the sediment cause remoulding and a reduction in shear strength. Scott and Zuckerman (1970) reviewed the topic of instability of the ocean floor and concluded that only limited evidence existed to support the theory that waves actually caused sea bottom failure. However, subsequent research by several others has shown evidence to the contrary.

Conclusive evidence of this phenomenon became available as a result of hurricane Camille in 1969, when hurricane generated waves produced lateral soil movements to at least 24 m below the mudline at one platform site (Sterling and Strohbeck 1973).

Figure 3 shows one mechanism of failure in terms of the disturbing moment, M_d, produced by gravity forces introduced by a sloping bottom, and a couple developed by the differential bottom pressures produced by surface waves (Henkel 1970).

$$M_d = \frac{2}{3} x^3 \beta \gamma' + \frac{L^2 \Delta p}{2\pi^2} (\sin \alpha - \alpha \cos \alpha) \qquad (13)$$

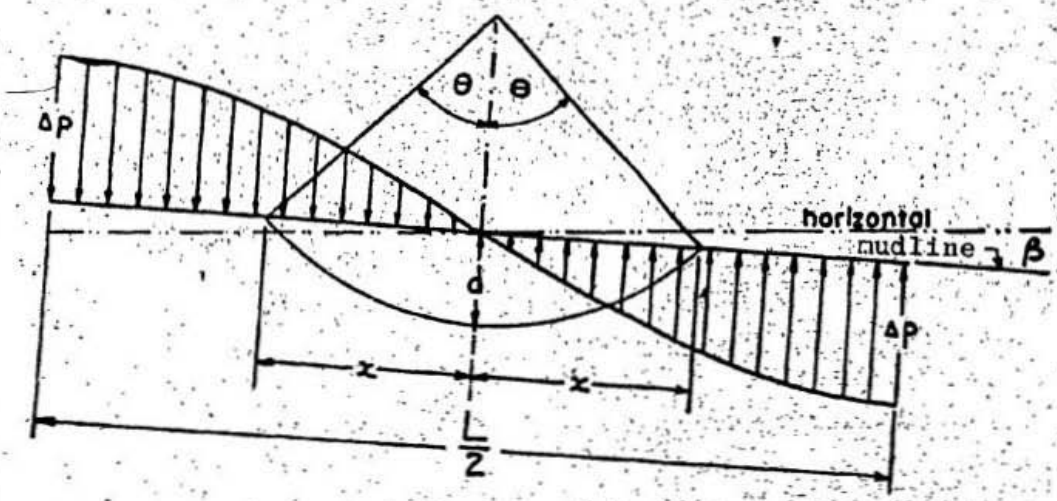


FIGURE 3 GEOMETRY OF ASSUMED SURFACE OF SLIDING (FROM HENKEL, 1970)

The dimensions of this possible slide surface are described by the half length, x, and the depth, d, to which sliding extends. The angle of the arc of sliding is 2θ, γ' is the submerged unit weight of soil, and $\alpha = 2\pi x/L$.

The moment of resistance, M_r, that can be mobilized within the soil is given by

$$M_r = 2\,x^3\,\left(\frac{c_u}{\gamma' z}\right)\,\gamma'\,\left(\frac{\sin\theta - \theta\cos\theta}{\sin^3\theta}\right) \qquad (14)$$

where c_u is the undrained shear strength.

The soil will be at the point of failure when $M_d = M_r$; and, when $M_d > M_r$, movement will take place. The limiting condition in which $M_r = M_d$ can be shown as

$$\frac{\Delta p}{k'\gamma' L} = 4\pi^2\left(\frac{x}{L}\right)^3 \frac{1}{\sin\alpha - \alpha\cos\alpha}\left\{\frac{\sin\theta - \theta\cos\theta}{\sin^3\theta} - \frac{\beta}{3k'r}\right\} \qquad (15)$$

where $k' = \frac{Cu}{\gamma' z}$. From this relationship Henkel (1970) showed that the bottom pressure effects due to waves are more than adequate to cause shear failure in soft sediments like those of the Mississippi delta.

A consequence of this effect in loose under-consolidated soils is that the material will tend to accumulate at a water depth where the wave effect becomes negligible. This depth is reported (Henkel 1970) to be about 120 m for the Mississippi delta. A marked change in slope from about 1:125 to 1:50 at this depth represents a change in the mechanism of sediment movement; i.e., in waters shallower

than 120 m, the sediments can be moved by wave forces, while in deeper water soil movement is primarily associated with gravity slides.

Henkel (1970) studied the above phenomenon using a glass tank 1.5 m long, 0.43 m high and 0.10 m wide. Tests were conducted with cohesive soils under a manually produced standing wave, to show qualitatively that waves could cause slope instability.

One of the factors which affects the depth of wave influence below the mudline and the consequent soil failure is the soil type and its strength profile. For clayey seabed sediments, it has been shown for a bottom of clay (Wright and Dunham, 1972) that the soil failure will be confined to shallow depths when the soil strength increases uniformly with depth. On the other hand for the type of soil encountered in the Mississippi delta where there is a surficial "crust" underlain by weak underconsolidated sediment, it has been shown (Wright and Dunham 1972, Wright 1976) that the failure zone could extend up to 30 m below the mudline.

Several types of laboratory tests to verify the existing theories have been reported in the published literature. The majority of data collected deal with cohesive soils. Under wave loading, the sediment was found to initially oscillate in sympathy with the standing waves,

and in time, mass movement of the soil occurred in the downslope direction (Singh 1971, Doyle 1973).

Tsui (1972) used a soil container 1.8 m long, 0.6 m deep and 0.15 m wide in which small amplitude progressive waves were passed over the soil by placing the soil container in a wave flume that measured 0.6 m wide by 1.2 m deep by 45 m long. It was concluded that for a particular shear strength and gravity stress a wave pressure below some critical value would result in an equilibrium condition within the soil such that only small irreversible shear strains developed. When the wave bottom pressure was at or above the critical, signfficantly large irreversible shear strains developed as indicated by a visible rupture zone and instability of the slope.

In order to arrive at suitable slope angles for the wave flume experiments Tsui (1972) considered the following relationship between slope angle and soil shear strength:

$$\frac{c_u}{\gamma' z_s} = \frac{c_u}{p'_m} = \frac{1}{2} \sin 2\alpha_f \qquad (16)$$

where:

z_s = depth of sliding surface

γ' = average submerged density

α_f = failure angle of slope

c_u = undrained strength

p'_m = vertical effective stress at depth of failure.

Good correlation was found between the shear strength at failure as determined from the static tilt experiment and in-situ vane shear test for the Bentonite clay used.

In the above tests, a reserve strength, S_r, was defined in terms of the critical bottom pressure, Δp_c, required to initiate mass movement of the sediment:

$$S_r = \frac{\gamma' z_s}{2} (\text{Sin } 2\alpha_f - 2\alpha) \qquad (17)$$

where α_f is the failure angle in static tests and α is the angle of slope subject to wave action. It was found that failure occurred when

$$\frac{\Delta p_c}{S_r} = 2.40 \qquad (18)$$

Tsui's approach assumes that gravitational forces alone cause downslope mass movement (failure) and that the wave serves only to cause strength reduction in the soil. This concept is different from earlier analyses in which it was assumed that some additional downslope force must be present to overcome a known shearing resistance and that (Terzaghi, 1956) the slope failure could occur without soil strength loss or forces other than gravity.

The necessary percentage reduction in soil shearing resistance (or measured undrained strength) to cause failure may be calculated as:

$$R = \frac{S_r}{c_u} = \left(1 - \frac{\text{Sin } 2\alpha}{2 c_u / \bar{p}_m}\right) \times 100\% \qquad (19)$$

and, for waves to initiate failures, the soil sensitivity must be

$$S_t = \frac{c_u \text{ undisturbed}}{c_u \text{ remoulded}} > F.S. \qquad (20)$$

Tsui (1972) found in his experiments that the bottom pressure required to initiate failure (Δp_c) could be given in terms of the soil strength and the slope angle (or F.S. against gravitational failure) as:

$$\Delta p_c = 2.4\, c_u \left(1 - \frac{\text{Sin } 2\alpha}{2\, C_u/p'_m}\right) \qquad (21)$$

$$\Delta p_c = 2.4\, c_u \left(1 - \frac{1}{F.S.}\right)$$

Equation 21 was found to predict the value of Δp_c to within ± 15% for the model tests. It was also concluded from the tests that the depth of sliding varied with the average degree of consolidation and that the wave characteristics had no influence on the depth of failure. (Tsui, 1972).

Hull (1973) extended the work of Tsui (1972), using the same tank, in order to quantify some of the phenomenon reported earlier. Cyclic subsurface pressures due to wave action were shown to cause remolding and loss of strength in fine grained submarine sediments and the depth of remolding was shown to generally increase with increased subsurface pressure. It was also concluded that the depth of potential

slope failure increases with increased subsurface pressure, generally in accordance with the relation proposed by Henkel (1970). Deep failure was considered to be impossible unless the sensitivity of the soil was in excess of the static factor of safety for the slope.

Doyle (1970) reported the results of tests in a tank 4.9 m long, 1.6 m deep and 1.2 m wide with a 1.1 m deep clay sediment, showing the effect of waves under several combinations of soil strength and wave loading conditions. It was noted that with a bottom slope, if the soil strength was high enough, oscillatory movements did not occur but a net downslope movement was observed.

Doyle (1970) also made qualitative observations about soil motion, remolding processes and effects, and mode of failure. He concluded that simple analytical tools such as the total stress slip-circle analysis and the elastic shear stress analysis appear to be useful in predicting soil instability. He also observed that the flexibility of the soil causes a reduction in bottom wave pressure.

The net downslope movement is to be expected intuitively, since there should be a soil strength range, in which the soil will move downslope when there is an added force, such as a wave load.

The slip-circle analysis that Doyle (1970) used is a total stress analysis in which a sinusoidal bottom

pressure acts as an overturning moment on the sea bottom. The shape of the failure surface is assumed to be circular with the soil shear strength along a circular arc providing the resistance to overturning. Bottom slope, if any, further acts to create instability in this analysis.

The wave shear stress analysis considered by Doyle (1970), used an elastic stress distribution below the mudline under an assumed sinusoidal wave loading. For this type of analysis the elastic shearing stress caused by some particular bottom wave pressure was plotted on a shear strength profile as shown in Figure 4. Wherever the wave shearing stress exceeds the insitu soil shear strength, failure of the soil is assumed to have occurred.

Doyle (1970) used the following relationship for the elastic shearing stress below the mudline. This was derived asuming an infinitely long sinusoidal bottom pressure wave:

$$\tau = \Delta p_o \frac{2\pi z}{L} e^{\left(\frac{-2\pi z}{L}\right)} \qquad (22)$$

where

τ = elastic shearing stress

Δp_o = bottom wave pressure amplitude under crest or trough

z = depth below mudline

L = wavelength

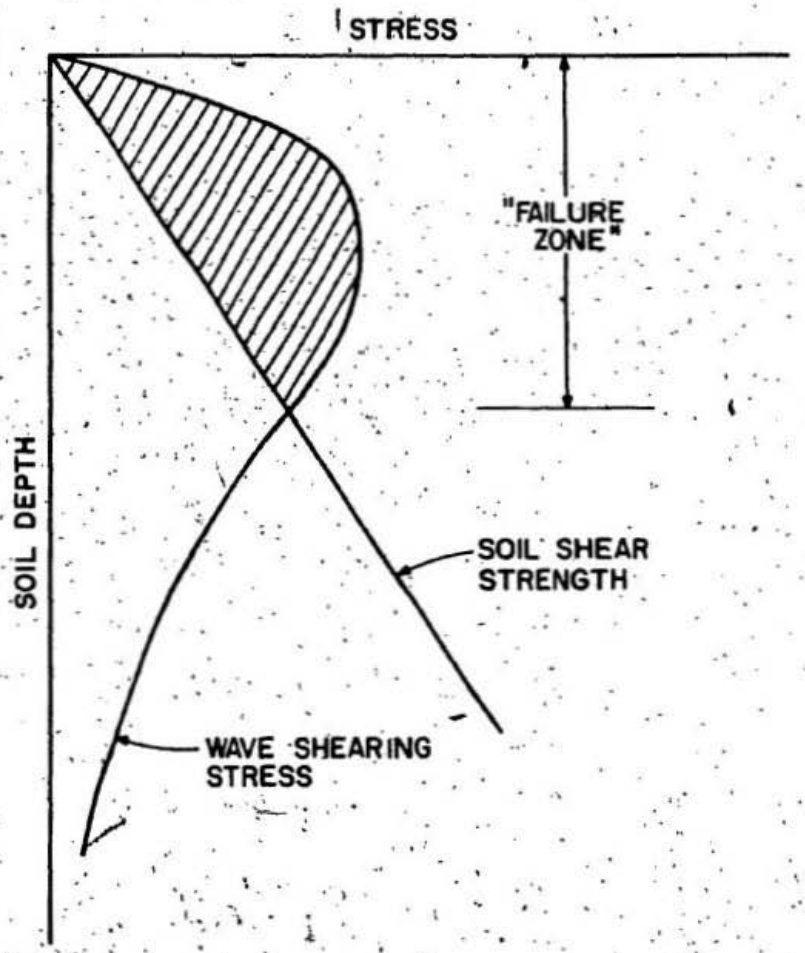


FIGURE 4 WAVE SHEARING STRESS SUPERIMPOSED OVER SOIL SHEAR STRENGTH PROFILE (FROM DOYLE, 1973)

Good agreement was noted between tank tests and the elastic stress analysis but agreement between tests and the slip-circle analysis was good only when the soil had relatively high strength near the soil surface, i.e. a "crust" profile (Doyle 1970).

2.2.2 Instability of Cohesionless Soils

Extensive slides in submarine deposits of loose sand are also well khown but often these slides are considered mysterious in that according to conventional stability analysis the slopes should be stable beyond any doubt (Andresen and Bjerrum 1967). A general description of a number of failures in loose sand has been given by Casagrande (1950); other examples are given by Terzaghi (1956).

Andresen and Bjerrum (1967) distinguish between two different types of slides, (1) retrogressive flow slide and (2) spontaneous liquefaction. A retrogressive flow slide generally starts in the lower part of a slope as a result of a local steepening due to erosion or due to the seepage pressures during falling tide. Following the initial slip, the slide develops retrogressively inland, slice by slice. This characteristic feature of successive slips is due to the fact that the sand liquefies as a result of the large strain imposed on it during the sliding movement. It then flows away and leaves an unsupported face of sand behind it which in turn fails and flows away (Andresen and Bjerrum 1967).

Spontaneous liquefaction can easily be demonstrated in the laboratory by shaking a container of submerged loose sand. During a brief period the sand will behave as a liquid such that heavy objects will sink and light objects will float. This loss of strength occurs when the pore water pressure is equal to the overburden pressure where the shear strength is given by $\tau_R = (\sigma-u)\tan\phi'$; when $\sigma=u$ then τ_R goes to zero.

The same phenomenon has been known to have occurred in nature. Slope failure in various cohesionless subaqueous sediments have been attributed to spontaneous liquefaction initiated by earthquake activity (Terzaghi 1956). Blasting is listed as another initiator for liquefaction of cohesionless soils (Andresen and Bjerrum 1967). Very little is known about the development and propagation of this type of failure. During earthquakes, for example, deposits of loose saturated sand on land have temporarily lost their bearing capacity, and embankments and buildings have settled or tilted as a result of foundation failures (Andresen and Bjerrum 1967), (Seed et al 1976), (Seed et al 1981), (Terzaghi 1956).

The liquefaction is believed to start at one point, spreading to neighbouring deposits of sand possessing metastable structures. The spreading can take place in all directions, downhill as well as uphill, and even large

horizontal areas can be involved in the failure. Slides of this type may propagate over large distances at a rate varying from 10 to 100 km per hour, depending on the topography. The essential feature of the mechanism of this type of failure is the temporary structural collapse of a volume of sand followed by re-sedimentation. During the short period of liquefaction the sand will flow down hill if it is located on a slope (Andresen and Bjerrum 1967).

Data from a number of such spontaneous liquefactions have been documented, the most impressive of which is the failure which occurred on the Grand Banks of Newfoundland following an earthquake on November 18, 1929. The rate and location of slope failure was recorded by the breaking of a series of telecommunications cables. The disturbance propagated approximately 550 km, with velocities of 20-110 km per hour over a slope of less than 1 percent (Terzaghi 1956).

A method used in Norway to determine whether or not a sand deposit may be subject to liquefaction has been described by Andresen and Bjerrum (1967). In 1959, the Norwegian Geotechnical Institute developed the "blasting test" to determine the susceptibility of a sand deposit to flow sliding. A small charge of dynamite is lowered into a boring and detonated. The effect of the blast is observed by measuring the settlement of the ground surface and by

recording the pore pressure at various distances from the charge. A similar technique has also been developed in the USSR (Andresen and Bjerrum 1967), (Florin and Ivanor 1961).

A third cause of instability in cohesionless soil is the cyclic loading due to the direct action of waves (Seed and Rahman 1978). This is manifested in its complete form as liquefaction.

A typical example of liquefaction is the failure of a 3.05 m diameter steel pipeline in Lake Ontario during a storm; it is believed that the backfill temporarily liquefied causing the pipe to float to the surface of the soil. The backfill was at least 2 m deep over the crown of the pipe, and the water was about 9 m deep over the sections that failed (Christian et al 1974).

Seed and Idriss (1971) developed a simple procedure for determining the pore pressure response of sand deposits on the ocean floor for evaluating the cyclic mobility or liquefaction potential of sand deposits during earthquakes. Christian et al (1974) used a slightly different method of analysis to study the problem of wave-induced liquefaction in sand around a pipeline (Seed and Rahman 1978).

Others (Yamamoto 1978, Yamamoto et al 1978) treated the pressures and effective stresses in seabeds induced by waves analytically, using Biot's three dimensional consolidation theory. Biot's (1941) theory takes into

account the elastic deformation of the porous medium, the compressibility of pore fluid, and the Darcian flow of pore fluid. In order to verify his theory, Yamamoto (1978) compared his calculated pore pressures with those measured from his laboratory experiments.

Yamamoto et al (1978) describes experiments done in a wave tank that measured 5 m wide by 1.5 m deep. Coarse and fine sand beds 0.5 m deep by 1.5 m wide by 10 m long were tested under 0.9 m deep water. Relatively small wave heights were used with wave periods between 1 sec. and 2.6 sec.

In the above tests, the stresses and deformations were not measured and therefore a complete verification of the theory could not be made. As an example, Yamamoto analyzed the stablity of North Sea sediments and found that the top portions of sand beds as thick as 2.5 m can be liquefied from the design wave and that the slide-failure zone can penetrate the sand beds as deep as 8.0 m.

Raman-Nair (1984) in a work done parallel with this present thesis, has also solved Biot's equations for a sand bed. Papkovich-Neuber solution was used from the theory of elasticity to predict stresses, pore pressures and failure depth within a soil bed. The predicted values of pore pressure and failure depths are compared with the present experimental results in this thesis.

During the past year several other papers have been published dealing with various aspects of the soil-wave

interaction problem (Tsui and Helfrich 1983, Nataraja and Gill 1983, Finn et al 1983, Denmars 1983).

Various techniques have been used to arrive at a solution for the transient effect of waves, but the analysis of the effect of a series of waves generally involves the Seed and Rahman (1978) approach.

Seed and Rahman (1978) developed an analytical procedure to evaluate the stability of ocean floor deposits against wave-induced instability and provide a quantitative evaluation of the complete time history of pore-pressure response of a soil profile to a selected design storm.

Their soil-wave interaction analysis showed a progressive buildup of pore pressure caused by the cyclic stresses induced by the direct action of a series of waves on a seabed composed of cohesionless soils. Pore pressure within a soil profile can build up during a series of progressive waves, to a stage where it becomes equal to the vertical effective stress. The rate and amount of pore pressure buildup will depend on: (1) wave characteristics, (2) cyclic loading characteristics of the soil, (3) the drainage and compressibility characteristics of the different soil strata comprising the soil profile (Seed and Rahman 1978).

The analysis of Seed Rahman (1978) considers a storm to be composed of a number of different waves having

characteristics in accordance with linear wave theory. The characteristics of a wave component are described by its period, length and height. The gently sloping ocean floor at a location under study is approximated to be horizontal. The wave-induced pressure on the ocean floor, due to each wave component is calculated by using linear wave theory (Wiegel 1964), given in Equation (10).

The progressive nature of the wave induced shear stresses implies that along any vertical line the amplitude of shear stress at the same depth will be the same. The phase lag is considered unimportant and all such lines are considered identical with respect to stresses induced by a given wave component; the problem is then considered as one-dimensional with regard to pore-pressure response.

The wave induced shear stresses are evaluated using the theory of elasticity. The following two assumptions are made:

(1) Linear elastic theory is applicable

(2) Wave-induced stresses on the ocean floor are not affected by the permeability of the ocean floor soil deposit.

Charts were then developed from the following relationships:

$$\left.\frac{\tau_c}{\sigma'_{v_o}}\right|_{z=0} = 2\pi \frac{\gamma_w}{\gamma'} \cdot \frac{H}{L} \cdot f_d \qquad (23)$$

and

$$\left.\frac{\tau_c}{\sigma'_{v_o}}\right|_{z=z} = f_z \cdot \left.\frac{\tau_c}{\sigma'_{v_o}}\right|_{z=0} \qquad (24)$$

where

$\frac{\tau_c}{\sigma'_{v_o}}$ is the cyclic shear stress ratio

$$f_d = \frac{1}{2} \cdot \frac{1}{\cosh\left(2\pi \frac{d}{L}\right)} \qquad (25)$$

$$f_z = \exp\left(-2\pi \frac{z}{L}\right) \qquad (26)$$

It has long been recognized that pore pressures in saturated sands under undrained conditions build up progressively under the action of cyclic shear stresses. At any instant the pore pressure, generated under undrained conditions, is considered to depend primarily on

(1) the relative density, D_r, of the soil.

(2) the induced cyclic shear stress ratio, $\frac{\tau_c}{\sigma'_{v_o}}$,

and

(3) the existing pore pressure.

The pore pressure will develop at different rates throughout the soil, depending on (1) the geometric details of the soil profile, and (2) the permeability and compressibility characteristics of the different soils in the profile. The net pore-pressure response will be the effects of generation and dissipation.

In order to develop the basic equation governing the pore-pressure response, Seed and Rahman (1978) assumed that the flow of water is governed by Darcey's Law

$$\frac{\partial}{\partial z}\left[\frac{k_z}{\gamma_w}\left(\frac{\partial u}{\partial z}\right)\right] = \frac{\partial \varepsilon}{\partial t} \qquad (27)$$

where k_z is the coefficient of permeability in the vertical direction, and ε is the volumetric strain, which is related to the vertical stress by means of the coefficient of volume compressibility, m_v.

Seed and Rahman (1978) used the following equation to account for the variation of soil compressibility with pore-pressure:

$$m_v = \frac{e^{Ar_u}\, B}{1 + Ar_u{}^B + A^2 r_u{}^{2B}/2\, m_{v_o}} \qquad (28)$$

where:

$A = 5(1.5 - D_r)$

r_u = pore pressure ratio, u/σ'_{v_o}

$B = 3/2^{2D_r}$

m_v = compressibility at r_u

D_r = relative density

m_{v_o} = initial compressibility at $r_u = 0$

The rate of pore-pressure increase, ψ, is given as:

$$\psi = \frac{\partial u_g}{\partial N} \cdot \frac{\partial N}{\partial t} \tag{29}$$

where N is the number of stress cycles during a storm, and $\frac{\partial u_g}{\partial N}$ is determined in the laboratory (Seed and Rahman 1978).

For many soils, the relationship between u_g and N can be expressed in terms of the number of cycles N_ℓ to cause liquefaction under the given stress conditions in the following form, (Seed and Rahman, 1978)

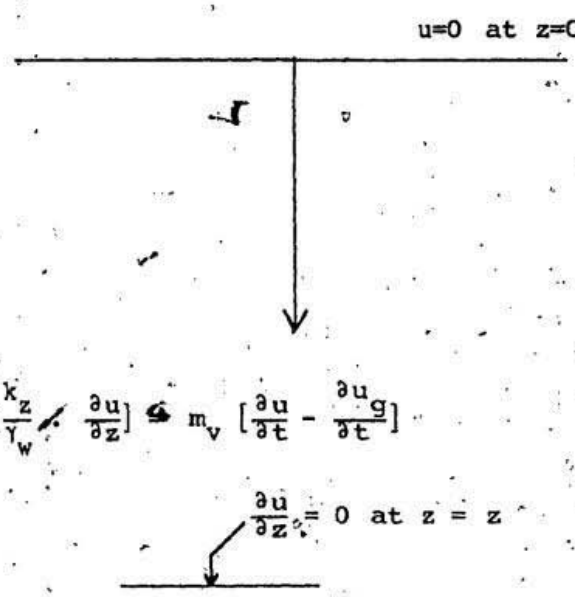
$$\frac{u_g}{\sigma'_{v_o}} = (2/\pi) \text{ arc sin } \left[\left(\frac{N}{N_\ell}\right)^{1/2\theta}\right] \tag{30}$$

where θ is an empirical constant.

This problem can be reduced to the solution of

$$\frac{\partial}{\partial z}\left[\frac{k_z}{\gamma_w} \cdot \frac{\partial u}{\partial z}\right] = m_v \left[\frac{\partial u}{\partial t} - \psi\right] \tag{31}$$

the solution of which has been done in finite element form and a comprehensive computer program (OCEAN 1) has been developed for this purpose. The end result of this program is the calculation of porewater pressures at various points and the prediction of porewater pressure history at these different depths in the seabed (Seed and Rahman 1978).



$$\frac{\partial}{\partial z}\left[\frac{k_z}{\gamma_w}\frac{\partial u}{\partial z}\right] = m_v\left[\frac{\partial u}{\partial t} - \frac{\partial u_g}{\partial t}\right] \qquad (32)$$

This concept of residual porewater pressure has been further developed by Finn et al (1983) to include the effects of increasing porewater pressures during a storm on the shear and bulk moduli. Others have published analysis of the transient effects. However, there has not been much work done in the laboratory to check either the transient effects of waves or the effect of a series of waves on the sea bed.

In the research reported in this thesis an attempt is made to study experimentally some of the effects of waves on soil. The design, fabrication and calibration of a wave-soil tank and the results of tests with flat and sloping beds of soil are reported here.

CHAPTER III

EXPERIMENTAL FACILITIES AND PROCEDURES

3.1 WAVE-SOIL TANK

3.1.1 Design Considerations

Two alternative experimental arrangements to model the effects of waves on seabed sediments were considered. One was the approach used by Tsui (1972) where a small soil tank is submerged in a larger wave flume. The other was to build a separate independent wave-soil tank similar to that of Doyle (1970) which can be tilted to form a sloping bed of soil. For this research, it would have been possible to use the 58m x 4.6m x 3 m deep University wave-tow tank in which a soil container of suitable size could have been placed for testing. However, it was decided not to pursue this option because of scheduling problems.

It was decided to design an independent test tank that could be tilted, and in which waves of about 0.5m to 3m length could be generated. It was necessary to pay attention to the design of the wavemaker and the beach in order that the generated waves were nearly sine waves and the reflection was a minimum.

An extensive review of the literature on wave tanks and wave generators was done before deciding the dimensions of the tank to be fabricated. A site visit was also made to

NRC laboratory facilities in Ottawa and Queen's University at Kingston, Ontario. A tiltable soil tank, 3.6 m x 0.76 m x 1 m deep with one long side of glass, which was earlier used for iceberg scour model tests, was readily available for use in the present research. However, it was felt that the length of the tank was not enough for use as a wave tank.

The available tank was extended at both ends, and the 3.6 m section with glass side was used as the main test section. An additional 1.8 m section was added at one end to incorporate a wave absorber. A 2.4 m section was added at the other end to contain the wavemaker of sufficient initial length so that the test section containing the soil was at least 3 times the water depth from the wave generator; this allows the wave to reach a steady form after leaving the wave maker (Keating and Webber, 1977). A smooth transition from the wavemaker bottom to the mudline of the test section for various mudline elevations is also provided. The above design changes required redesign of the structural supports for the tank. The tilting arrangement and the hydraulic jack for tilting also required suitable modifications. The redesigned tank is shown in Figure 5.

Several wave generating systems listed below were considered as possible generators for the present tank.

1. Piston type
2. Paddle, hinged at the bottom

3. Pneumatic

4. Wedge

5. Salter Duck in reverse

A paddle type wave generated hinged at the bottom, was finally chosen. The design incorporates a continuous flexible seal as shown in Figure 6, so that the back of the waveboard is dry. The drive and guide mechanisms for the hinged paddle are simple and easily maintained and adjusted. The main disadvantage of the other systems is that they require more elaborate guide systems or that the performance is not well documented in the literature. The Salter Duck has an advantage that a water tight seal is unnecessary and there will be no splashing behind the wavemaker, but again the performance is not well documented in the literature.

The size of the motor for the wavemaker is dependent on the characteristics of the waves to be generated. Gilbert et al (1971) have published graphs which correlate motor capacity and wave characteristics for various combinations of water depth, period and desired wave heights. In order to generate 0.1 m high waves with periods in the range 0.5 sec to 2.0 sec in the tank a 1/4 hp motor is necessary and waveboard frequency must be adjustable from 0.5 Hz to 2.0 Hz. The 1.5 hp motor which came with the tank was found to be suitable. The output speed can be varied to give wave board frequencies from 0.5 Hz to 1.7 Hz.

The paddle is connected to the motor by a 1 m long shaft through an adjustable eccentric wheel as shown in Figure 7. The maximum eccentricity is 25 cm, which makes possible a total wave board rotation of up to 20 degrees.

The wave board is constructed of 13 mm aluminum plate, and is 64 cm deep and 71 cm wide. Wings projecting backward from the waveboard enable a proper connection and operation of the watertight membrane along the bottom and sides of the tank. Streamlined fins were attached to the wet side of the wave board (Figure 6) to prevent cross waves at the board. Tests done without the fins, resulted in excessive crosswaves at the board when the wavelength was nearly equal to the width of the tank. Any crosswave developed at the board was found to progress along the length of the tank. Excessive splashing near the waveboard was also a problem before the fins were installed.

In order to reduce the disturbance of the soil in the main test portion of the tank, the entire wave generator section is isolated from the main tank by using a flexible connection. Further, the section which contains the wave generator is mounted on rubber pads, aproximately 2.5 cm thick by 5 cm diameter. Thus vibration from the wave generator and motor are isolated from the test soil.

The 1.8 m length of the tank from the wave generator to the main test section has an adjustable bottom

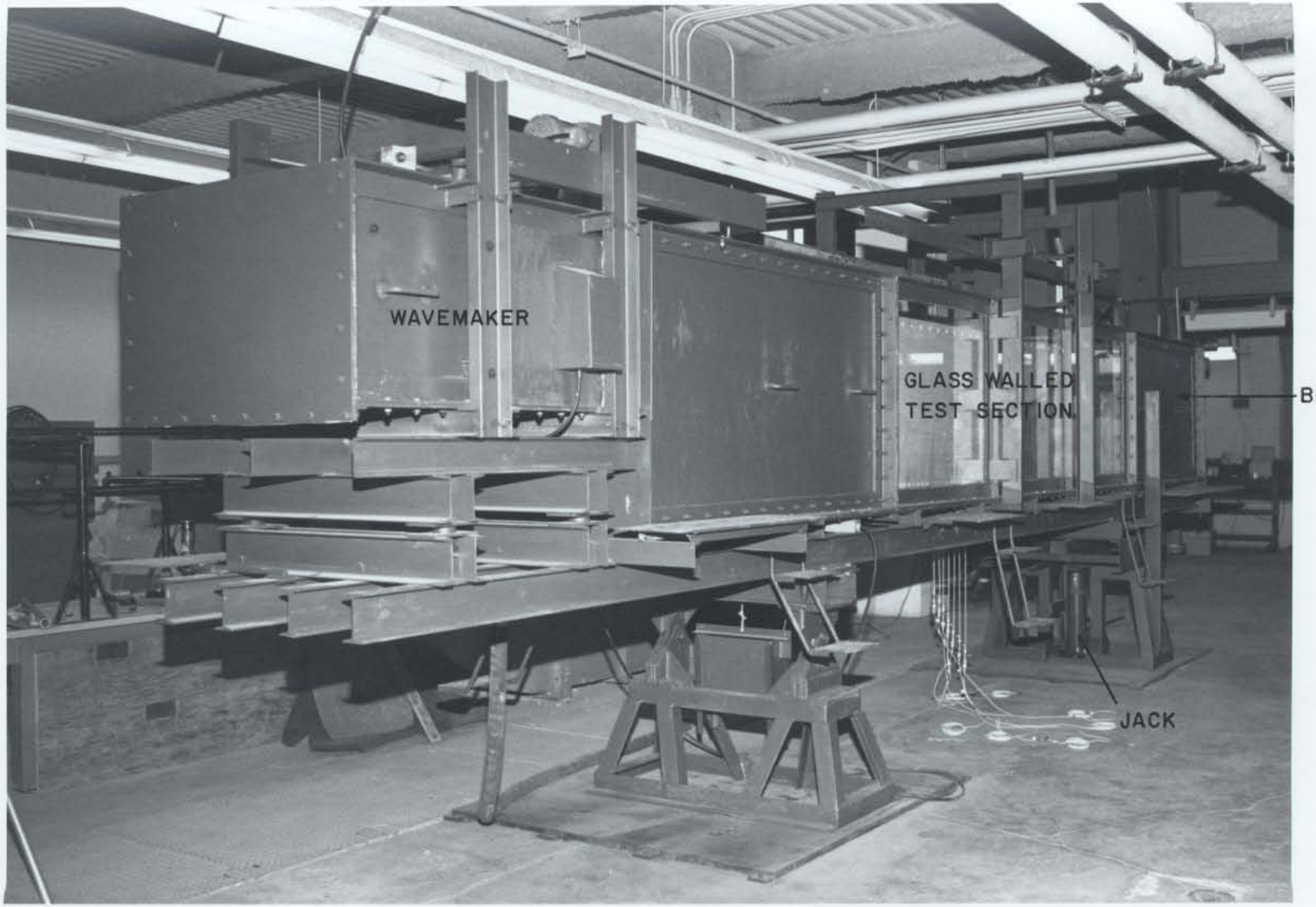


FIGURE 5 WAVE-SOIL TANK

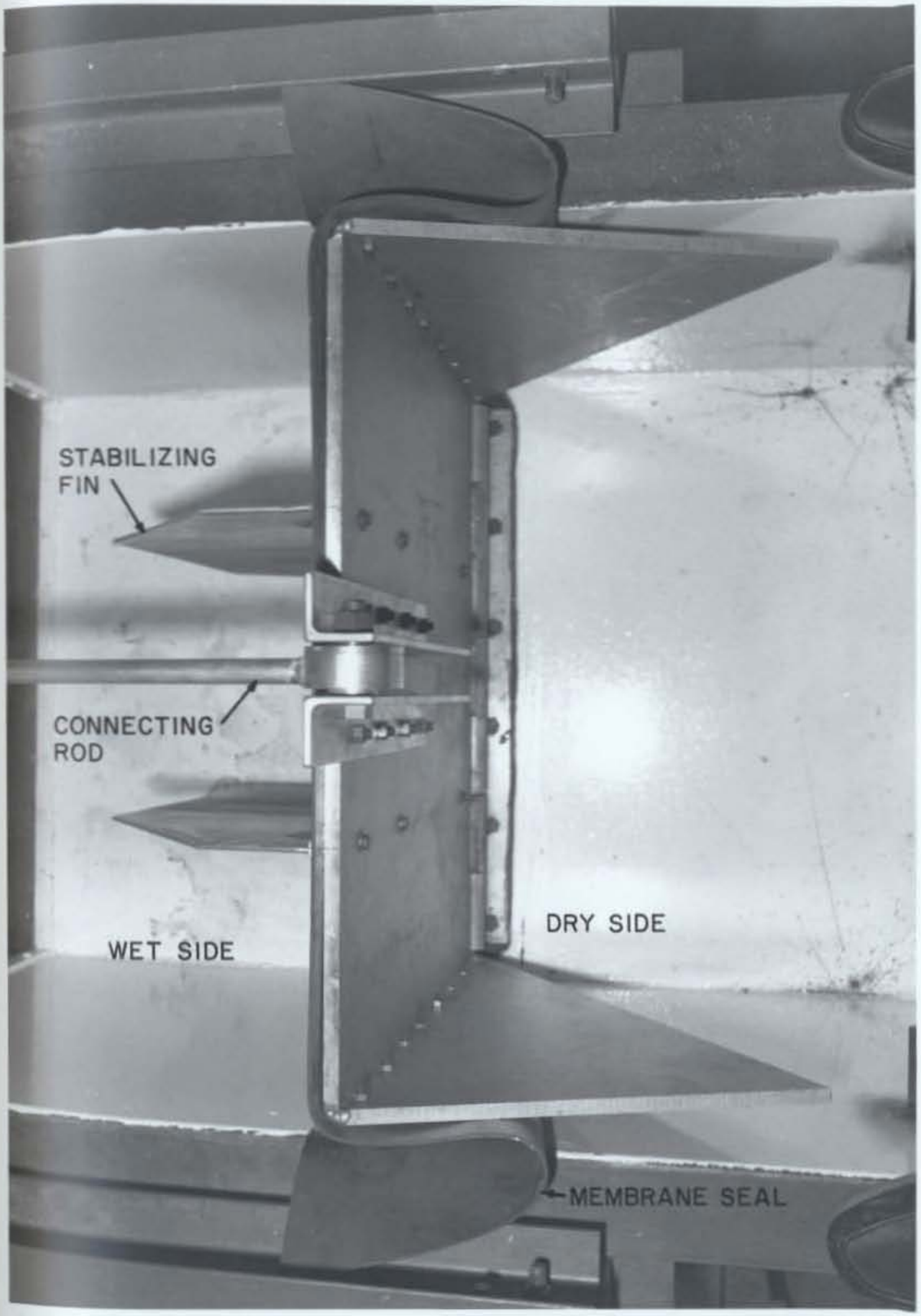


FIGURE 6 WAVE BOARD (TOP VIEW)

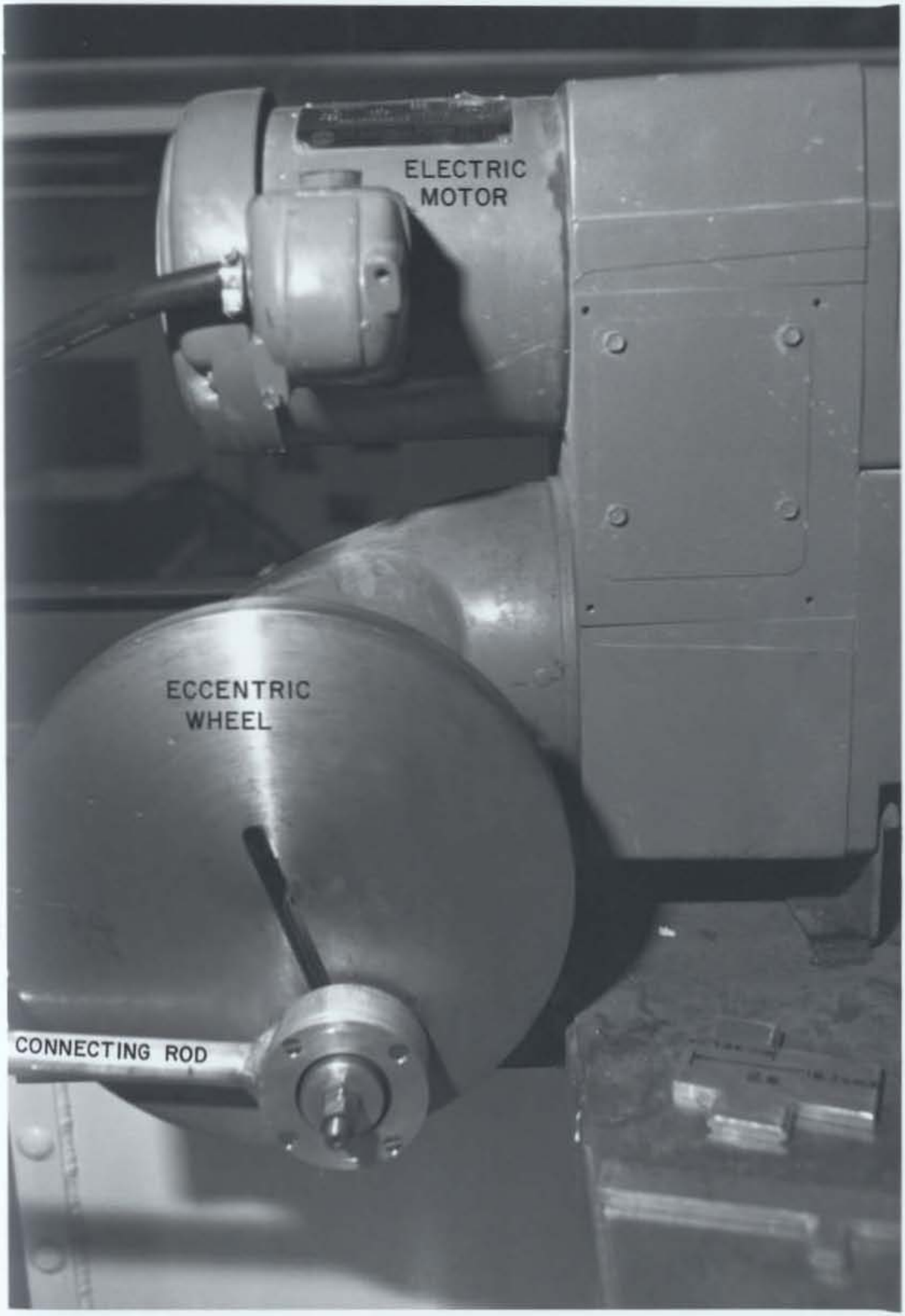


FIGURE 7 WAVEMAKER DRIVE

to provide a smooth gentle transition from the wave maker to the soil test bed. Details of the arrangement are shown schematically in Figure 8.

The central test section of the tank containing the soil is 3.8 m long with one side of 12 mm thick glass. Soil is held in place by plates at the ends, the total height of which can be adjusted to obtain different elevations for the mudline.

The tank is supported by a hinge near the wavemaker end and a 20 ton hydraulic jack with a removable support at the beach end (Figures 5 & 8). The hydraulic jack has a maximum displacement of 56 cm. The support at the beach end can be adjusted to give vertical movement of ±50 cm at this support. Thus soil slopes of ±1:10 may be obtained along the mudline in the test section.

A grid made of 13 mm diameter copper pipe is located at the bottom of the central test section. These pipes with 2 mm holes drilled at approximately 10 cm intervals enabled water to be forced through the soil when the soil sample was prepared for the tests. Soils of different densities were prepared using the forced jet technique through the pipeline grid.

A carriage which was capable of traversing the length of the test section, was mounted in the central section of the tank and was used to support the wave probes.

As indicated earlier, one of the requirements of the tank is to produce waves that are simple and consistent. Since the tank is of a finite length, waves will be reflected causing the wave height to change along the length of the tank. It is thus necessary to minimize the effects of reflection by installing a suitably designed beach at the far end. A very common and effective wave absorber is a gentle sloping beach of about 1:20 slope, covered with a layer of porous material. The size of the tank used in this research precluded the use of such a flat beach due to the constraint of length. The following alternatives were considered of which the first five were tested, since these offered easy construction and adjustment. They are shown schematically in Figures 9 and 10.

Beach #1 - A wedge of horse hair (Resilitex)

Beach #2 - A parabolic beach with transverse wooden strips. Radius = 2.5 m, Arc length = 0.84 m

Beach #3 - Similar to Beach #2 without a runner

Beach #4 - Similar to Beach #2 without the wooden strips

Beach #5 - Similar to Beach #4 but covered with 2 cm thick horse hair

Beach #6 - Perforated vertical baffles (Hamill, 1963)

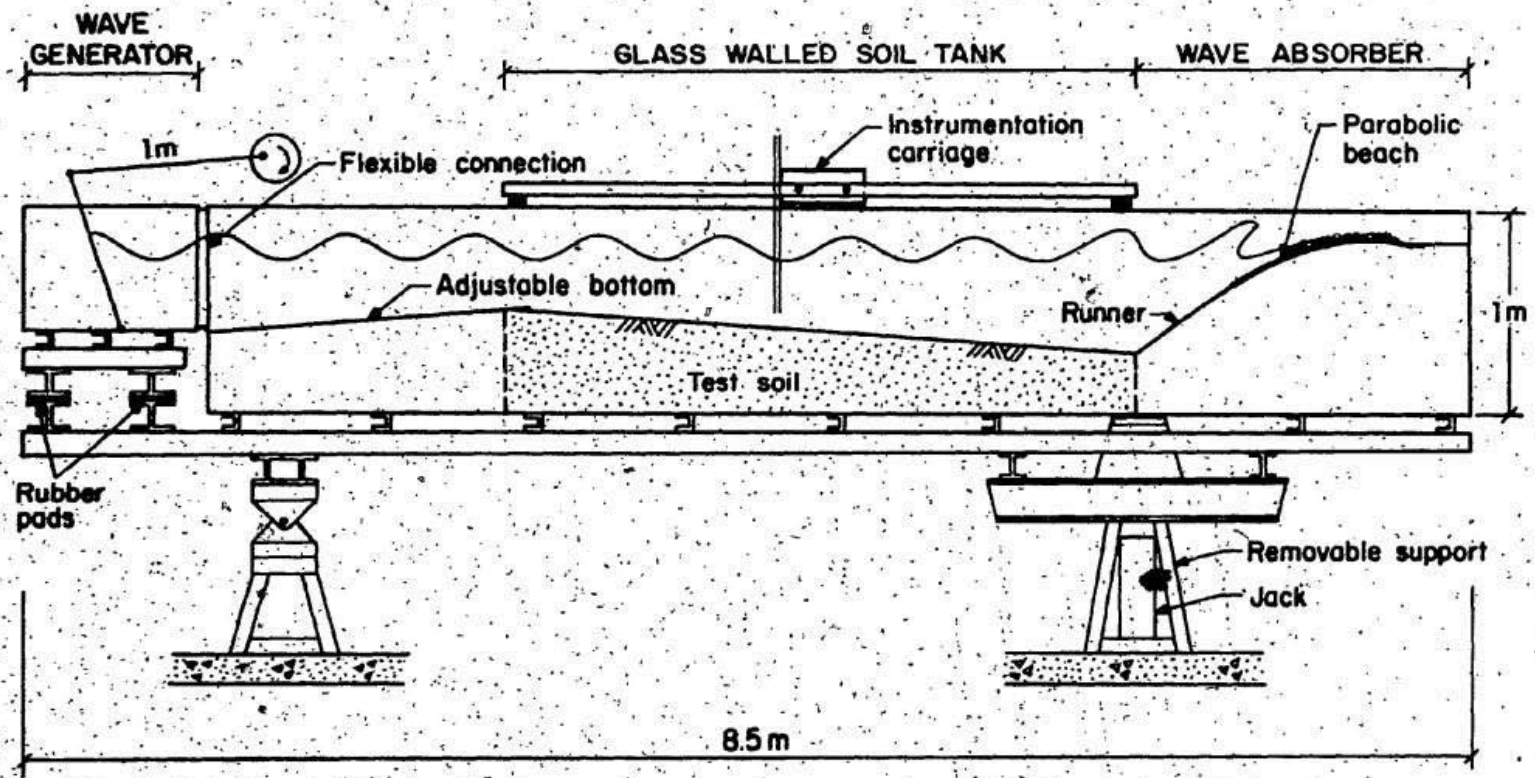
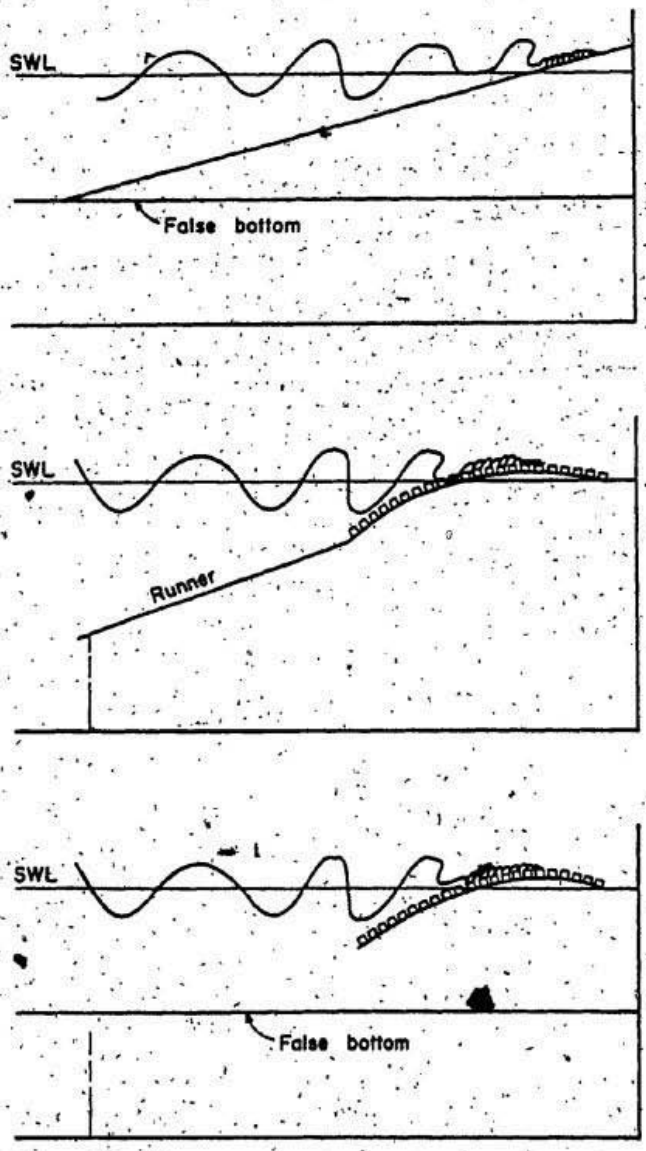


FIGURE 8 SCHEMATIC OF WAVE-SOIL TANK

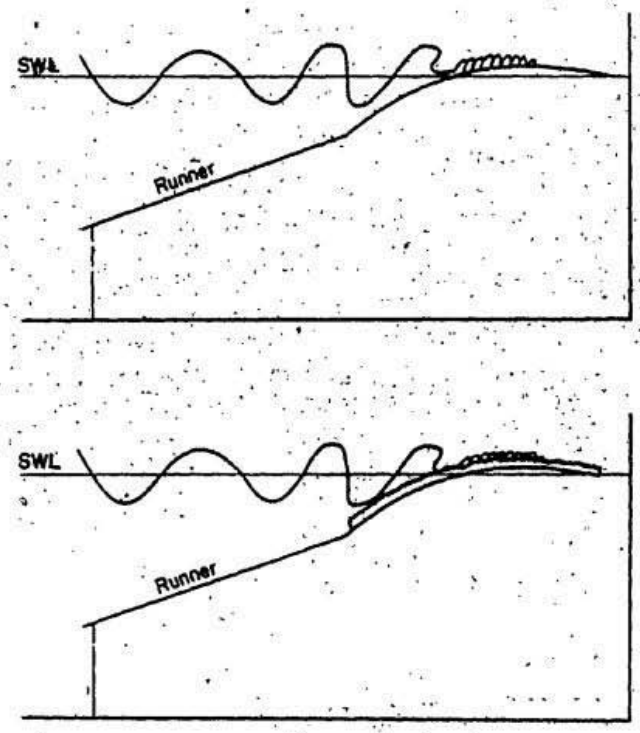


BEACH No. 1
Wedge of horse hair — Resilitex held in place with wire mesh.

BEACH No. 2
Parabolic beach — Rigid, impermeable beach with 2 cm. x 2.5 cm. wooden strips.

BEACH No. 3
Parabolic Beach — Rigid, impermeable beach with 2 cm. x 2.5 cm. wooden strips but no runner.

FIGURE 9 SCHEMATIC OF BEACHES TESTED



BEACH No. 4
Parabolic beach
—Rigid, impermeable, smooth.

BEACH No. 5
Parabolic beach
—Rigid, impermeable, covered with 2 cm. thick horse hair.

FIGURE 10 SCHEMATIC OF BEACHES TESTED

Beach #7 - A sloping bank of honeycomb material (Aveiro, 1982)

Beach #8 - A sloping gravel beach

Beach #9 - Rectangular bars

Beach #10 - Perforated inclines (Hamill 1963)

While most of the above types of beaches, or versions thereof, are described in the literature, there is no published data of their performance which could be extrapolated to meet the requirements of the present tank and experiments. In order to determine the most suitable type of beach, a series of experiments was carried out on the first five types listed above. The details of the test results are given in section 4.1.8.

Physically, the wedge of horse hair was quite acceptable and could be easily adjusted to accommodate various soil slopes and water depths. Likewise, the parabolic shapes were quite adaptable since these could be adjusted for different wave types to give a minimum reflection in each case.

The other alternatives were not suitable since they are less adaptable for adjustment to suit various wave characteristics and water depths. The wave absorber which was not tried, but which may be a good system for this tank is Beach #10. This system of perforated inclines is reported to produce low reflection coefficients and occupy a relatively short section of wave flume (Hamill 1963).

The wave absorber finally selected was a parabolic beach similar to that described by VanLammeren and Lap (1964) and used in the Wave and Current Laboratory of the Netherlands Ship Model Basin. A runner was attached to the beach by a hinge and extends to the beach end of the soil to give a smooth continuous bottom along the length of the tank as shown in Figure 8 and Figure 11. This arrangement was necessary to prevent the beating type response of the waves and to prevent drifting of sand outside the test section.

The performance of this modified parabolic beach is described in a later section.

3.2 Experimental Set-Up

3.2.1 Instrumentation

Wave height measurements at various locations along the length of the tank were made by a wave probe which was mounted on the carriage and could be moved along the length of the tank. The wave probe, shown in Figure 12, was a resistance type and consisted of two 3 mm diameter stainless steel rods hardwired to the wave monitors. The excitation voltage and the output voltage were provided and linearized using "Churchill Controls" wave monitors. The linearized signal was then recorded on a strip chart recorder.

Water pressure fluctuations at the mudline and pore water pressure changes inside the soil were measured using

four IPT-1100 "Kulite" pressure transducers with the following capacity range:

Rated Pressure	35 kPa
Maximum Excitation	12 VDC
Sensitivity	1 mV/kPa

The necessary power supply and amplification units were manufactured in-house. The output signals were amplified and either recorded directly using a strip chart recorder or were digitized by an HP 3497A Data Acquisition Unit, shown in Figure 13, and recorded on diskette using an HP 86 micro-computer.

Pressure variation at the mudline and inside the soil was measured using a row of 4 pressure transducers. These were positioned to read porewater pressures at 7 cm, 20 cm and 30 cm below the mudline (Figure 14). The fourth was used to measure pressure variations at the mudline due to the surface waves. The initial readings of the pressure transducers were suitably adjusted in order that the hydrostatic head of the still water was offset. The readings recorded during the experiment directly gave the pressure fluctuations due to wave loads.

The recording system for the pressures was similar to that used for the wave probe except that each transducer required a separate chart recorder. When the HP 3497A Data Acquisition/Control Unit was used, the rate of the data

logging was about 40 samples per second. Appropriate computer software was developed for data logging, retrieval and final plotting, and is listed in the Appendix.

3.2.2 Soil Sample

The sand used in this work was natural sand excavated from an open pit, fractioned, fabricated and commercially designated as #00 Alwhite Silica Sand. (Nova Scotia Sand & Gravel Co. Ltd.). The grain size distribution given below is plotted in Figure 15. For purposes of comparison, the grain size distribution of the surficial sand from the Hibernia area is also shown.

Grain Size Analysis of the Soil Sample

Sieve No.	% Passing
20 (.841 mm)	100.0
30 (.594 mm)	98.6
40 (.419 mm)	80.7
50 (.300 mm)	45.0
60 (.249 mm)	34.0
70 (.212 mm)	21.0
80 (.178 mm)	10.3
100 (.150 mm)	2.6
200 (.075 mm)	0.0

The coefficient of uniformity, C_u, is 2.13, and the coefficient of concavity, C_c, is 0.88.

The permeability of the sand at various densities was determined using a slightly modified standard laboratory procedure (ASTM #D2434). A loose specimen of the soil (ρ_d = 1372 kg/m^3) was prepared in a standard 7.62 cm diameter

by 20 cm long test cylinder by allowing the dry sand to fall through a column of water. The permeability was determined for this initial dry density. Then the soil was densified by tapping and vibrating the container and the permeability test was repeated. This procedure was repeated for several densities and a relationship between the permeability and void ratio was obtained as shown in Figure 16.

3.2.3 Preparation of Sand Bed

Two general density conditions were used in the experiments, loose sand and dense sand. In some cases soil samples with intermediate densities indicated later were also studied.

The loose sand condition was achieved in the tank by forcing water upwards through the soil from the grid of 13 mm diameter copper tubing, at a rate of approximately 5 liters per second for 30 seconds. The resulting dry densities were determined by slowly draining the soil and using a 146 cm^3 thin wall sampler; these values were checked using the mudline elevation observed through the glass wall. Care was taken during drainage to ensure that the soil volume remained unchanged. Dense sand conditions were achieved by vibration, or wave action as indicated later.

Before the soil was placed in the tank, the performance of the facility as a wave tank and the wave generation characteristics were evaluated. Results of these and other tests are discussed in the next chapter.



FIGURE 11 BEACH END OF TANK

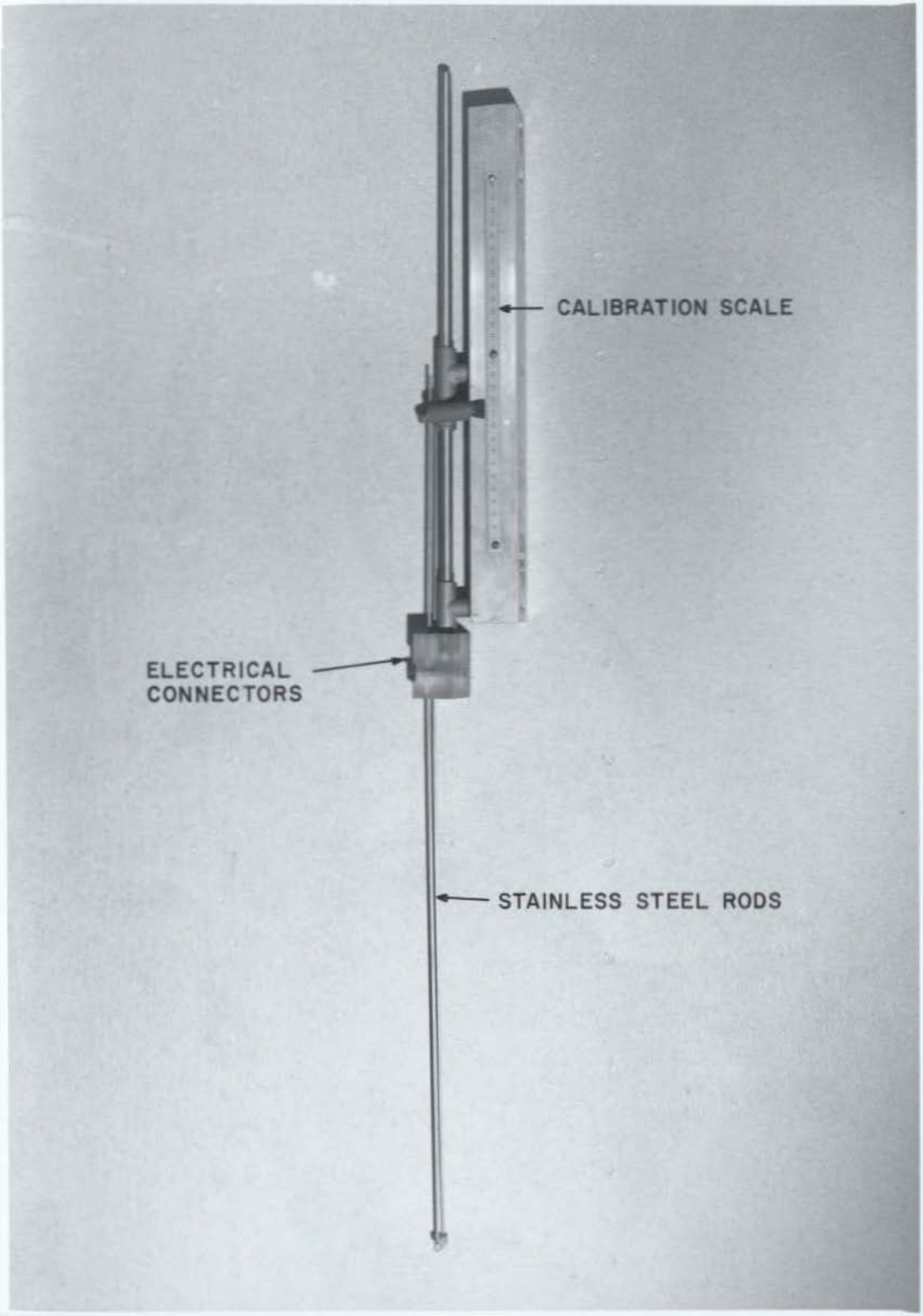


FIGURE 12 WAVE PROBE

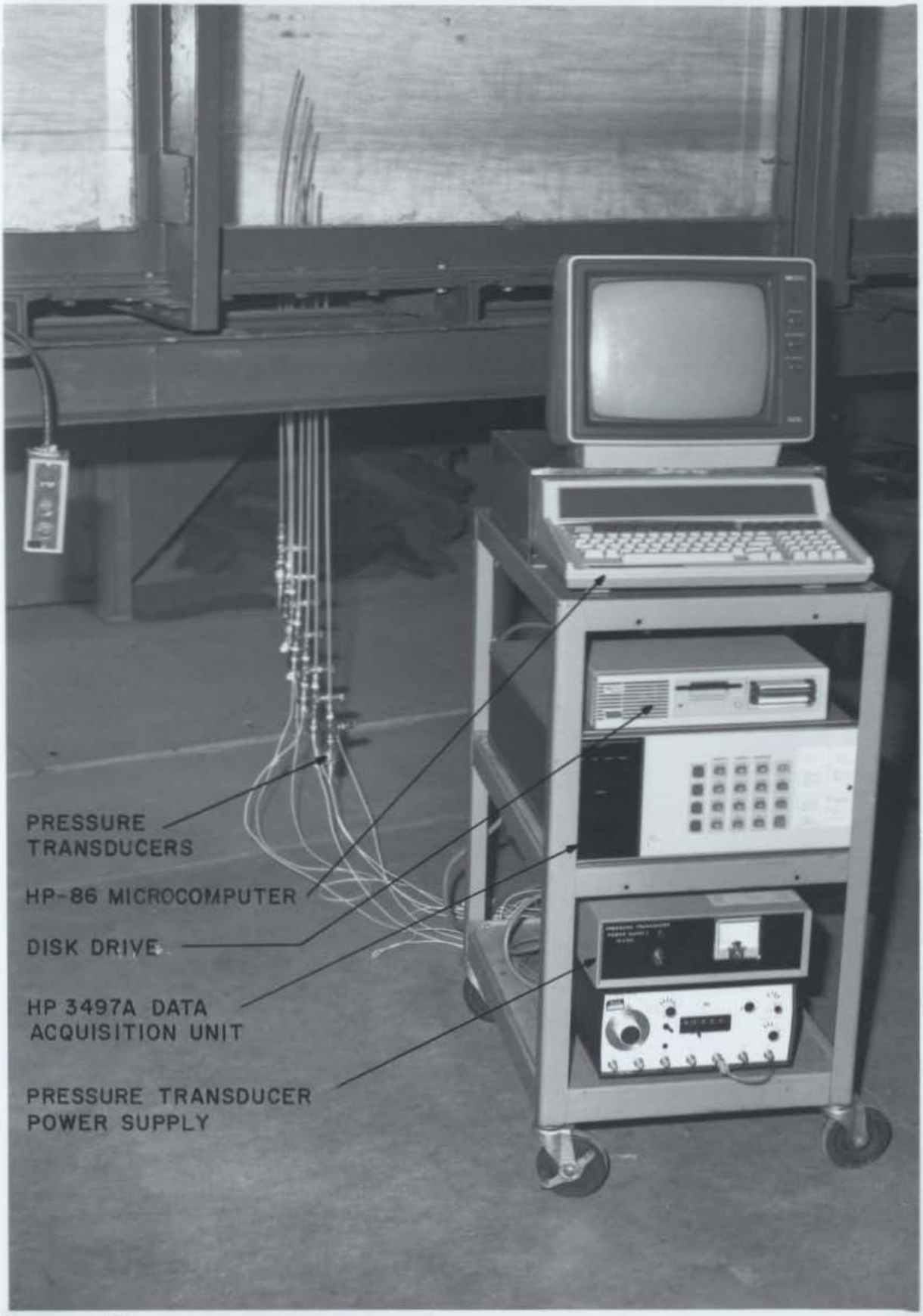


FIGURE 13 INSTRUMENTATION

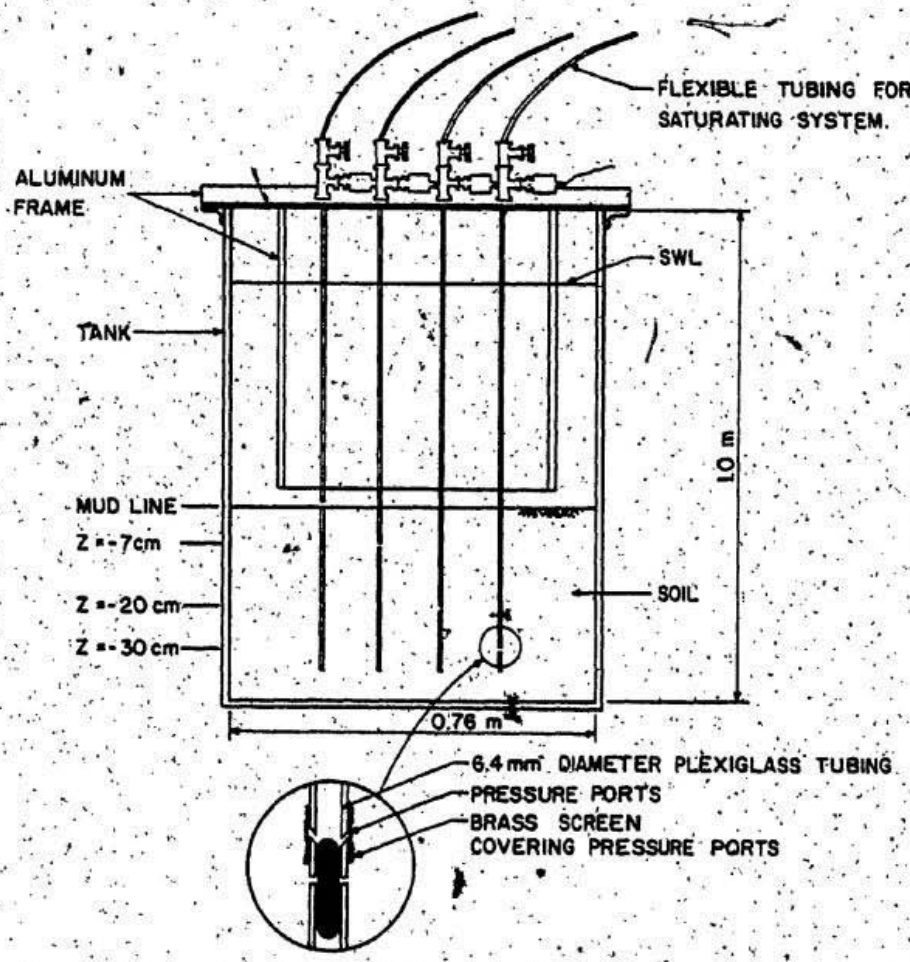


FIGURE 14 PRESSURE TRANSDUCER ARRANGEMENT

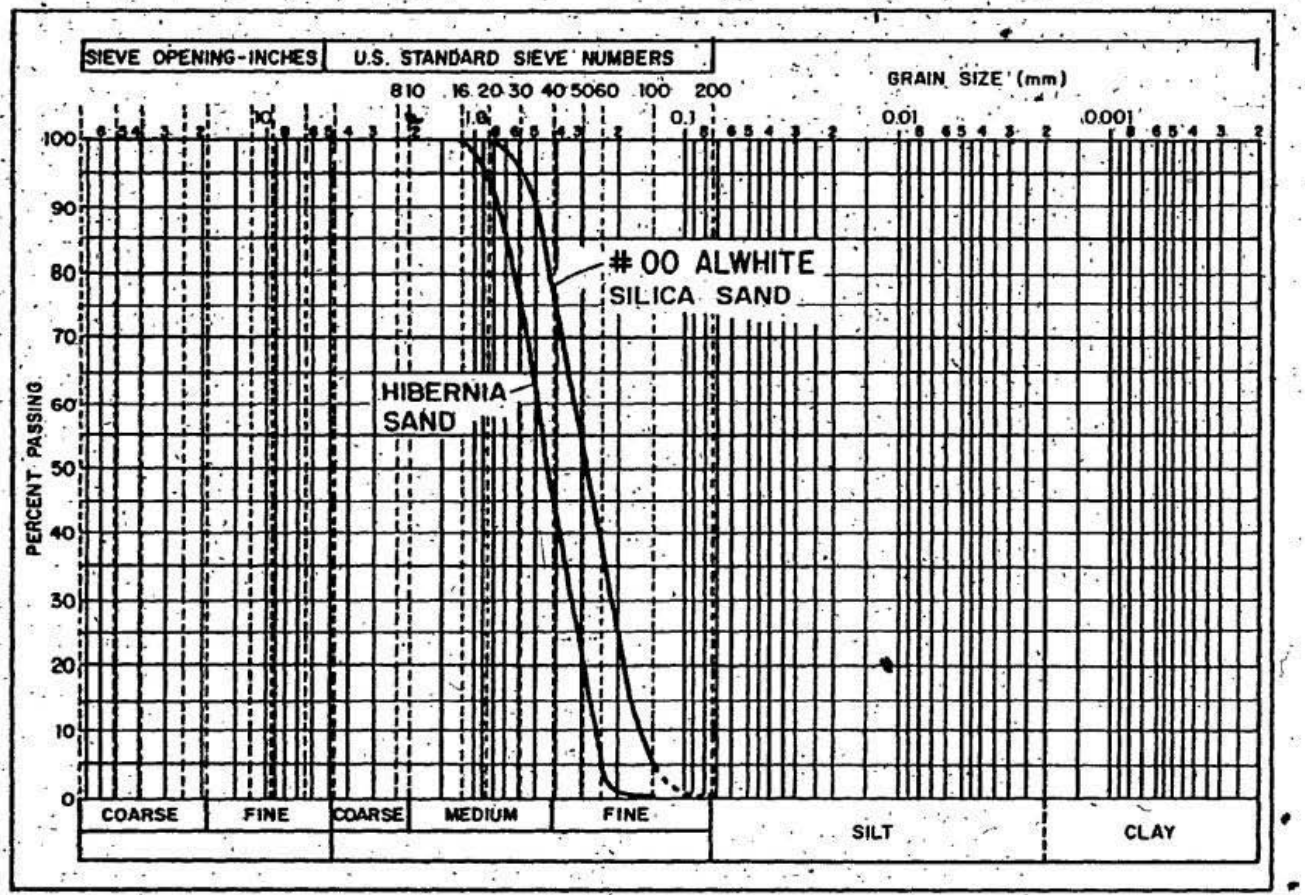


FIGURE 15 GRAIN SIZE DISTRIBUTION

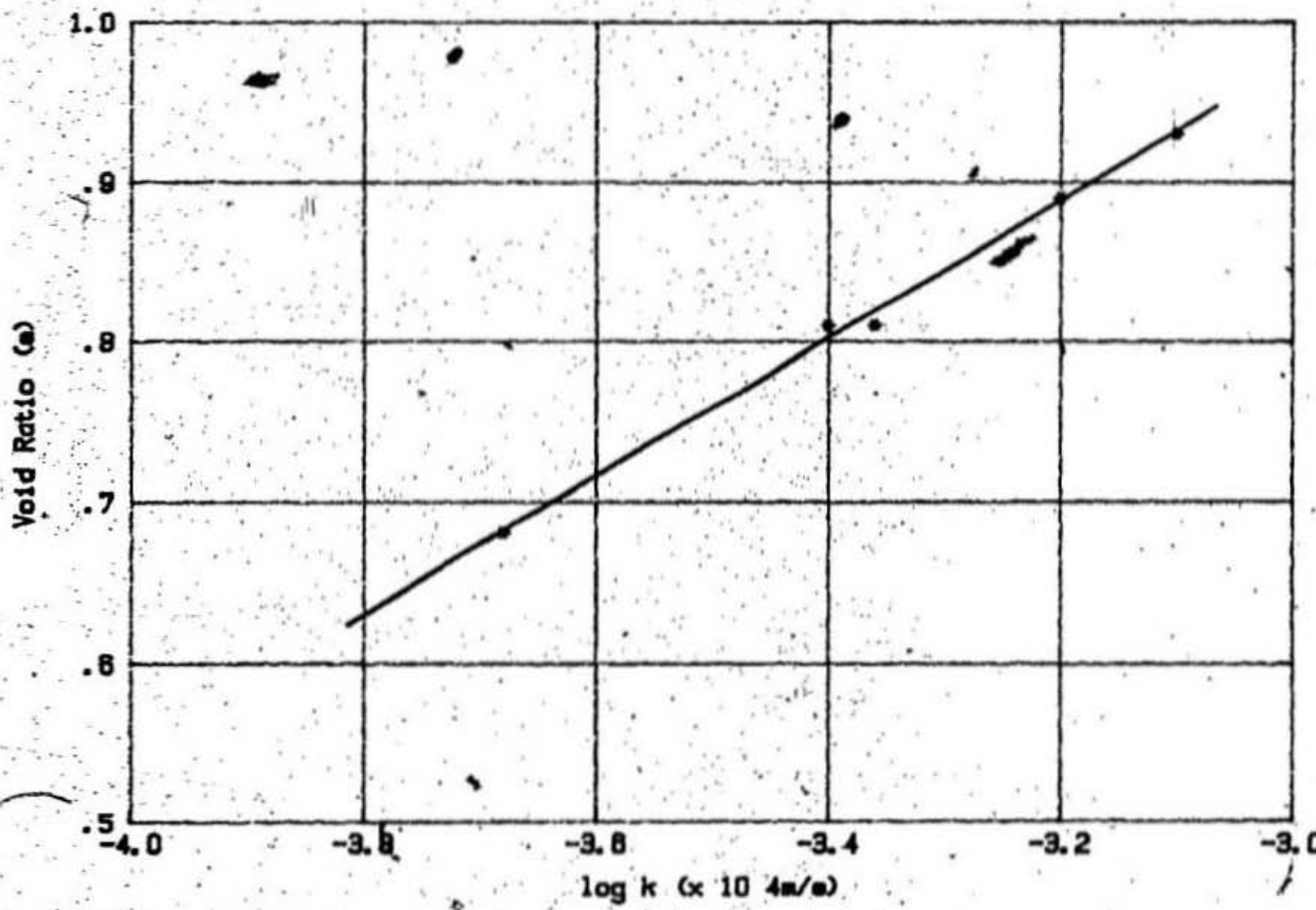


FIGURE 16 SOIL PERMEABILITY AT VARIOUS VOID RATIOS

Table 1

PROPERTIES OF THE SOIL USED

$G_s = 2.646$

	ρ_d $(\frac{kg}{m^3})$	e	k(m/s)
$\rho_{d\ min}$	1346	0.97	
$\rho_{d\ max}$	1617	0.64	
$\rho_{d\ min}$ (by pouring sand through a column of water)	1339	0.98	9.77×10^{-4}
$\rho_{d\ max}$ (by vibrating in saturated state with no surcharge)	1613	0.64	1.66×10^{-4}

CHAPTER IV

EXPERIMENTAL RESULTS AND DISCUSSION

The scope and focus of this research may be divided into two broad categories:

1. Evaluation and calibration of the test tank as a wave flume.
2. Examination of the effect of waves on soil stability.

The purpose of the performance evaluation of the tank was, to assess its capabilities and limitations and to document the performance characteristics of the wave generator and beach for use in further tests. An evaluation of the wave characteristics is also necessary to determine the wave theory most appropriate for the waves generated.

4.1 Wave Tank Performance Tests

Tests to evaluate the performance of the wave generator and the beach were performed without soil in the tank. However, in order to simulate the presence of a soil bed, a false bottom of 20 mm thick plywood reinforced with 25 mm x 50 mm wooden ribs underneath and anchored to the bottom of the tank was used to represent a bed of impermeable soil.

In any study of seabed stability the height of the water column above the soil is a very important parameter and the performance of the wavemaker was therefore evaluated for several water depths above the false bottom.

4.1.1 Wave Characteristics

The wave flume was tested using wave board frequencies between 0.56 Hz and 1.67 Hz, water depths between 30 cm and 50 cm, and paddle displacements up to a maximum of 15°, to produce mainly intermediate water waves.

Wave characteristics at three different water depths are given in Table 2. These characteristics were plotted in the wave classification chart (Shore Protection Manual, 1977) as shown in Figure 17; it may be observed that most of the waves generated can be described by Stokes' 2nd and 3rd order wave theories.

Typically for frequencies below 1 Hz, Stokes' 2nd order theory applies and for frequencies higher than 1 Hz. Stokes' 3rd order theory appears to be more appropriate. A comparison is made in a later section of the experimental values of wavelength vs frequency, and measured bottom pressure against theoretical values.

4.1.2 Wave Height and Wavemaker Stroke Correlation

Theoretical relationships have been given by Ursell et al (1960) for the performance of piston type wave makers and flap type wave makers. For piston type wave makers, the wave height is given as

$$\frac{H}{e} = \frac{2(\cosh 2k_o d - 1)}{\sinh 2k_o d + 2k_o d} \qquad (33)$$

TABLE 2

TYPICAL WAVE CHARACTERISTICS USED IN THIS RESEARCH

PERIOD (sec)	1.78	1.4	1.12	0.97	0.84	0.79	0.74	0.6
d = 30 cm								
L(m)	2.8	2.1	1.6	1.3	1.12	0.97	0.87	0.63
H_{max}(m)	.027	.017	.031	.042	.041	.049	.061	.068
d/T^2	.095	0.15	0.24	0.32	0.43	0.48	0.55	0.83
H/T^2 max	.0086	.0087	.025	.045	.058	.079	.11	.19
d = 36 cm								
L(m)	3.2	2.2	1.7	1.4	1.1	1.0	0.88	0.62
H_{max}(m)	.025	.032	.045	.067	.070	.072	.087	0.62
d/T^2	0.11	0.18	.29	.38	.51	.58	.66	1.0
H/T^2	.0079	.016	.036	.071	.099	.12	.16	.15
d = 50 cm								
L(m)	3.5	2.6	1.8	1.4	1.2	1.1	0.91	
H_{max}(m)	.048	.067	.098	.118	.116	.114	.096	
d/T^2	0.16	0.26	0.34	.53	.71	.80	.91	
H/T^2	0.015	.034	.078	.125	.164	.18	.18	

where the wave height, H, is evaluated at a distance not less than 3d from the wavemaker, $\frac{2\pi}{k_o}$ is the wave length, and e is the wavemaker stroke at the still water level. The above equation has been verified in laboratories and a good correlation has been shown to exist as shown in Figures 18 and 19. (Ursell et al 1960, Muggeridge and Murray 1981).

For a flap type wave generator, the wave height is given as

$$\frac{H}{e} = \frac{4 \sinh k_o d}{k_o d} \cdot \frac{k_o d \sinh k_o d - \cosh k_o d + 1}{\sinh 2 k_o d + 2 k_o d} \quad (33a)$$

The above equation has been tested experimentally by the Neyrpic engineers (Ursell et al 1961).

The tests done in the present research to evaluate the performance of the wavemaker were compared with the theoretical values of Ursell et al (1960) and shown in Fig. 20. Wave heights, H, were monitored in the tank at a number of locations between 2.5 m and 6 m from the mean position of the waveboard using the wave probe described earlier. The stroke, e, of the waveboard was measured by attaching a pen at an arbitrarily chosen point in the connecting rod; the stroke was measured as the longer axis of the ellipse formed by the moving pen. The wave length was determined using the relationship C = L/T. The speed, C, was determined by

measuring the time required for a wave to travel a distance of 3.5 m. The period, T, was determined by counting the number of waves passing a point during 30 seconds. The time was measured using a manually operated electronic stopwatch.

Measured values of H/e and $2\pi d/L$ for 0.36 m deep water over the range of $0.01 < H/L < 0.14$ and $0.1 < d/L < 0.5$ were compared with the theoretical values of Ursell et al (1960) as given by Equation 33a. The comparison is shown in Figure 20.

The experimental values are about 20% less than the theoretical estimates. The theoretical relationship developed by Ursell et al (1961) applies to wavemakers that are hinged at the bottom; it is most likely that the difference in the experimental values is due to the fact that the present wavemaker is hinged 4 cm above the bottom which is approximately 10% of the total height of the wavemaker. The correlation obtained is therefore considered acceptable.

4.1.3 Wavelength and Frequency Correlation

The computed wavelength, using linear or second order wave theory, can be shown (Shore Protection Manual, 1977) to be given by:

$$L = \frac{g T^2}{2\pi} \cdot \tanh\left(\frac{2\pi d}{L}\right) \qquad (34)$$

This relationship was also checked experimentally in the present facility. Figures 21, 22 and 23 show the

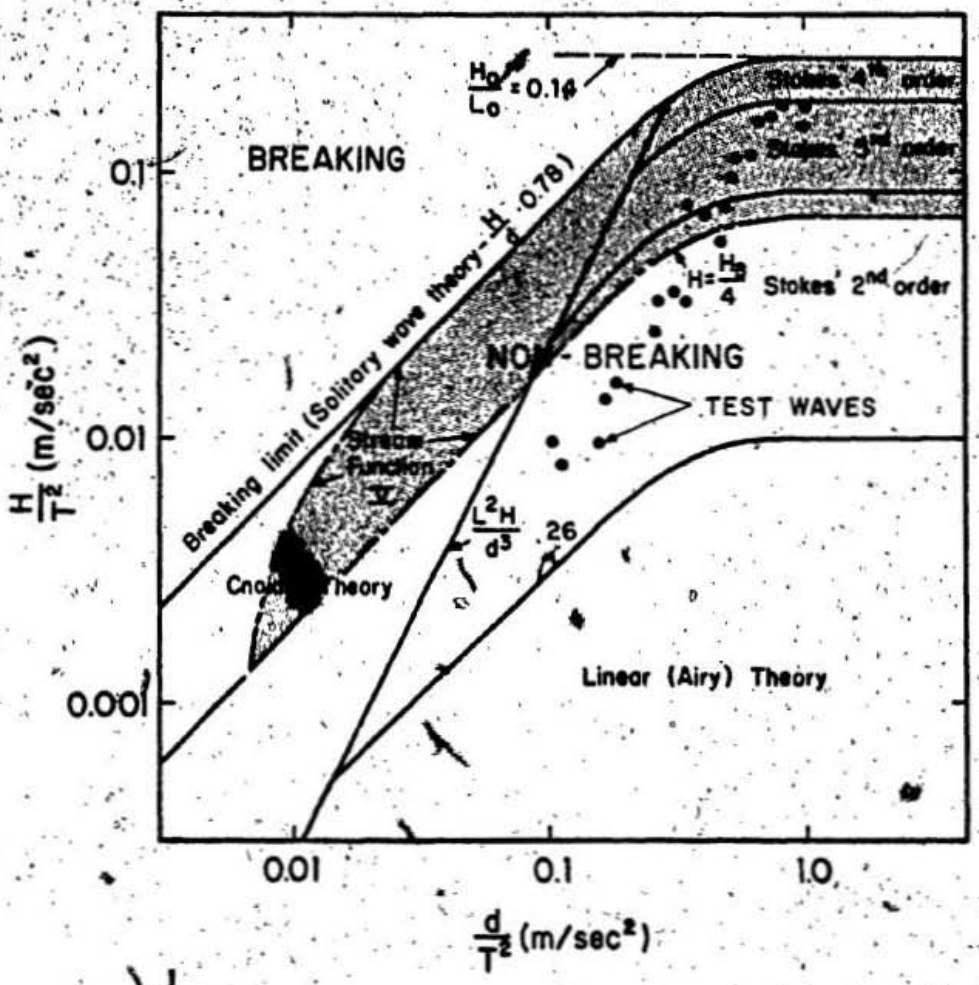


FIGURE 17 REGIONS OF VALIDITY FOR VARIOUS WAVE THEORIES (FROM U.S. SHORE PROTECTION MANUAL, 1977). • TYPICAL WAVES USED IN THIS RESEARCH

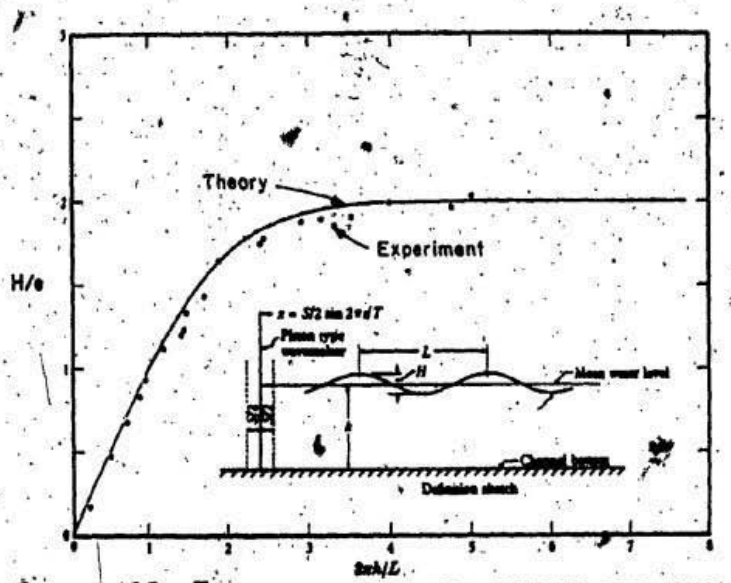


FIGURE 18 TEST OF WAVEMAKER THEORY FOR SMALL WAVE-STEEPNESS (FROM URSELL ET AL, 1960)

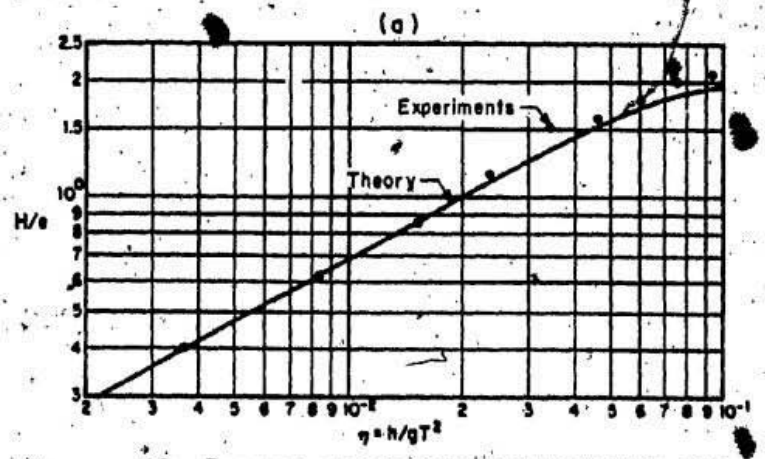


FIGURE 19 PISTON GENERATOR PERFORMANCE FOR REGULAR WAVES (FROM MUGGERIDGE AND MURRAY, 1981)

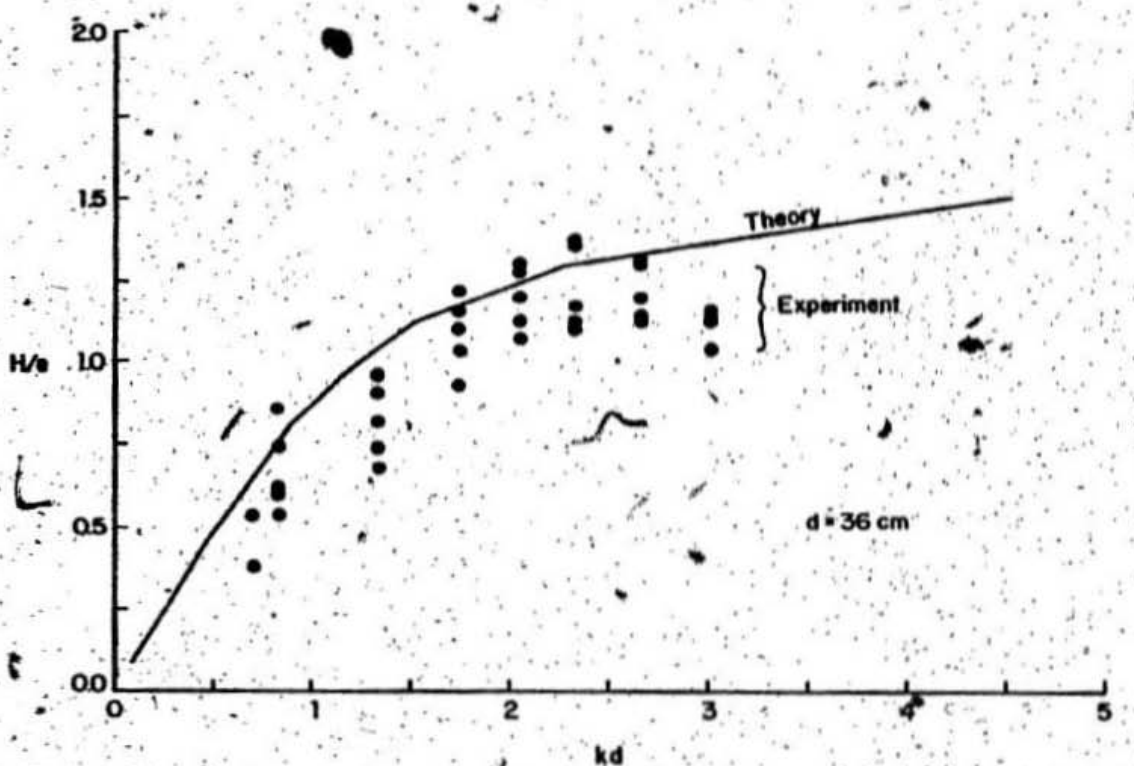


FIGURE 20 WAVE-MAKER PERFORMANCE

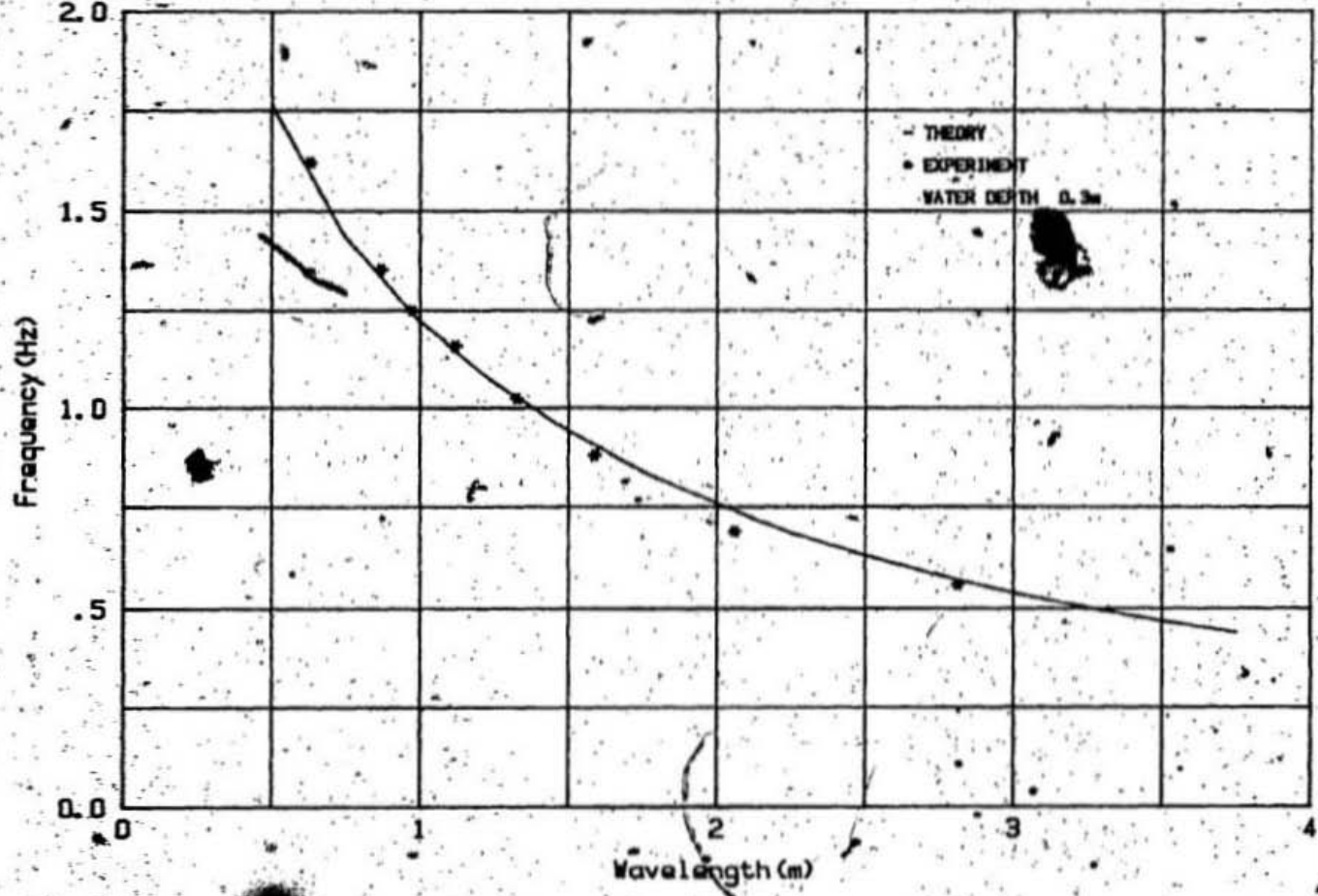


FIGURE 2 FREQUENCY VS WAVELENGTH (D = 300 MM)

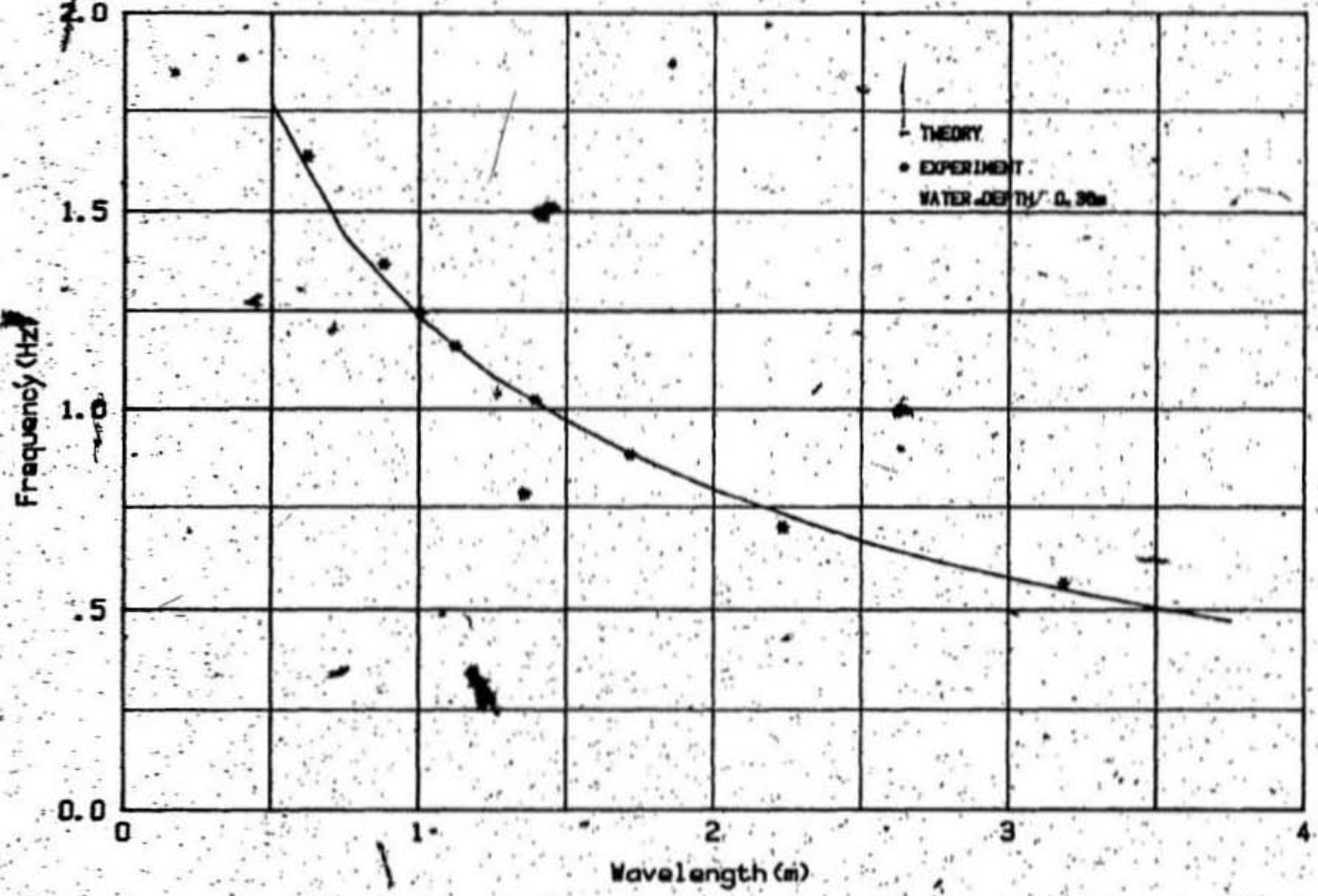


FIGURE 22 FREQUENCY VS WAVELENGTH (D = 360 MM)

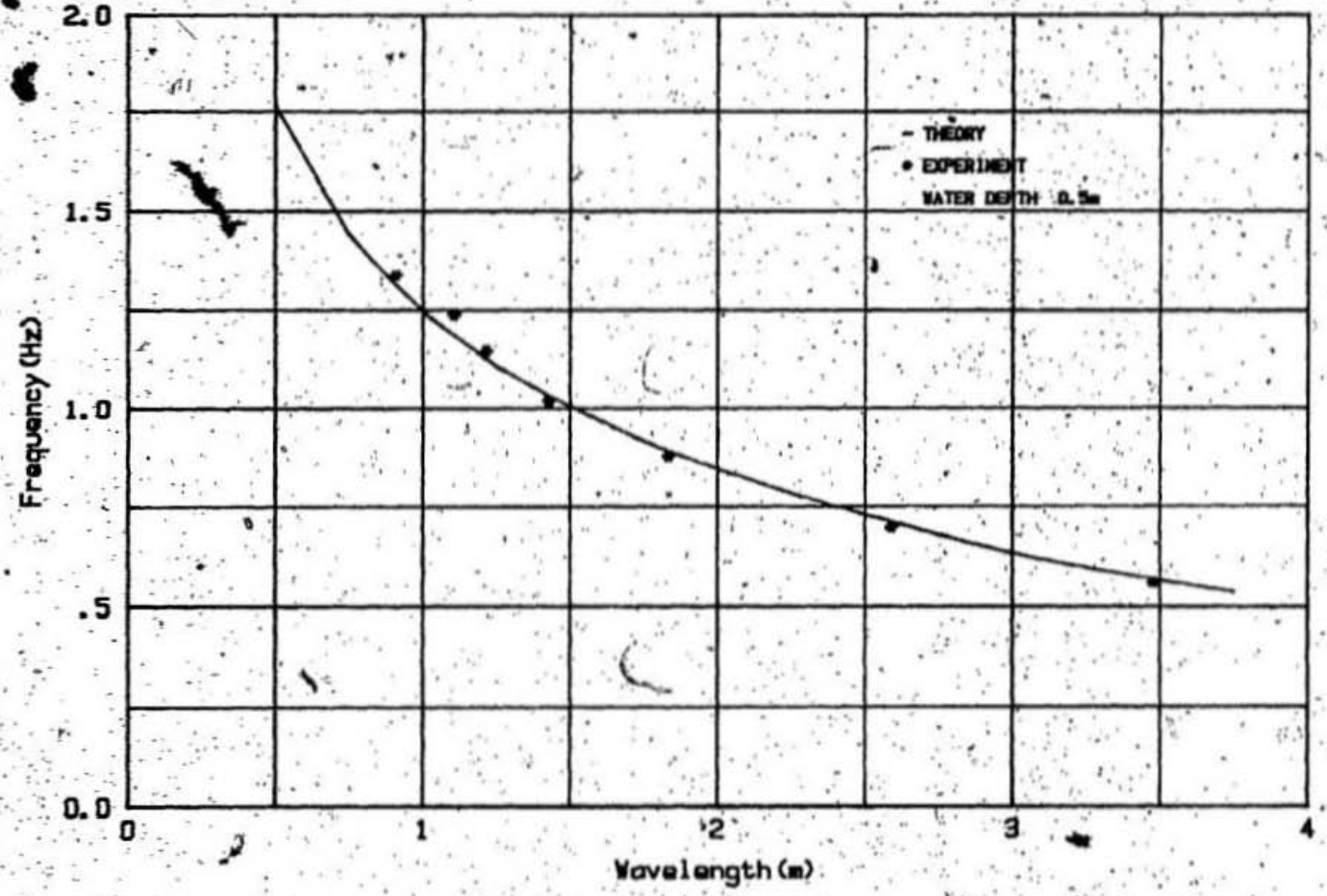


FIGURE 23 FREQUENCY VS WAVELENGTH (D = 500 MM)

theoretical wavelength-frequency relationship for water depths, d = 30 cm, 36 cm and 50 cm. The experimental values obtained are also plotted in the figure and a good correlation is observed.

4.1.4 Wave Form

Waves produced by the periodic motion of a flap type wave generator do not have the ideal constant form which might be expected from the regularity of the flap motion. As waves propagate they slowly change form in a periodic way, which depends on wave steepness, H/L, and relative water depth, d/L. (Hansen and Svendsen, 1974).

Figure 24 from Hansen & Svendsen (1974) shows, in an extreme case, the time variation of the surface elevation at different points along a wave flume. This pattern is typical for most laboratory wave tanks and is present because a rigid flap cannot exactly produce the variation of the particle motion which corresponds to a progressive wave of constant form.

A qualitative explanation of this motion is that a smaller wave is travelling down the flume, superimposed on the main wave, but with a somewhat smaller speed. This wave is denoted as a "free second harmonic wave" as shown in Figure 25.

The wave pattern not only shows itself as a disturbed wave profile but also exhibits an apparent

variation in mean water level from place to place along the tank. The upper and lower wave envelopes meander along the length of the tank as shown in Figure 26. The amplitude of the meander will equal the amplitude of the free second harmonic wave. The maxima and minima for the envelopes appear at fixed points down the wave flume, the position of which depends only on the main wave and the free second harmonic wave at the generator (Hansen and Svendsen, 1974).

Figure 27 shows typical surface displacements obtained in the present research for frequencies ranging from 0.56 Hz to 1.35 Hz. The measurements were made at a fixed position in the tank over a period of time. The 0.56 Hz wave has a form that is similar to that described by Hansen and Svendsen (1974).

Figure 28 shows a compressed plot of wave heights as the wave probe was moved about .1 cm per sec. along the length of the tank. The meandering effect demonstrated is very similar to that described by Hansen and Svendson (1974).

The physical manifestation of this phenomenon is in some way similar to, but should not be confused with reflection, which will be discussed later.

An additional limitation in producing a gravity wave in the shape of a pure sine, is the non sinusoidal motion of the wave maker. When the length of the connecting

rod is more than 10 times the wave board displacement, the second harmonic should be less than 5% of the fundamental harmonic (Keating and Webber, 1977). For the present equipment, the connecting rod is about 10 times the maximum board displacement at the average still-water level.

In general, the form of the waves generated appear to have the same characteristic anomalies that have been reported by other researchers. Even though these anomalies have been demonstrated to be similar to those reported by others it is important to recognize that these phenomena can have significant effects on tests performed in the tank. For certain tests it may be desirable to eliminate or at least reduce these effects.

4.1.5 Beating

A phenomenon called "beating" has been described by Flügge (1962). When the difference between the frequencies of two component vibrations of harmonic form is small, the resultant vibration takes a form that is called "beating" as shown in Figure 29 (Flügge 1962). If there are two generating mechanisms that oscillate at slightly different frequencies, then the expected result is that at any given location along the length of the tank, the two waves add together so that the wave envelope is not constant with time.

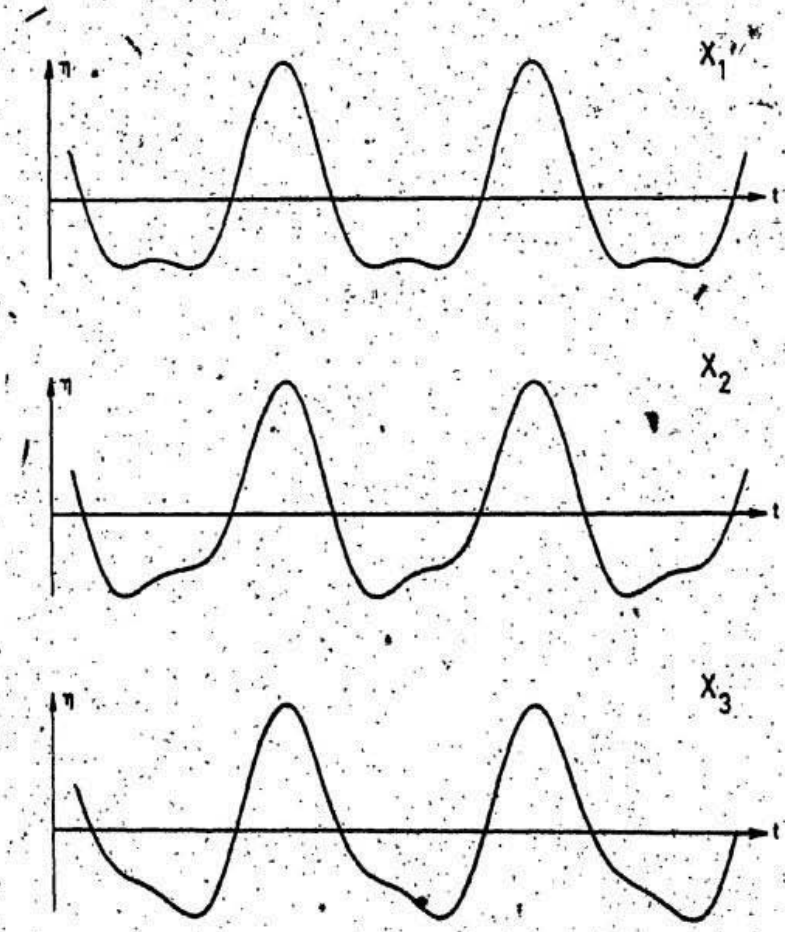


FIGURE 24 WAVE PROFILE AT DIFFERENT STATIONS IN A WAVE FLUME (FROM HANSEN AND SVENDSEN, 1974)

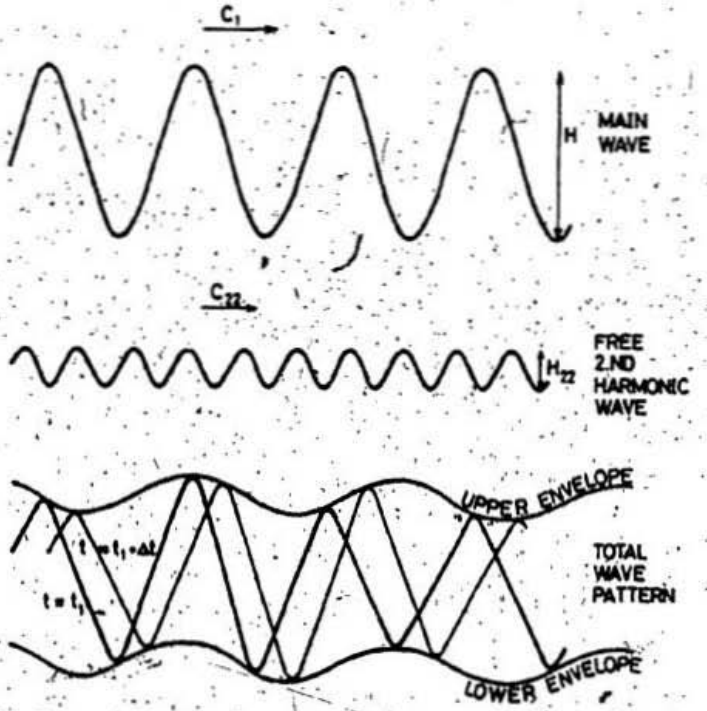


FIGURE 25 SUPERPOSITION OF SECOND ORDER STOKES MAIN WAVE AND FREE SECOND HARMONIC WAVE (FROM HANSEN AND SVENDSON, 1974)

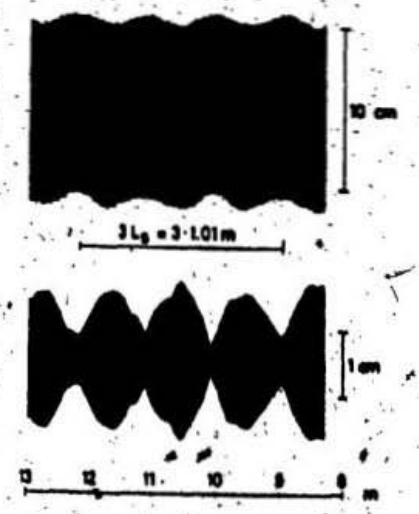


FIGURE 26 RECORD OF TOTAL WAVE MOTION AND TOTAL SECOND HARMONIC MOTION (FROM HANSEN AND SVENDSON, 1974)

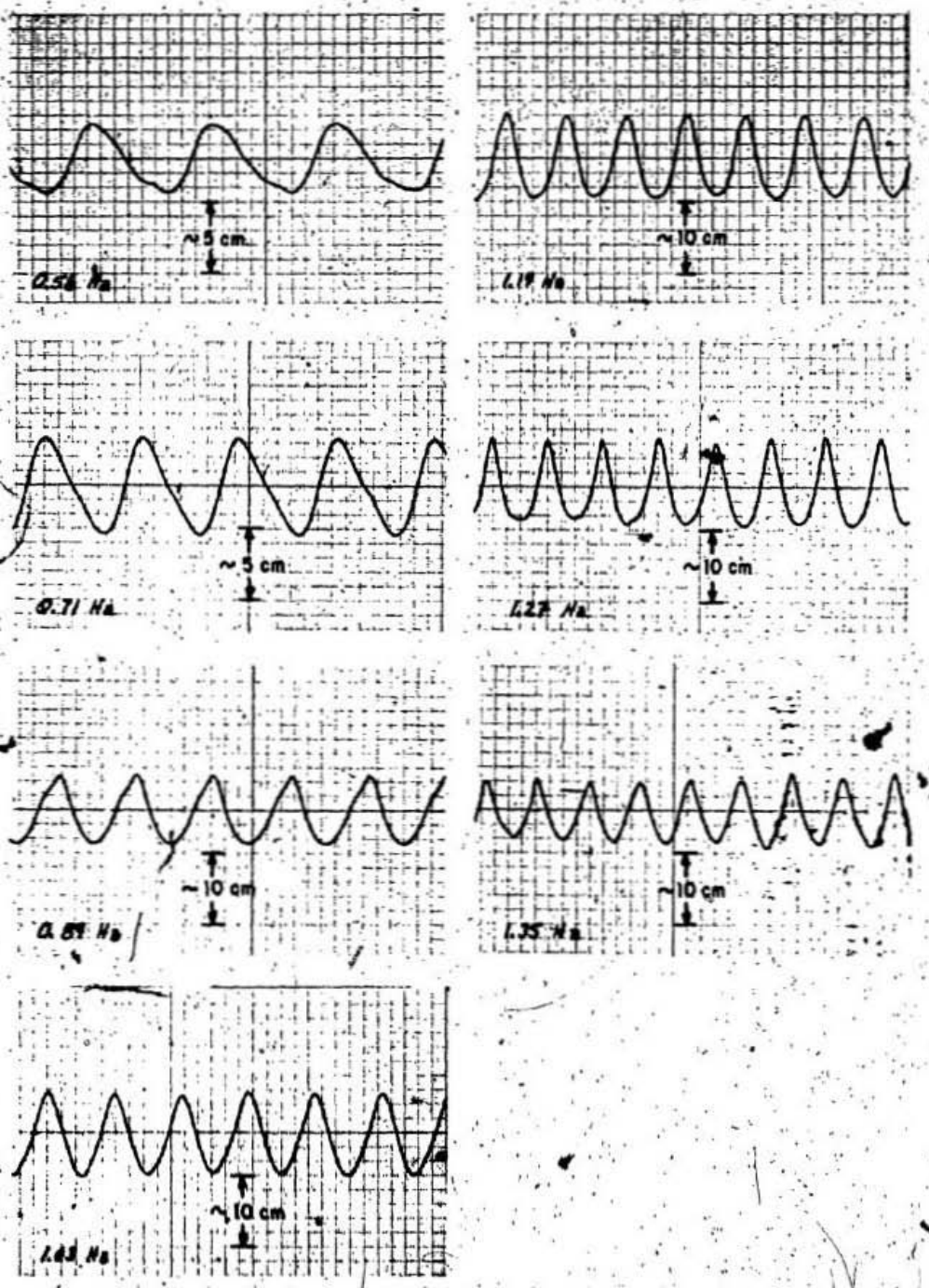


FIGURE 27 TYPICAL SURFACE WAVES IN THE WAVE-SOIL TANK

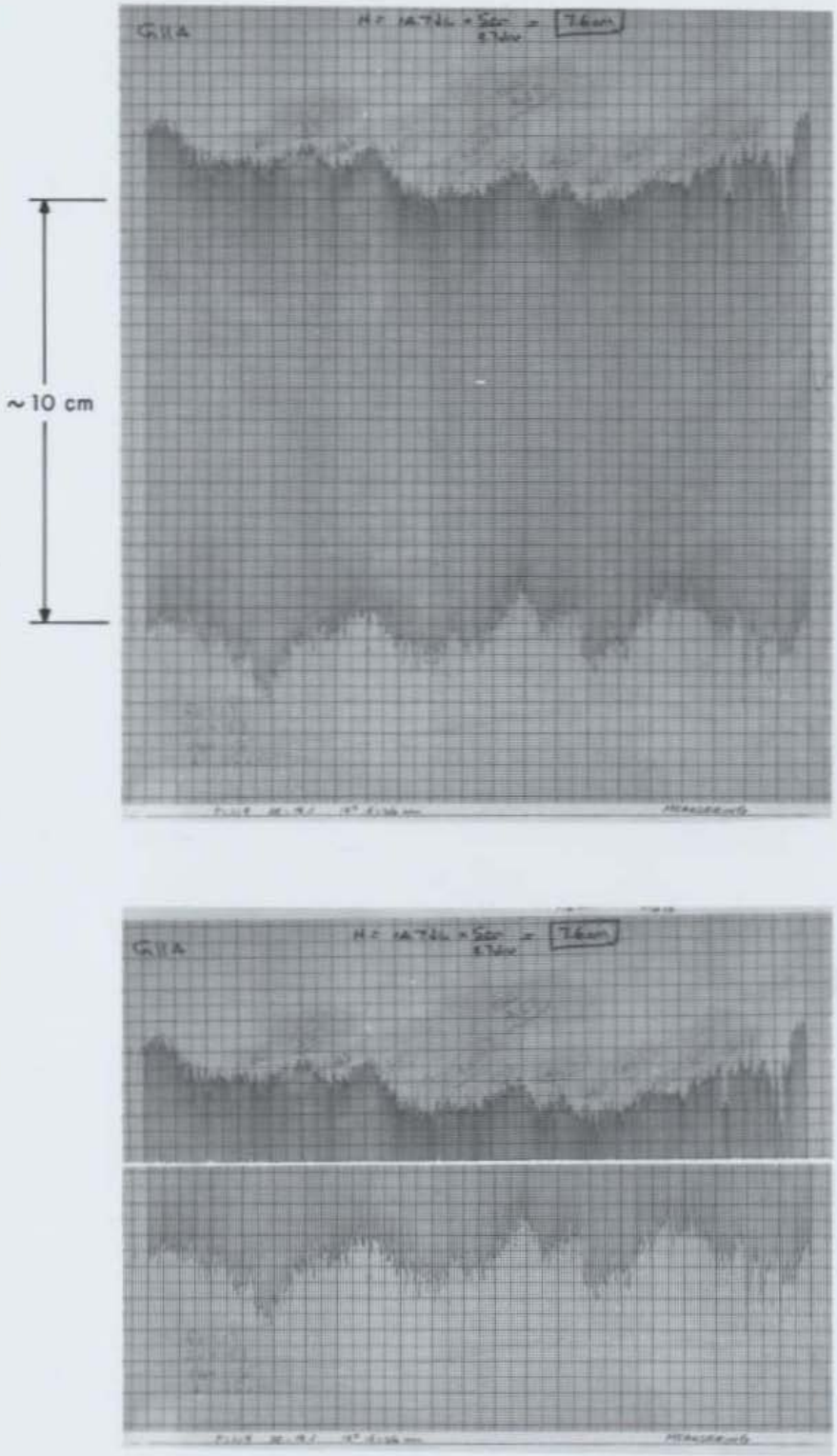


FIGURE 28 A TYPICAL RECORD OF MEANDERING

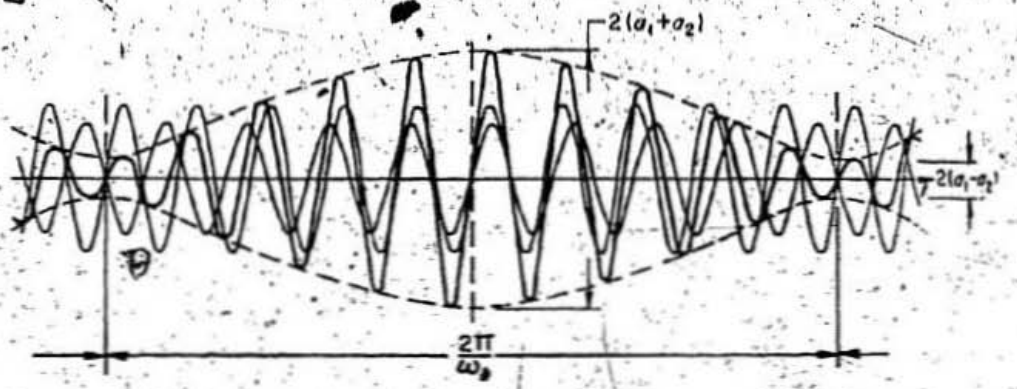


FIGURE 29 AN EXAMPLE OF BEATING (FROM FLÜGGE, 1962)

This beating was observed during the calibration of this tank and when present, it is very difficult to measure the effects of wave reflection and meandering because the wave heights are not constant over time. The phenomenon of beating was observed when the following deficiencies occurred:

1. The beach was loose and moved excessively.
2. Tank movement was excessive.
3. The water level behind beach was free to oscillate with wave action.

While the term beating has not been found in the published literature to describe a wave tank phenomenon, under some conditions this phenomenon can occur in wave tanks as demonstrated in this work.

Examples of beating which were observed in this are shown in Figures 30, 31, 32, 33, 34. The periods of such beats were approximately 8 seconds or 16 seconds. In some of the preliminary tests which were not recorded, beating with periods in the order of 60 seconds was observed.

In any research of this type, if waves with predetermined characteristics are required, preliminary calibration tests should be done to verify this beating phenomenon, identify the potential causes and if necessary to minimize the effects through appropriate remedial measures.

1.6 Buildup and Decay Time

Figure 35 shows a typical plot of surface displacements at a station in the test section as the wavemaker is started, run, and turned off. It may be seen that the buildup time to steady state is very short, in the order of a few seconds.

For some wave frequencies, at the beginning soon after the wavemaker is turned on, waves higher than the steady state heights were obtained. This has some consequence in the study of the wave effects on soil as the higher waves set up pore water pressure in the soil which may be different from the steady state pressures. Although for the tests done in this research the above anomaly was not a major problem, the implications of this will be discussed in a subsequent section.

Also, when the wave generator is turned off a large wave always appears. This can be attributed to the slowing down of the wave board. As the wavemaker motor slows down to a stop, the period of the final wave becomes larger. Since wave speed $C = L/T$, and L is proportional to T^2, an increase in period, T, causes an increase in wave speed, C. The longer period wave travels faster than the steady state waves, and actually catches up; the energies are added resulting in a higher wave height. There was a clear demonstration of the importance of this effect during soil

testing; a soil may not fail under steady state waves but would fail as the large wave passed over the test section after the generator was turned off. The increase in porewater pressure due to these large waves is also very noticeable and will be discussed later.

The natural decay of the waves is also shown in Figure 35 and a resonance frequency of about 0.1 Hz may be observed. In order to verify this resonance phenomenon further, under still water conditions, one end of the tank was quickly lowered and the water elevation variation with time at the end of the tank was monitored. The period of the resulting oscillations was 8.0 seconds. Approximate multiples of 8 seconds (8, 9, 15, 16, 80 seconds) were noticed in the beating phenomenon described earlier. The resonance frequency for the system is thus estimated as 0.125 Hz.

4.1.7 Maximum Wave Heights

Figure 36 shows the maximum possible wave heights for the given water depths, using the maximum wavemaker stroke. The maximum wave height is limited by two different criteria; one is the maximum stroke of the wavemaker and the other is the phenomenon of wave breaking. Waves break when $H/L > 0.14$ or when $d/H < 1.25$.

The wave generator can generate waves of maximum height of 0.12 m at a corresponding wavelength of 1.3 m with a water depth of 0.5 m.

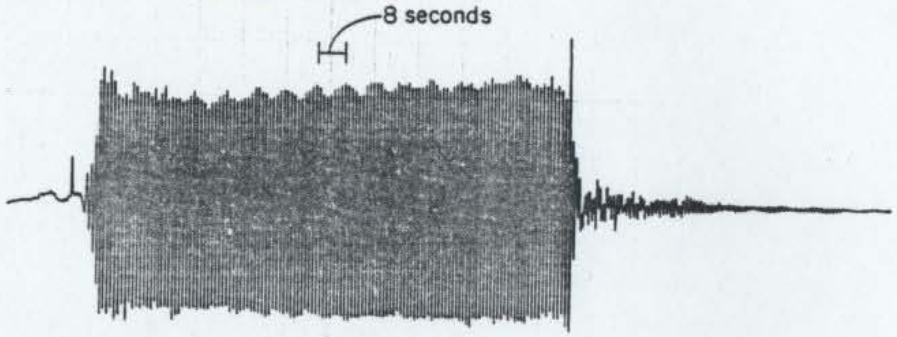


FIGURE 30 AN EXAMPLE OF BEATING. PERIOD IS 8 SECONDS FOR 1 HZ WAVES

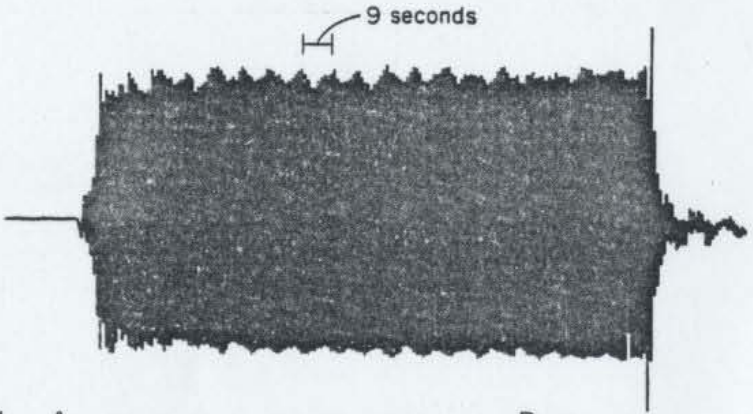


FIGURE 31 AN EXAMPLE OF BEATING. PERIOD IS 9 SECONDS FOR 1.19 HZ WAVES

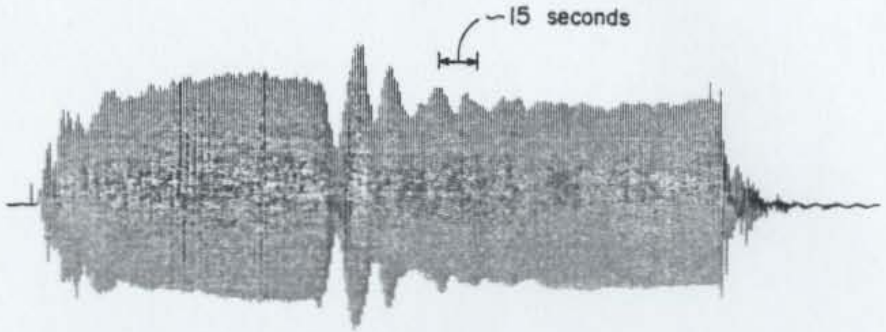


FIGURE 32 AN EXAMPLE OF BEATING. PERIOD IS 15 SECONDS FOR 1.03 HZ WAVES

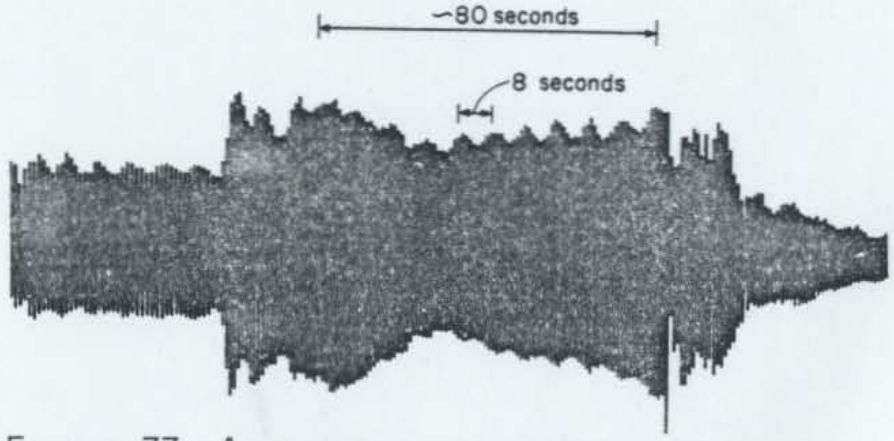


FIGURE 33 AN EXAMPLE OF BEATING WITH PERIODS OF 8 SECONDS AND APPROXIMATELY 80 SECONDS FOR 1.03 HZ WAVES

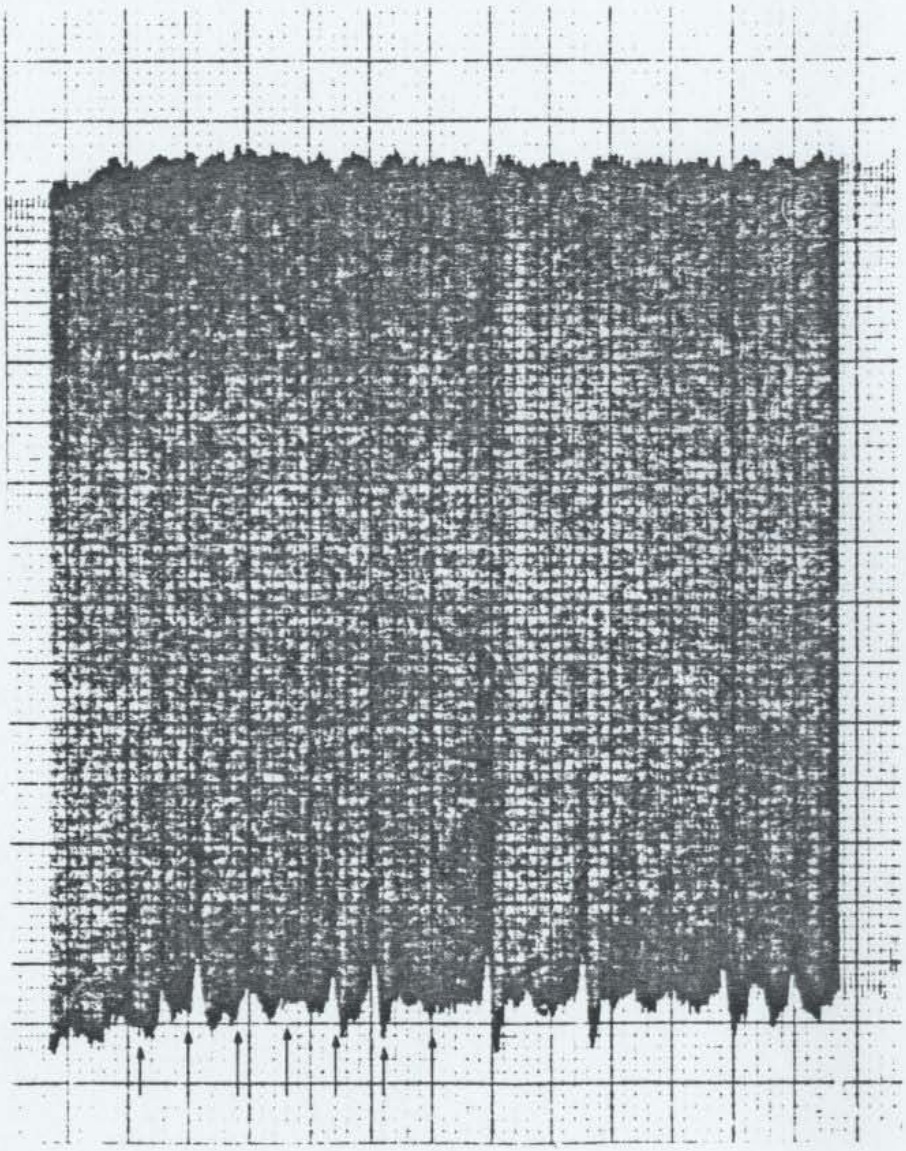


FIGURE 34 AN EXAMPLE OF BEATING. APPROXIMATE PERIOD OF BEATS IS 16 SECONDS

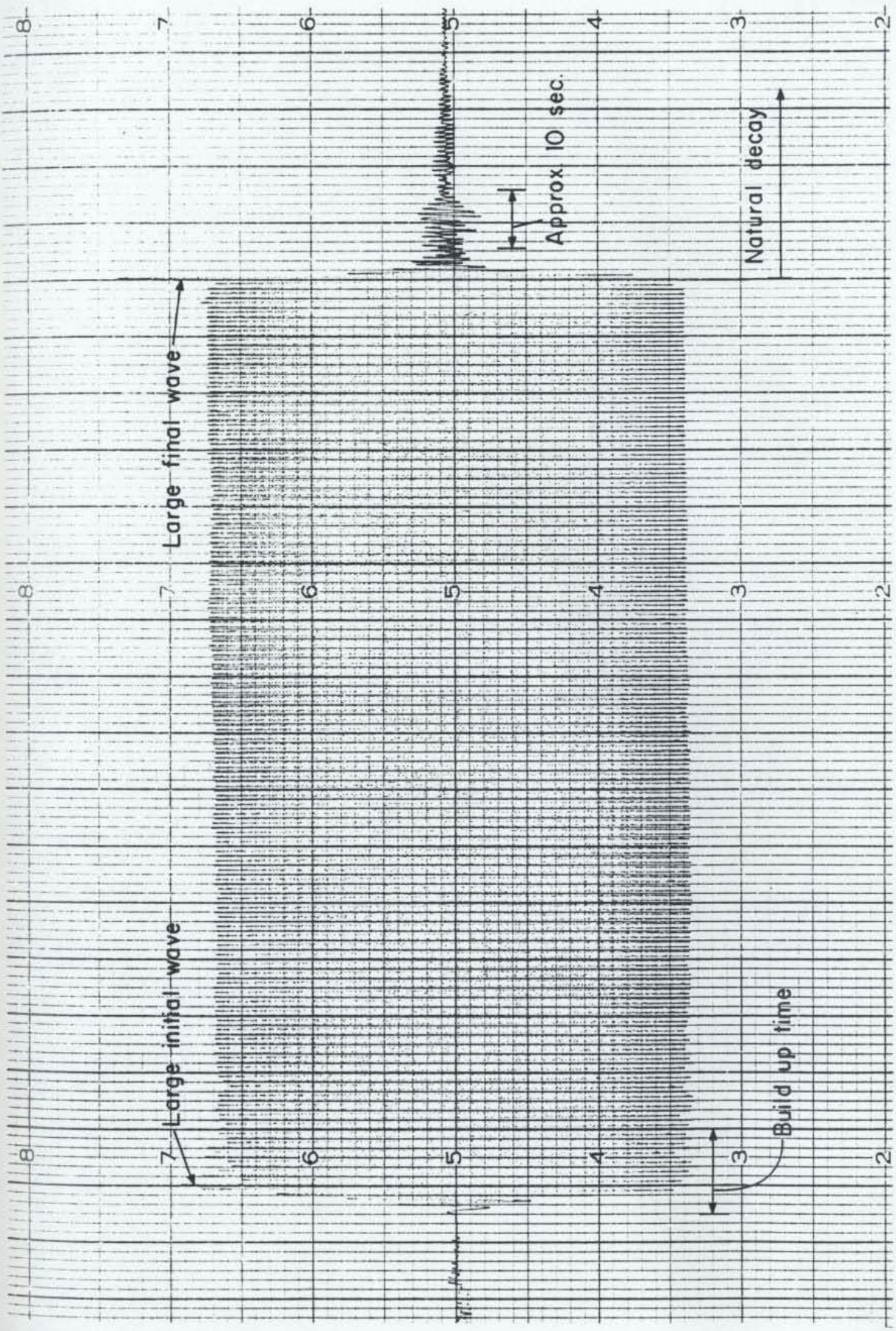


FIGURE 35 TYPICAL WAVE RECORD

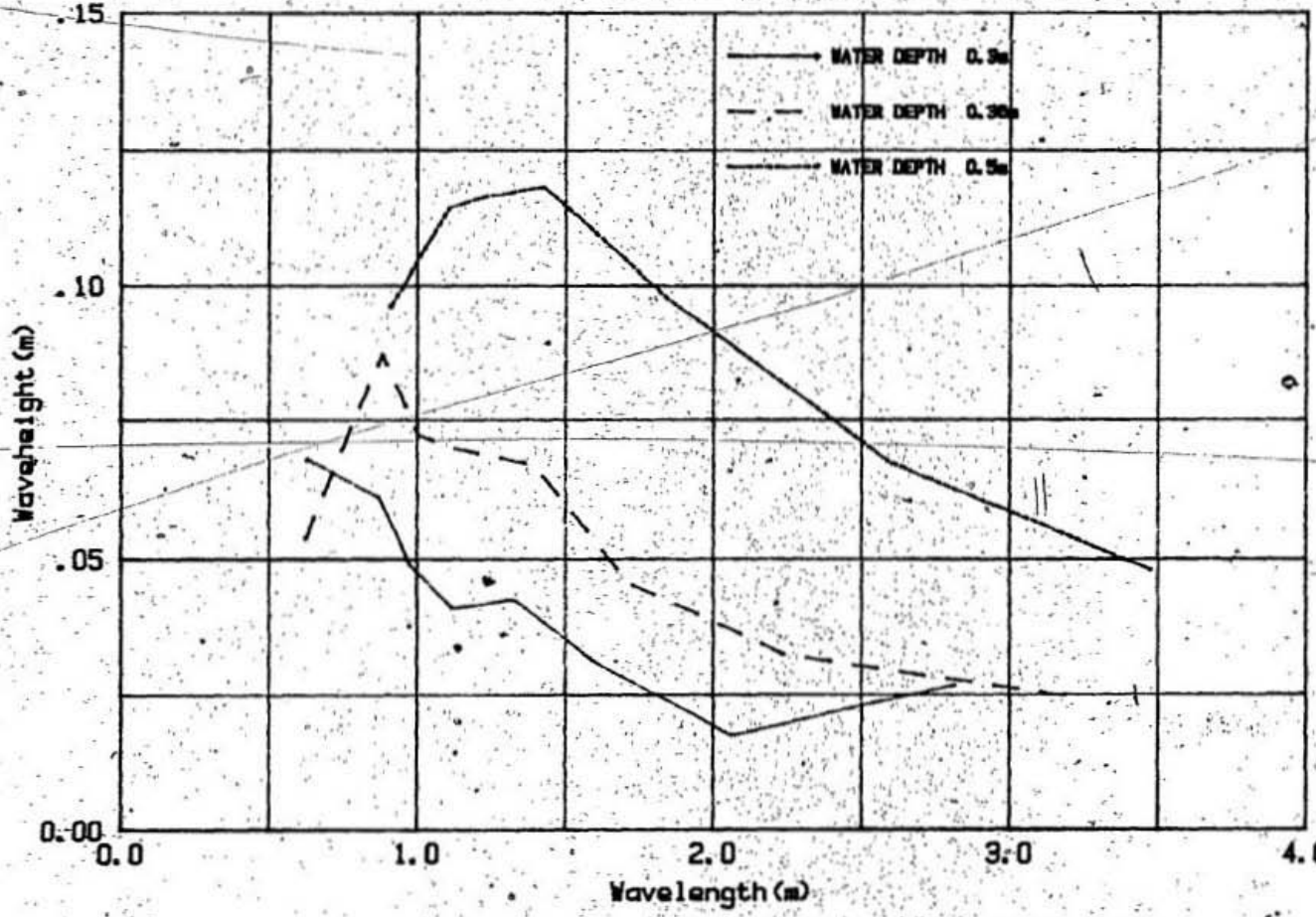


FIGURE 36 PERFORMANCE ENVELOPE OF THE WAVE GENERATOR

The height of the short waves of Figure 36 were limited by breaking; the height of the longer waves were limited by the maximum wave board stroke.

4.1.8 Reflection

As a wave board is forced to oscillate, a progressive primary incident wave, is created which travels from the wave board to the beach at the opposite end of the tank. At the beach end of the tank, only part of the wave energy is absorbed, and the rest is reflected. This reflected wave is then the primary reflected wave. The amplitude of the reflected wave depends on the characteristics of the surface on which the primary wave impacts and generally the amplitude of the primary reflected wave will be small for a well designed beach. In the extreme case when the reflecting surface is vertical, impermeable and smooth, the amplitude of the reflected wave can be nearly as much as that of the incident wave.

When the reflected wave reaches the wavemaker it reflects as a secondary incident wave; thus a series of multiple order incident and reflected waves are created. The reflected waves progressively attain smaller amplitudes and a steady state is attained after a certain time interval depending on the length of the tank. If the primary reflection is 10% or less, the secondary reflected wave is less than about 1% of the primary incident wave and is generally negligible (Ursell 1960).

In any series of experiments involving porewater pressure in soil, it is desireable to simulate a condition where the wave heights not only have reached steady state but are uniform along the length of the tank. If the reflection is significant then the wave height can vary substantially along the tank. For example with 25% reflection, the ratio of the minimum wave height to the maximum wave height, H_{min}/H_{max}, measured L/4 apart will be 0.6. It is therefore necessary to determine the extraneous effects of the reflection phenomenon on the waves used for testing.

The reflection coefficient C_R is defined as the ratio of the reflected wave height, HR, to the incident wave height HI. This can be shown to be given by:

$$C_R = \frac{H_{max} - H_{min}}{H_{max} + H_{min}} \qquad (35)$$

where H_{max} and H_{min} are the resultant heights of the incident wave HI and the reflected wave HR, as shown in Figure 37. Physically in a wave tank H_{max} and H_{min} are separated by a distance of L/4.

There are different methods of calculating C_R. In the conventional method it is assumed that the waves are sinusoidal and the evaluation of the reflection coefficient is based on direct measurements of H_{max} and H_{min}. A small error may be introduced in this method because of the assumption of a sinusoidal wave profile (Hamill 1963). Goda

and Suzuki (1976) have proposed a two point method for calculating C_R by analyzing the fourier components of the amplitude by the fast fourier transform technique.

The direct method was used for this research, in which H_{max} and H_{min} were measured by travelling the wave probe along the length of the test portion of the tank. For wavelengths less than 1 m, readings were taken at stations spaced 0.05 m since the distance between H_{max} and H_{min} would be less than 0.25 m. Up to 10 waves were sampled at each station and averaged to give the wave amplitude. For wavelengths greater than 1 m, the readings were taken 0.1 m apart. In some cases continuous records were made by travelling the probe along the length of the test section at a speed of about 1 mm/s.

A typical record is shown in Figure 38. Some experience and judgement is necessary in using such a record. A steady state must be reached before the records are of any value and only the maxima and minima that are approximately L/4 apart may be used. It is also necessary to use caution near the beach end of the tank so that other extraneous effects are not misinterpreted as reflection. In this example, it may be seen that the wave heights at stations 4, 10, 16 and 22 are 6.9 units, 11.5 units, 6.7 units and 11.5 units respectively. These maxima and minima gave reflection coefficients of 25%, 26.3% and 26.3% which was then averaged as 25.9% for the test.

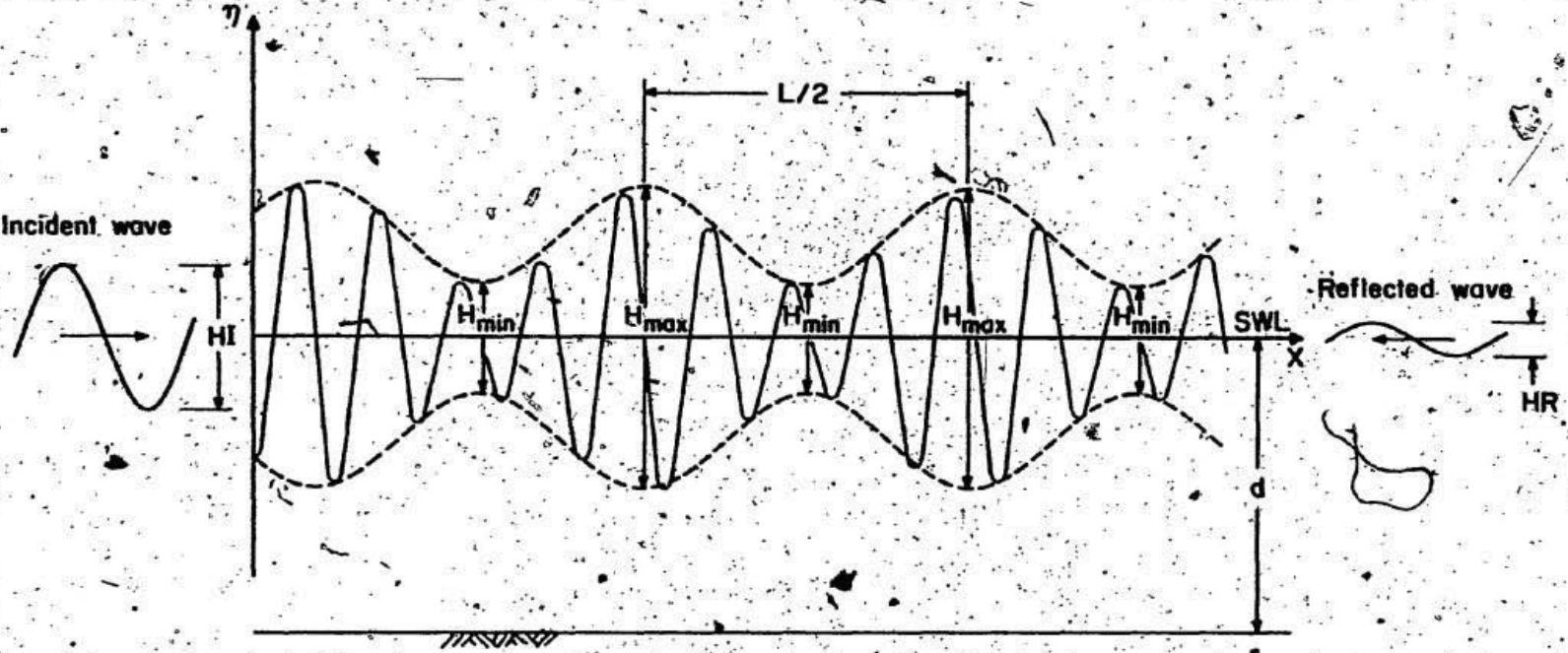


FIGURE 37 CHANGE IN WAVE HEIGHT ALONG THE TANK DUE TO THE SUMMATION OF INCIDENT AND REFLECTED WAVES

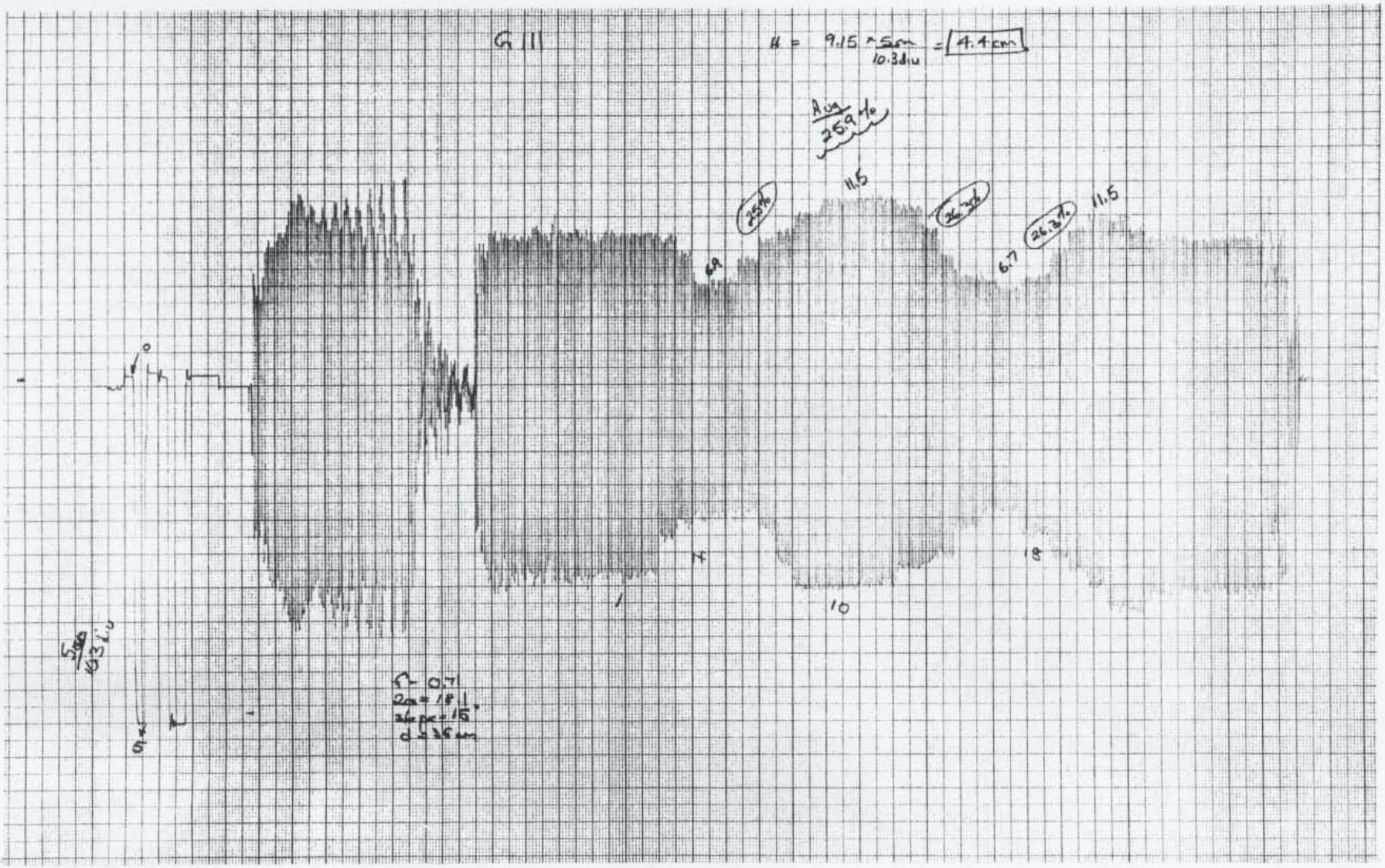


FIGURE 38 A TYPICAL EXAMPLE SHOWING THE CALCULATION OF THE REFLECTION COEFFICIENT

Five wave absorbers were assembled and tested over a range of wave periods, water depths and wave heights. The beach types were briefly discussed in the previous chapter (Figures 9 and 10) and are listed below:

Beach #1 - Wedge of Resilitex (horsehair).

Beach #2 - Rigid parabolic beach with wooden strips and runner.

Beach #3 - Rigid parabolic beach with wooden strips but no runner.

Beach #4 - Smooth parabolic beach with runner.

Beach #5 - Smooth parabolic beach with runner. Curved section covered with 2 cm thick Resilitex.

Beach #1 produced very low coefficients of reflection in the order of 3-10% for most frequencies tested. However, for some frequencies the beating condition as described above was excessive and unacceptable.

Similarly Beach #3 gave acceptable reflection coefficients as seen in Table 3 but again the beating was excessive and considered unacceptable.

The reflection coefficients of Beaches 2, 4, 5 are shown in Figures 39 and 40 for two different inclinations of the beach.

For frequencies of less than about 1.1 Hz the parabolic beach with 2 cm Resilitex covering has

TABLE 3
REFLECTION COEFFICIENTS FOR DIFFERENT BEACH TYPES AND SLOPE ANGLES

Wave-board displacement, 2e = 8 cm Water depth, d = 36 cm

Run No.	Beach Slope	Board frequency (Hz)	Reflection Coefficient CR (%)	Avg CR	HI (cm)
G101	6°	0.71	9.0,11.8,13.2,13.2,9.1	11.3	3.5
G102	6°	0.89	9.5,3.6,3.6,4.5,4.5,5, 5,5.9,8.6,9.4	6.0	4.4
G103	6°	1.03	10.7,9.4,11.0,15.8,8.1 6.8	10,3	6.25
G104	6°	1.19	5.4,5.7,9.7,5.3,7.9	6.8	7.4
G105	6°	1.27	9.2,8.9,7.5,9.8,7.0	8.5	8.2
G106	12°	0.71	23.2,23.2,24.7	23.7	3.9
G107	12°	0.89	9.6,10.6,13.8,13.8	12	4.6
G108	12°	1.03	13.2,12.8,11.5,7.7, 11.7,11.7	11.4	6.9
G109	12°	1.19	8.5,8.5,3.7,6.8,8.4	7.2	7.9
G110	12°	1.27	7.4,6.4,8.9,4.3,9.8	7.4	8.5
G111	15°	0.71	25,26.3,26.3	25.9	4.4
G112	15°	0.89	16,15.1,18.4,19.3	17.2	4.5
G113	15°	1.03	13.2,15.4,15.4,12.8	14.2	6.6
G114	15°	1.19	6.5,1.2,5.6,4.6,4.3, 5.3	4.6	7.6
G115	15°	1.27	10.4,9.1,9.1,3.5,8.1, 7.7,8,8	8.1	8.1
G116	12°	0.71	5.8,5.2,4.4	5.1	3.5
G117	12°	0.89	9.1,8.8,8,6.5	8.1	5.4
G118	12°	1.03	7.5,6.4,3.3,4.7	5.5	7.0
G119	12°	1.19	9.5,7.1,8.2	8.3	7.6
G120	12°	1.27	9.5,7.8,9.2	8.8	8.2

For Test G101 to Test G115, Beach #4 was used.
For Test G116 to Test G125, Beach #5 was used.

TABLE 3 (continued)
REFLECTION COEFFICIENTS FOR DIFFERENT BEACH TYPES AND SLOPE ANGLES

Wave-board displacement, 2e = 8 cm

Run No.	Beach Slope	Board frequency (Hz)	Reflection Coefficient CR (%)	Avg CR (%)	HI (cm)
G121	15°	0.89	9,9,7.5	8.5	5.4
G122	15°	0.71	6.9,6.9,7.7	7.2	3.3
G123	15°	1.03	10.6,9.2,8.3,9.4,8.5, 8.2	9	6.4
G124	15°	1.19	1.8,0.3,5.4,0.7,5.6, 6.9,4.1	4.8	7.7
G125	15°	1.27	7.1,5.4,8.8,7,8.4	7.3	8.1
G126	~8°	0.71	10.5,10.5,10.5	10.5	3.9
G127	~8°	0.89	12.4,12.4,13.2,11.9	12.5	4.8
G128	~8°	1.03	5.9,10.3,9.7,9.7,9.2	9	6.4
G129	~8°	1.19	8.6,3.6,7,7.1,7.1,4.6	6.2	7.7
G130	~8°	1.27	3.2,3.2,5.3,3.4,5.6	4.14	8
G131	12°	0.71	13.6,14.5,13.4	13.8	4.1
G132	12°	0.89	15.5,15.2,14.8,14.5, 16.2	15.2	4.7
G133	12°	1.03	10.5,13.4,14.3,9.3, 12.7,11.1	11.9	6.8
G134	12°	1.19	8.4,5.5,10,12.4,13.5 10.6,10	10.1	7.2
G135	12°	1.27	7.3,6.1,6.1,6.2,6.4, 6.4,6.8	6.2	8
G136	15°	0.71	22.4,22,22.2	22.2	4.8
G137	15°	0.89	21,19.8,17.6,19.1	19.4	4.4
G138	15°	1.03	11.7,11.1,17.6,17.6	14.5	6.4
G139	15°	1.19	7.4,7,9.2,7.3,11.1, 10.3,9.3	8.8	7.6
G140	15°	1.27	6.9,6.2,9.1,8.7,6.9 7.8	7.8	8.3

For Test G126 to Test G140, Beach #2 was used.

TABLE 3 (continued)
REFLECTION COEFFICIENTS FOR DIFFERENT BEACH TYPES AND SLOPE ANGLES

Wave-board displacement, 2e = 8 cm

Run No.	Beach Slope	Board frequency (Hz)	Reflection Coefficient CR (%)	Avg CR
X101	12°	.89		
X102	12°	.71	15.2, 16.9, 16.5	16.2
X103	12°	1.03	13.6, 11.6, 6.7	10.6
X104	12°	1.19		
X105	12°	1.27	3.0, 2.0	2.5

For Test X101 to Test X105, Beach #3 was used. Beating was excessive so that data for some frequencies were not obtained.

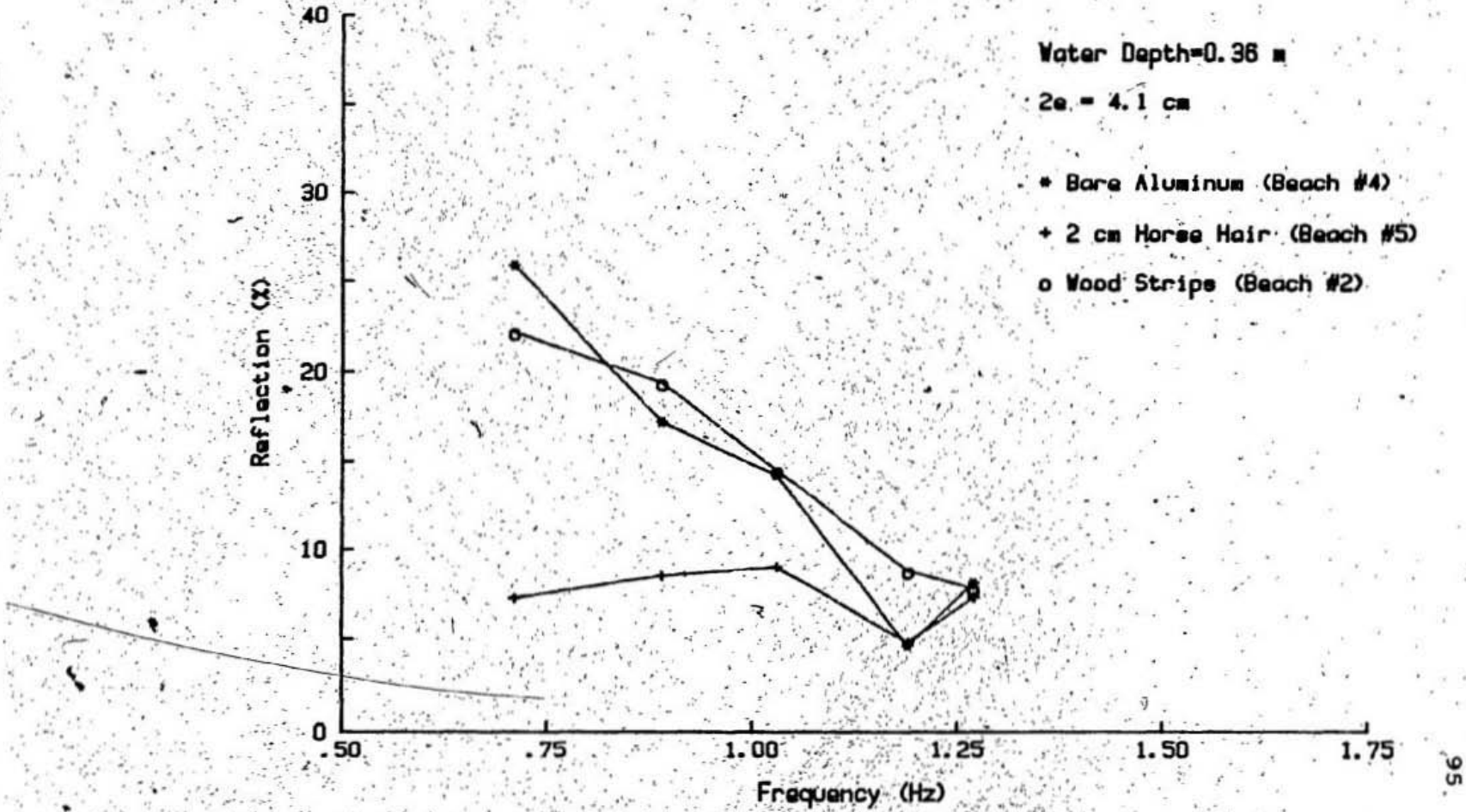


FIGURE 39 PARABOLIC BEACH PERFORMANCE (15 Deg)

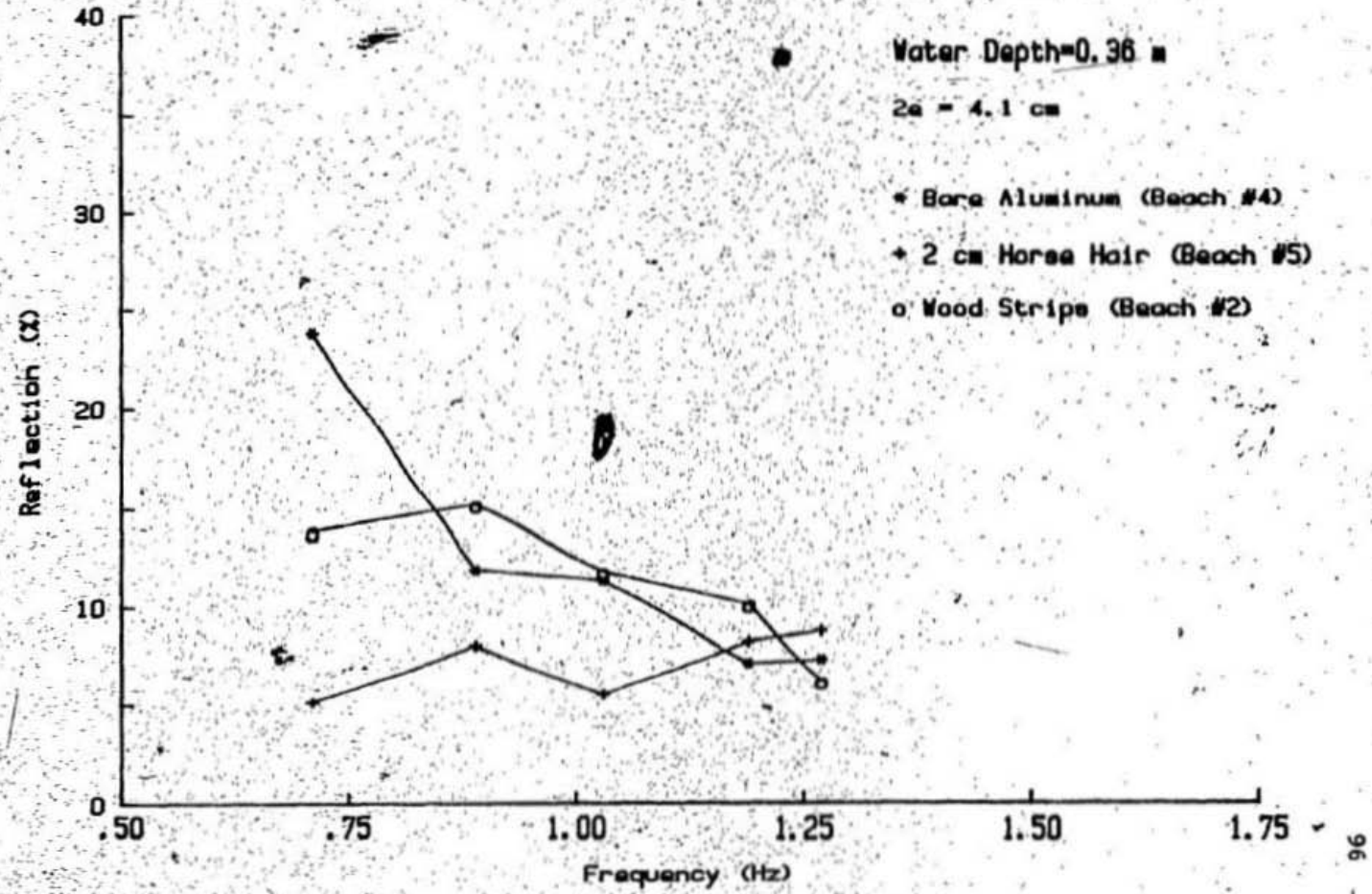


FIGURE 40 PARABOLIC BEACH PERFORMANCE (12 Deg)

significantly lower reflection coefficients than the other two. For frequencies above about 1.1 Hz the bare aluminum beach gave a better performance.

In comparing the beach performance, the length of the wet arc of the parabola was kept constant for all the tests. The inclination of the tangent to the parabola at the waterline was designated as the beach angle. Figure 41 summarizes the effect of the beach slope on its efficiency. This effect of the beach inclination is pronounced for frequencies less than about 1 Hz.

For the tests with the soil in place, the smooth aluminum parabolic beach with a runner was finally selected. To minimize reflection, the beach angle was tuned to suit the wave characteristics used.

The performance of the wave generator, the generation of nearly steady state waves and the minimization of reflection are aspects which are as important as the main tests on wave-soil interaction. A substantial proportion of this research was devoted to evaluating the above aspects in order to generate waves that were repeatable.

4.2 Influence of Waves on a Bed of Fine Sand

After the calibration of the wave tank to assess the capability of producing repeatable waves, the false bottom was removed and the test portion of the tank was

filled with white silica sand. The properties of the sand were discussed in Chapter III. The dry sand was weighed and the total quantity placed in the tank was recorded for cross checking with insitu density measurements.

The wave-soil interaction experiments were conducted after preparing the sand bed as described in Chapter III. Surface waves with various characteristics were passed over the soil with a view to examine the following phenomena:

1. Cyclic pressure changes at the mudline due to the effect of surface waves.
2. Variation of pore water pressure inside the soil due to the cyclic pressure change at the mudline. This included the examination of potential quick sand conditions and response to shock effects. These observations were subsquently used for determining liquefaction or soil failure condition. Porewater pressure variation was examined for both horizontal and sloping sand beds.
3. Densification due to waves.

A video record of the visible effects of waves on the soil was also made as part of Memorial University's ETV program "Experiment" for public telecasting.

4.2.1 Wave Pressure at the Mudline

Figure 42 shows a typical surface wave generated in the tank and the corresponding pressure developed at the mudline. It is obvious from the figure that the water depth is less than L/2 and consequently a measurable cyclic pressure is developed at the mudline. This is consistent with the pressure variation that has been conventionally assumed for the analysis of seabed stability (Henkel, 1970).

Theoretically the pressure at the mudline is given by linear theory as:

$$\Delta p = \gamma \frac{H}{2} \frac{1}{\cosh\left(\frac{2\pi d}{L}\right)} \tag{36}$$

Using Stoke's second order relationship the bottom pressure can be expressed as the right hand side of Equation 36 plus the second order term:

$$\frac{3}{8} \frac{\gamma \pi H^2}{L} \frac{\tanh 2\pi d/L}{\sinh^2 2\pi d/L} \left[\frac{1}{\sinh^2 (2\pi d/L)} - \frac{1}{3}\right] \tag{37}$$

Theoretical computations were made using the above two theories and a comparison with the experimental values is shown in Table 4. It may be seen from the comparison that the experimental values are slightly different from the theoretical computations; this may be due to the fact that the waves are assumed to be symmetrical and sinusoidal but the experimental waves are not perfectly sinusoidal or symmetrical. The nature of the experimental waves has been

TABLE 4

MEASURED AND COMPUTED BOTTOM PRESSURES

Depth = 0.43 m

Run	Freq. (Hz)	Wavelength		Wave Height (m)	Δp (theory)		Experiment		Theory/ Experiment
		Theory (m)	Exp (m)		Linear (kPa)	2nd order (kPa)	Crest (kPa)	Trough (kPa)	
1	0.71	2.32.	2.66	.062	±.194	±.198	.1	-.14	1.6
2	0.89	1.7	1.83	.070	±.149	±.148	.15	-.16	0.96
3	1.03	1.38	1.45	.079	±.117	±.116	.12	-.12	0.97
4	1.19	1.1	1.19	.074	±.074	±.074	.08	-.08	0.93
5	1.27	.95	1.0	.088	±.058	±.057	.05	-.08	0.88
6	1.35	0.85	0.86	.083	±.035	±.035	.04	-.05	0.78

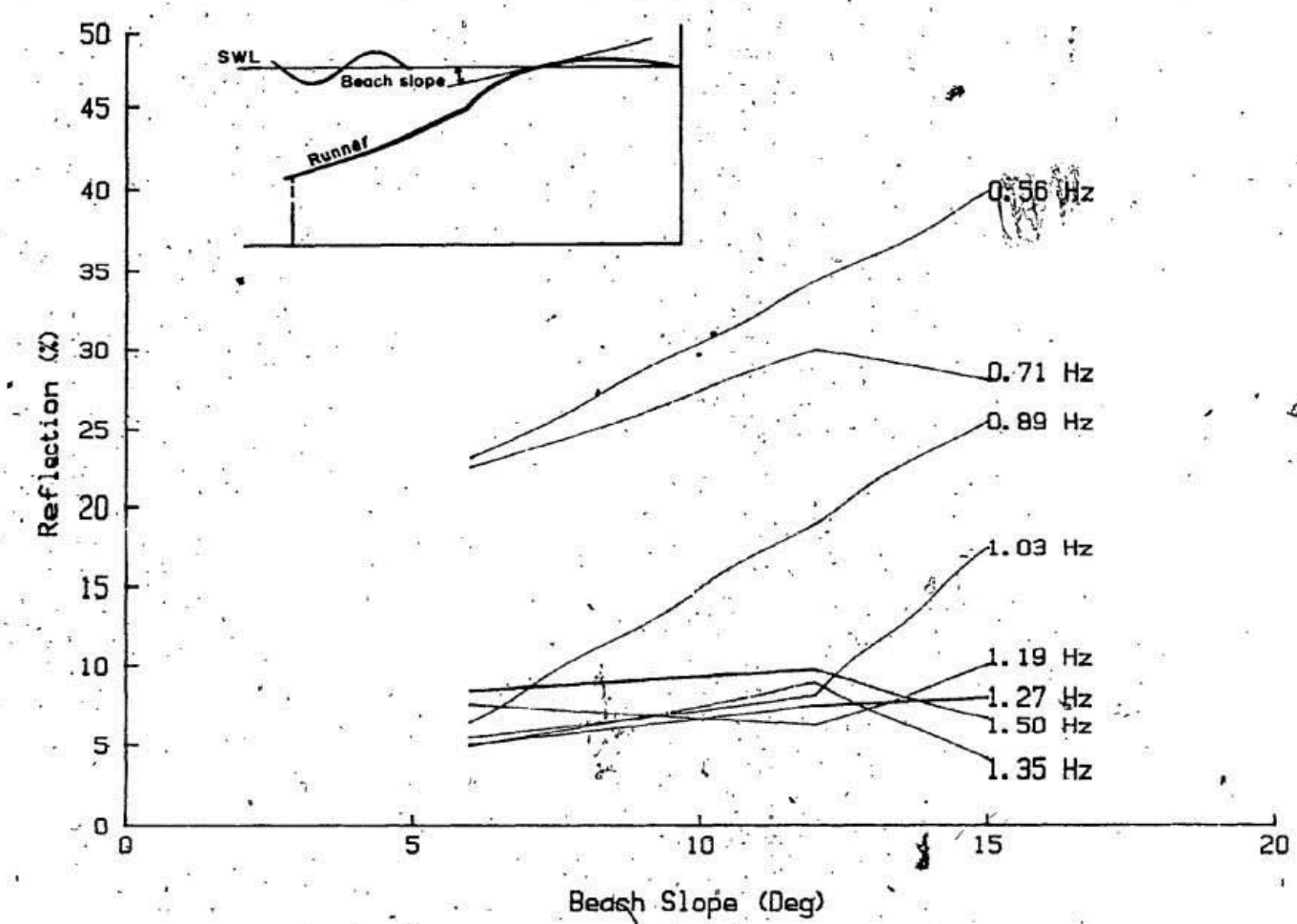


FIGURE 41. BEACH PERFORMANCE AT DIFFERENT SLOPES

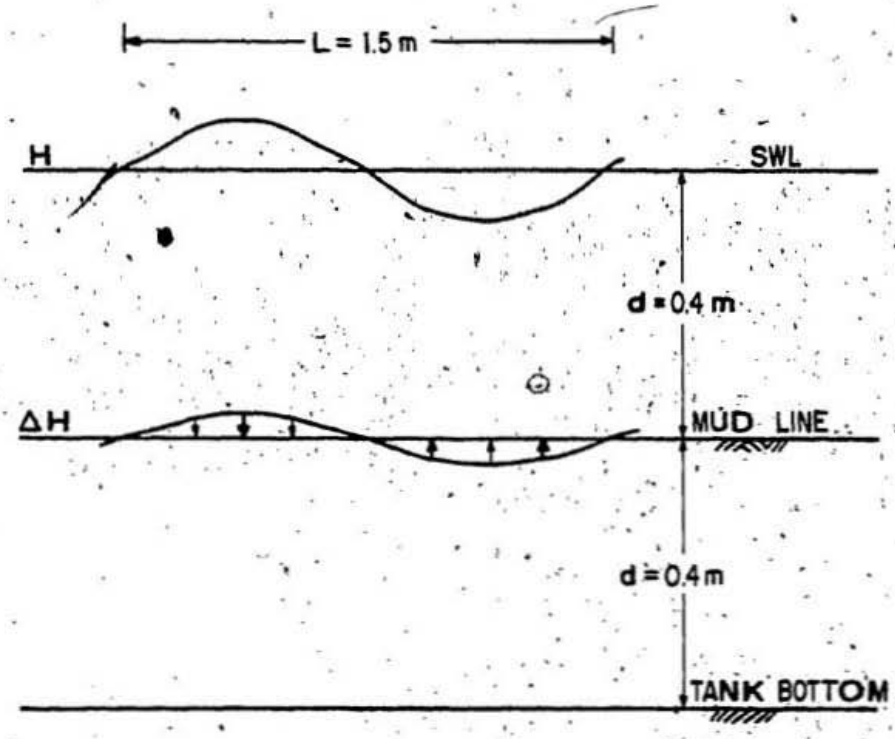


FIGURE 42 TYPICAL SURFACE WAVE AND RESULTING BOTTOM PRESSURE

discussed earlier in this chapter. A further explanation for any difference is that the theoretical values assume an impermeable rigid bottom whereas in the test, the sand bed is permeable.

From the measured pressures shown in Table 4, it is obvious that there is a pressure wave developed at the mudline; the intensity of this pressure wave can be continuously monitored and the effects observed.

4.2.2 Effects of Wave Pressure on a Flat Bed of Sand

The effect of waves on a flat sand bed was examined to study the conditions for soil failure by liquefaction and the subsequent pore water pressure dissipation and densification.

Preliminary theoretical computations were made to determine pore water pressures necessary to cause liquefaction. Also, experiments were conducted in which back pressure was developed by pumping water through the pipe-grid system at the bottom of the tank until the sand bed liquefied. These preliminary studies were used to correlate the measured pressures under the effect of progressive surface waves and to delineate the instant when the soil near the mudline and immediately below reached a no-strength condition.

Before waves were run, back pressures during liquefaction were measured. Pressure transducers were

used for subsequent tests under wave loads to identify soil failure.

In a second series of experiments without waves, it was attempted to measure the pore water pressure due to shock and the subsequent dissipation of the pressure.

The soil was brought to a loose state (ρ_d = 1250 kg/m^3) and the back pressure removed. Under this condition there was no excess pore water pressure in the soil. This is shown in the initial stages of Figure 45, from time = 0 - 2.4 seconds. The bottom of the wave tank was then tapped gently with a 4 kg mass of steel. There was a sudden development of excess pore water pressure in the soil causing liquefaction as confirmed by the pore-water pressure measurements at 7 cm, 20 cm and 30 cm depths below the mudline.

The measured pore pressures are plotted on Figure 46 and compared with the calculated overburden stresses. The measured pressures show that the excess pore water pressure is dissipated gradually, starting from the bottom of the tank. This is consistent with the fact that drainage is only in one direction and there is gradual densification in the sand bed from the bottom gradually proceeding to the surface. After a period of 7 seconds it was observed that drainage was complete and the soil reached a dry density of 1320 kg/m^3.

embedded in the soil as described in Chapter III and the water level in the tank was at 80 cm elevation under still water conditions. Water was forced under pressure into the sand bed through the pipe-grid system at the bottom of the tank. It was possible to maintain the still water level by manipulating the outflow and inflow valves. Pressures were continuously recorded at different depths inside the soil. A typical record of change in pore water pressure in the soil at different depths is shown in Figure 43.

At time = 2.8 seconds, the water was turned on, and at 4 seconds full flow was achieved. Between 4 and 6 seconds the smooth curve represents the time at which the soil was being raised upward as a block by the incoming water. At 6 seconds the block crumbled and the soil began to boil and hence the fluctuation in pore water pressure. It may be seen from the recorded pressures that the effect of this fluctuation is more pronounced at 30 cm depth which is obviously due to the longer soil column undergoing an erratic change in its state.

The theoretically calculated effective overburden pressures at 7 cm, 20 cm and 30 cm depths for a quick condition are respectively 0.56 kPa, 1.61 kPa and 2.41 kPa which compares well with the measured pore water pressures of 0.4 kPa, 1.6 kPa and 2.4 kPa shown by the dashed line in Figure 44. The above observation for quick condition was

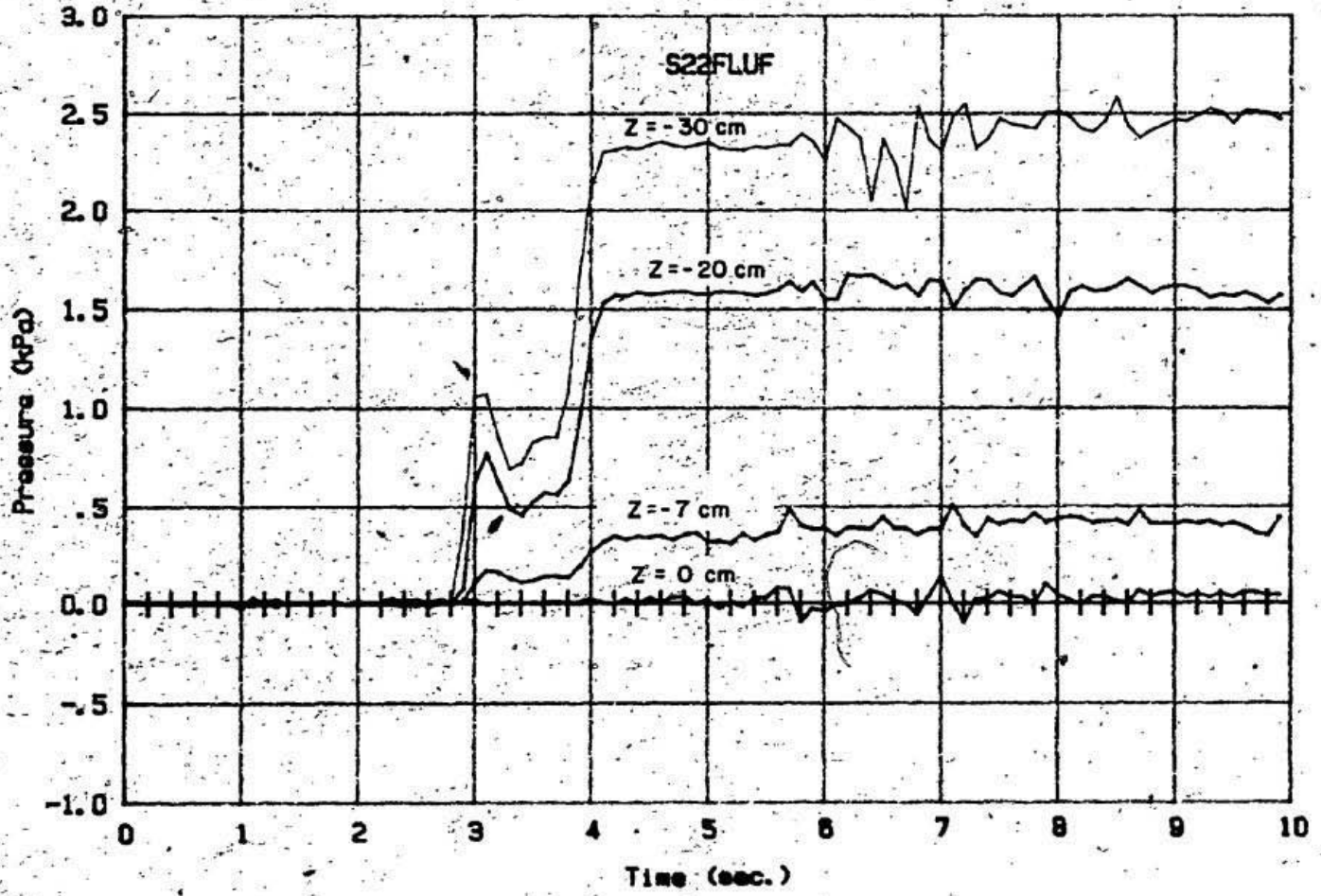


FIGURE 43 PORE-WATER PRESSURE CHANGE DUE TO SEEPAGE INDUCED LIQUEFACTION

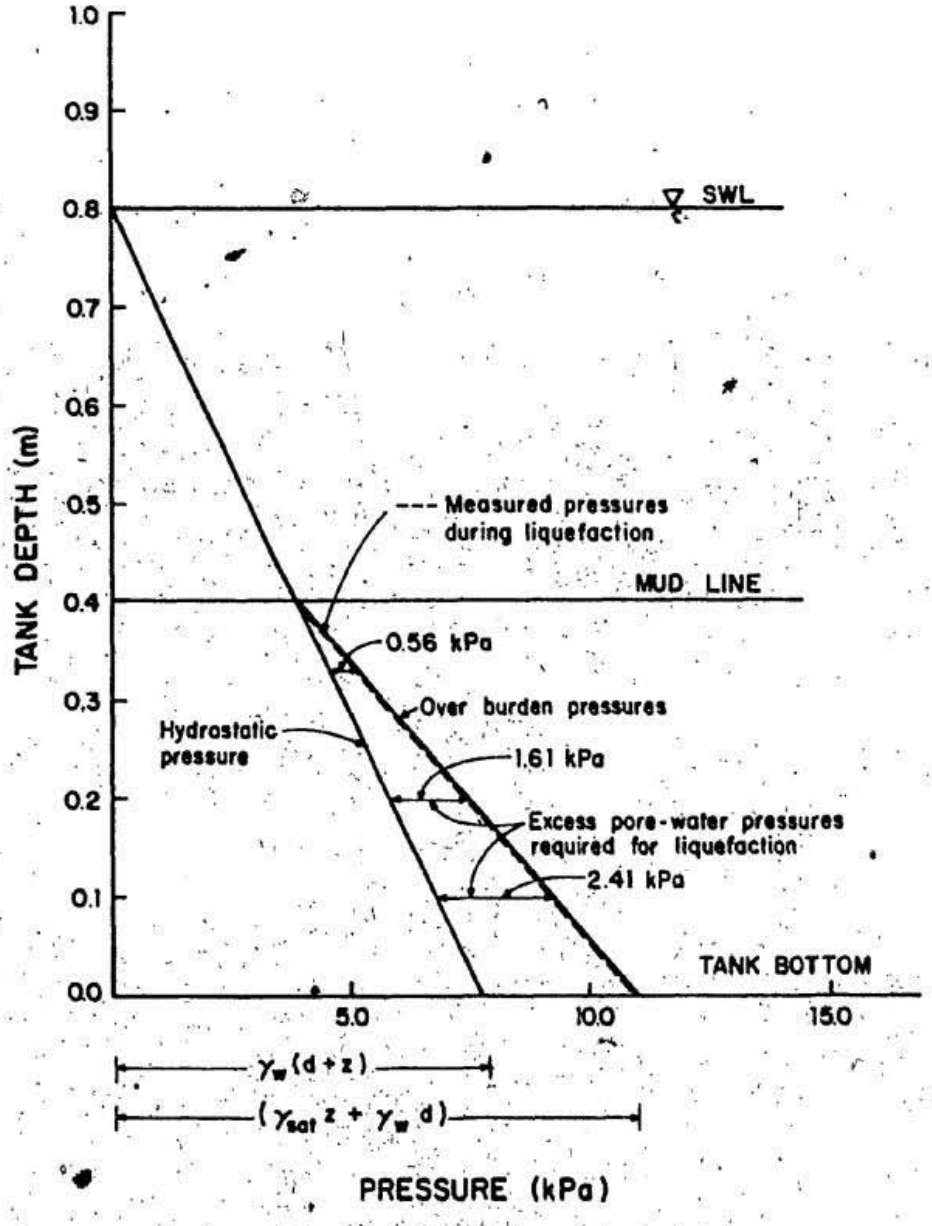


FIGURE 44 THEORETICAL AND MEASURED POREWATER PRESSURES AT LIQUEFACTION

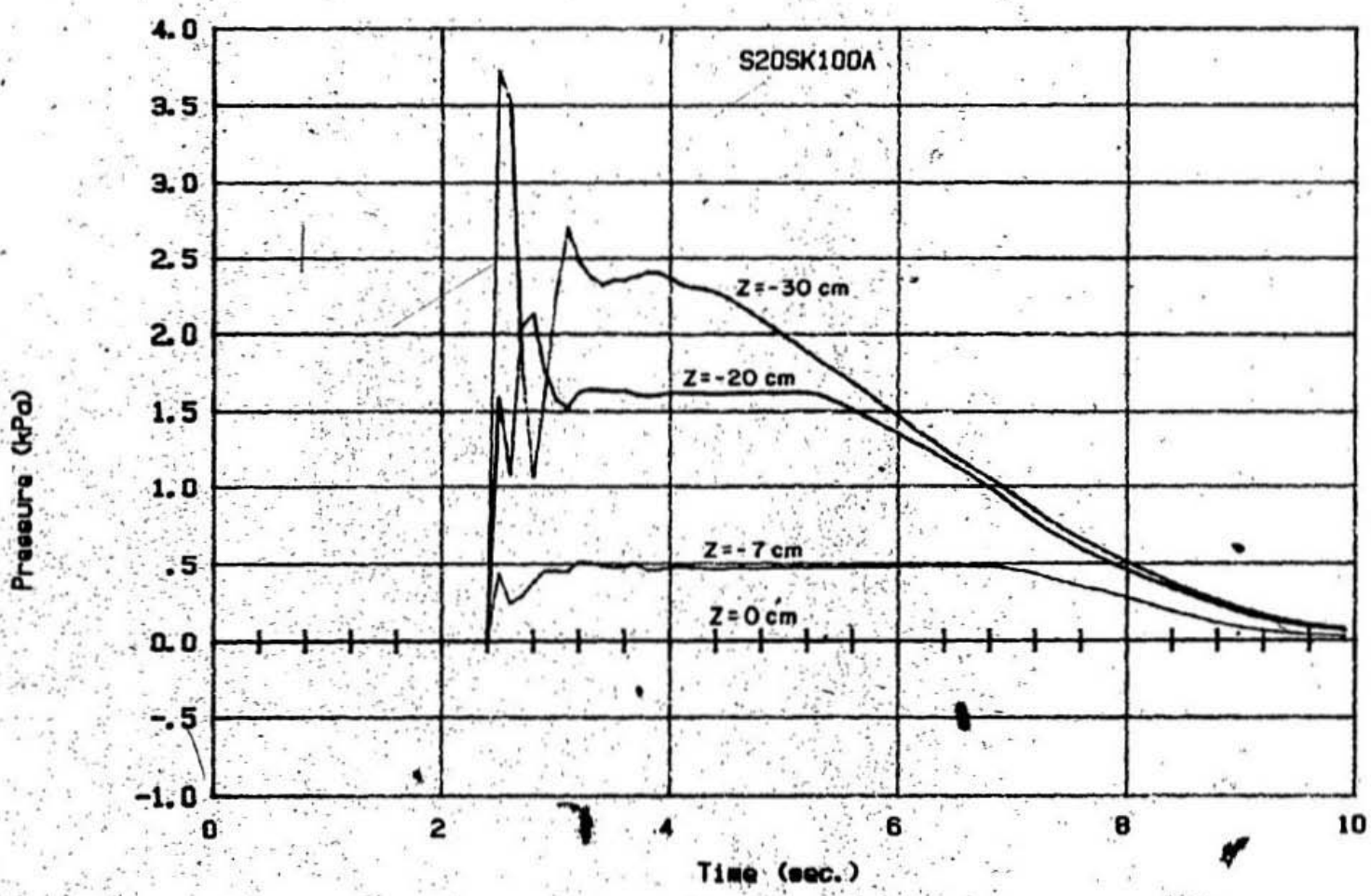


FIGURE 45 EXCESS PORE-WATER PRESSURE DURING SHOCK INDUCED LIQUEFACTION

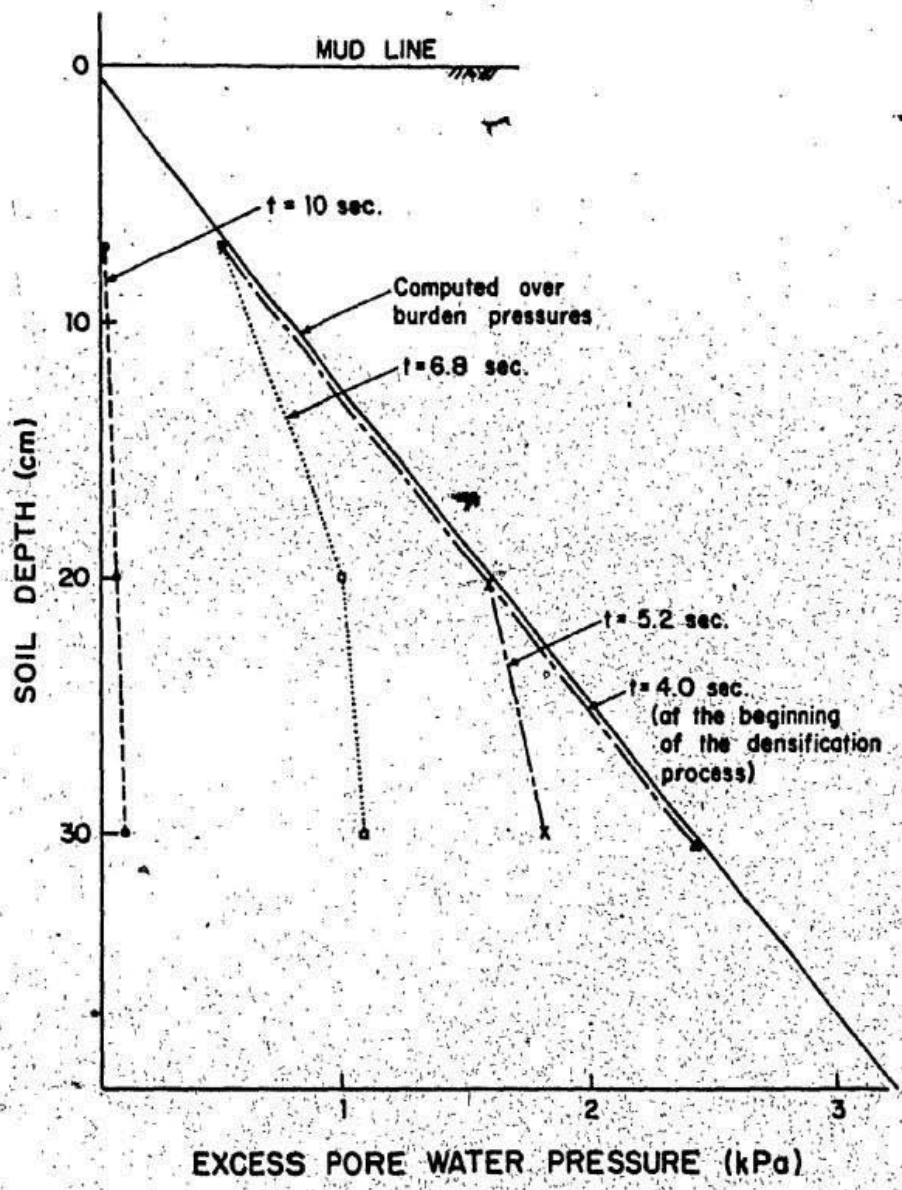


FIGURE 46 VARIATION OF EXCESS POREWATER PRESSURE AFTER SHOCK INDUCED LIQUEFACTION

As an additional confirmation and as a method of visually observing the liquefaction phenomenon, a weight was placed on the soil surface and was seen to suddenly sink into the soil as the porewater pressures rose soon after the application of the impact load.

After the above tests to determine the liquefaction susceptibility of the soil, the porewater pressure response of the soil due to wave load was studied by passing waves of various frequencies over a flat sand bed. The excess porewater pressures within the soil were directly obtained as explained in Chapter III.

Two types of observations were made. In the first set, the pressure transducer output was continuously recorded on a strip chart recorder; these records were used for a qualitative interpretation of the pressure variation inside the soil. In the second set of observations the pressure transducer output was recorded on computer diskettes through the data logging system described in Chapter III. These records extend for periods of 10 and 20 seconds and were used for quantitative evaluation of the excess pore water pressures and to identify failure criteria.

Sets of typical strip chart records are shown in Figures 47, 48, 49 and 50. The change in pressure at the mudline and the change in excess pore water pressure at 30 cm below the mudline are shown in the figures together with the

record of the exciting surface wave for wave frequencies between 0.7 Hz and 1.35 Hz. The magnitudes of the pressures in these figures are not plotted to exact scale and so only a qualitative interpretation is possible. Figure 47 shows the bottom pressure response and the resulting porewater pressure response when a 0.71 Hz wave passes over the test site. In this case the surface wave appears skewed while the resulting bottom pressure and porewater pressure pulses appear near sinusoidal. The pressures generally follow the water surface displacements at the same frequency but with a reduced magnitude. In the case of 1.03 Hz waves shown in Figure 48(a), the pattern was similar with an even closer resemblance between surface wave form and that of the resulting pressures. It can be seen that as the surface waves start, the magnitudes of the pressures increase according to the increase in wave height and a steady state is reached where the pressure response is near sinusoidal.

However, in the case of higher frequency waves in Figure 48(b), Figure 49, and Figure 50, the pressure response is different. It may be seen from Figure 48(b) that the pressure change with time inside the soil at 30 cm is not uniform. When the first 1.27 Hz wave passes across the test location the pressure change at 30 cm depth is somewhat similar to the pressure responses at other lower frequencies. However, this pattern changes after about 10-15 waves. When

the wave frequency is increased to 1.35 Hz, the initial excess porewater pressure at 30 cm depth due to the initial test wave is much larger (Figure 49a) than that under a steady condition. Similarly, towards the end of an experiment when the last generated wave passes the test location there is a sudden increase in the excess porewater pressure.

A relative comparison of Figures 48 to 50 shows that when the wavemaker is turned off, pressure attenuation inside the soil is also different for different surface wave frequencies. For example, at 1.03 Hz when the wave generator was turned off the surface wave height (Figure 48a) reduced to approximately 10%, while the pressure at 30 cm depth reduced to approximately 30% of the steady state pressure. When the frequency was 1.27 Hz (Figure 48b), after the wave generator was turned off, the wave height reduced to about 20%, but the porewater pressure at 30 cm depth increased by about 50% instead of decreasing. In Figure 49, it may be seen that at 1.35 Hz, the surface wave reduced approximately 10% while the magnitude of the pressure change at 30 cm depth had no significant change.

It was also noted that in addition to the pressure variations with time, the response inside the soil did not always correspond to the form of the surface wave or the form of the wave at the mudline. Figure 50 shows a surface wave

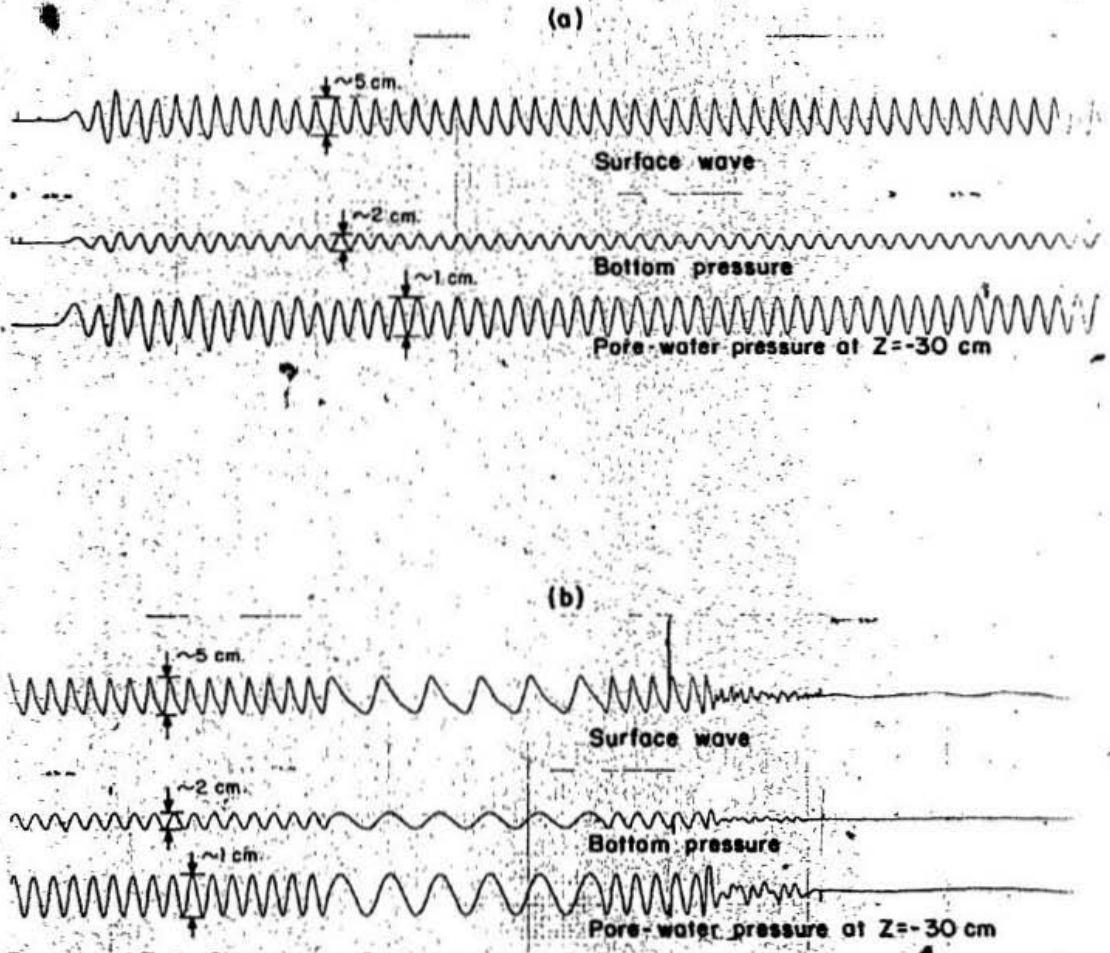


FIGURE 47 PRESSURE RESPONSE TO 0.71 HZ WAVES

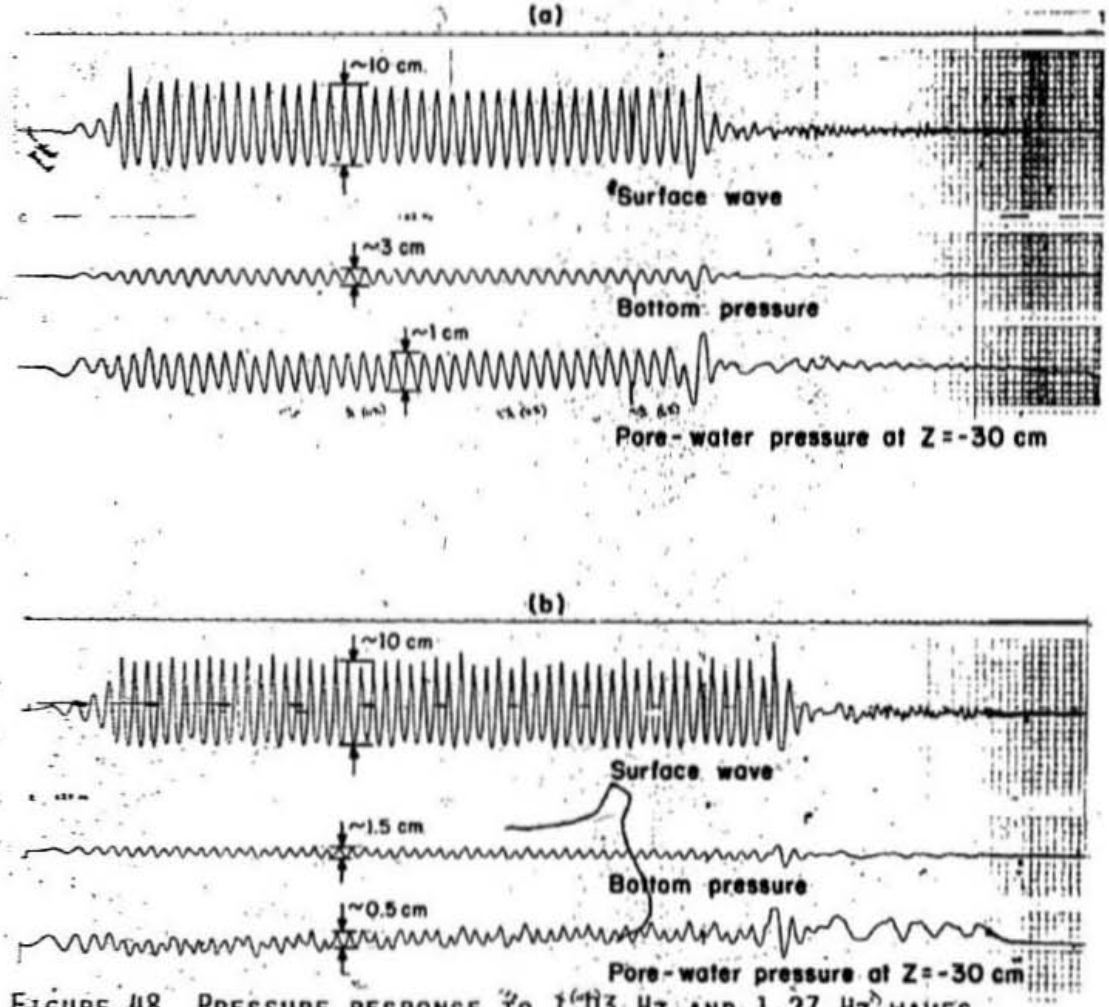


FIGURE 48 PRESSURE RESPONSE TO 1.03 Hz AND 1.27 Hz WAVES

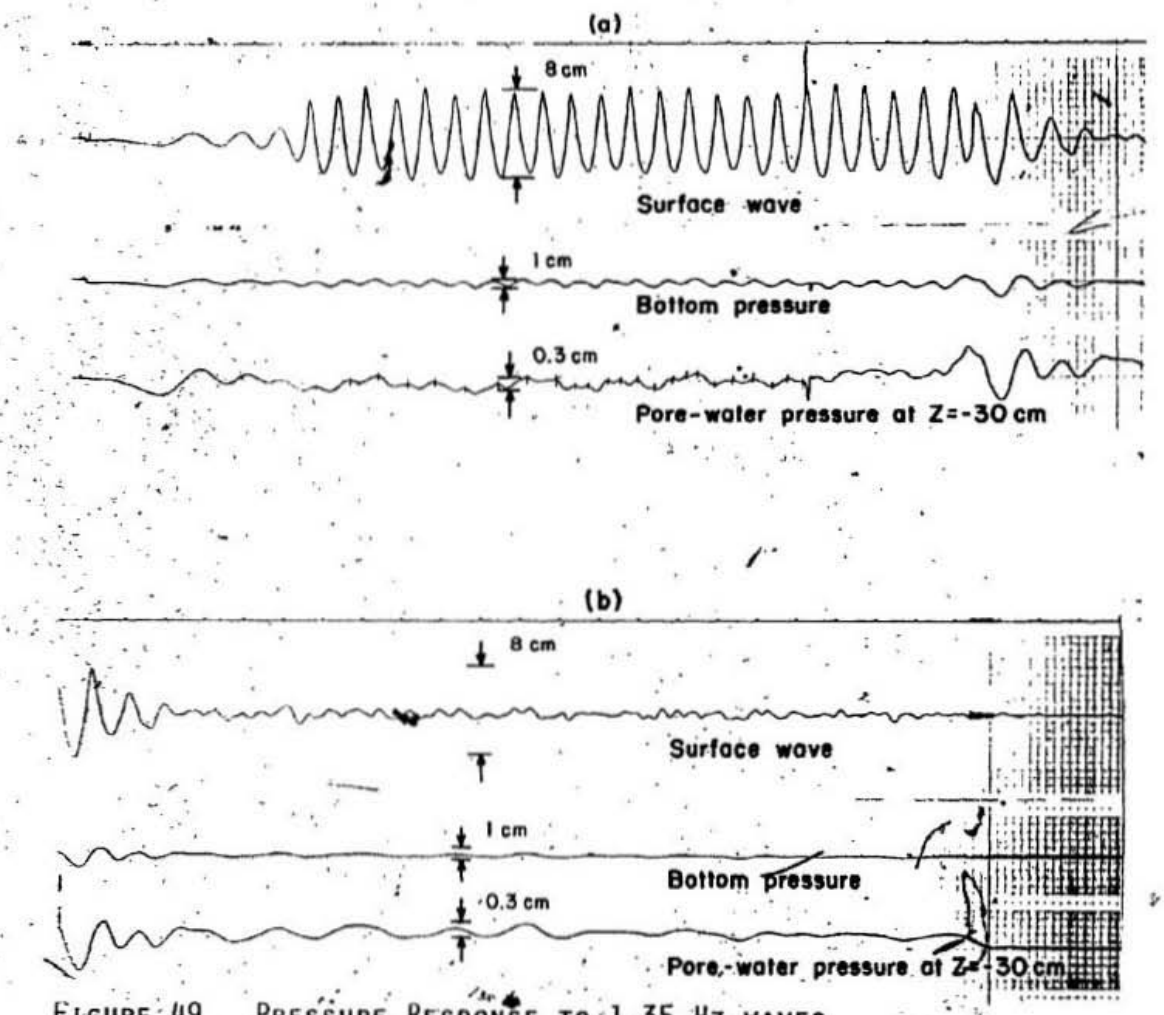


FIGURE 49 PRESSURE RESPONSE TO 1.35 HZ WAVES

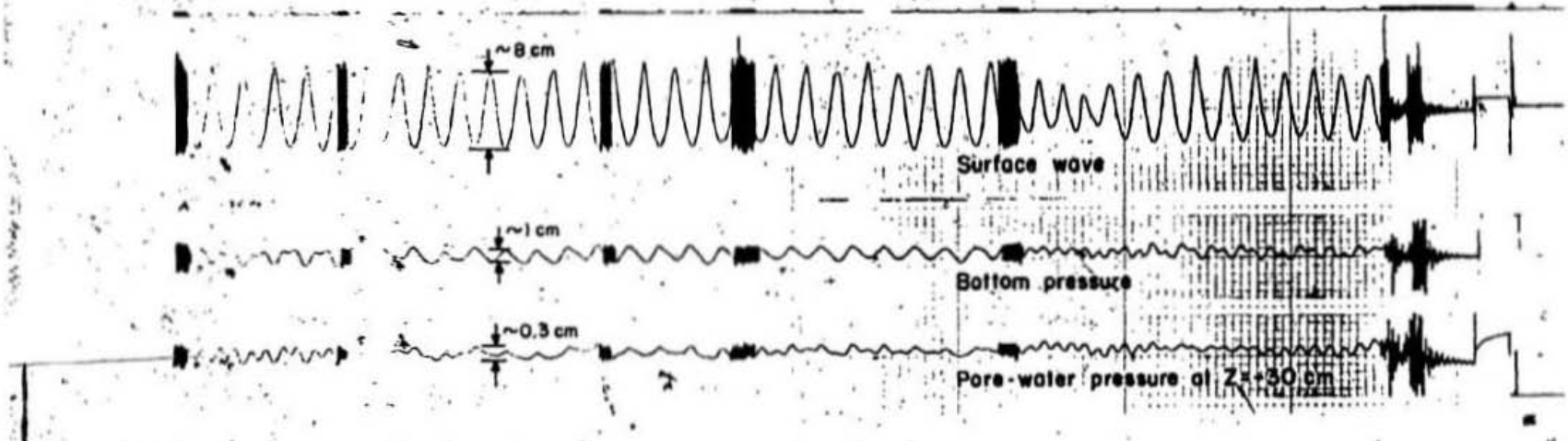


FIGURE 50 PRESSURE RESPONSE TO 1.35 HZ WAVES SHOWING HOW THE PRESSURE RESPONSE CHANGES WITH TIME

at 1.35 Hz that produced a bottom pressure somewhat similar in form, but the sub-bottom pressure at 30 cm was considerably different. The frequency of pressure change at 30 cm depth at higher frequencies is twice that of the surface and bottom pressure waves.

It was also noticed that the pressure variation inside the soil was out of phase with the wave pressure at the mudline. This phenomenon has been reported by others (Sleath, 1970; Yamomoto, 1978; Tsui, 1983; and Raman-Nair, 1984). Table 5 and Figure 51 give a summary of phase lag between mudline pressure pulses and the pressure change at 30 cm depth within the soil found in the present work. The phase lag varies between 5.8% and 17.2% depending on depth below the mudline, frequeney of the waves and soil characteristics.

In summary, qualitative observation of the strip chart records shows that the pressure at the mudline follows the general pattern of the surface waves. However, the type of porewater pressure response inside the soil is dependent on the wave frequency which appears to influence the magnitude of the porewater pressure, the type of pressure attenuation, the form of the pressure wave, the frequency, and the phase lag. It is also most likely that the properties of the soil, particularly its drainage characteristics will influence all the variations listed

TABLE 5
PHASE LAG OF THE PRESSURE FLUCTUATION
BELOW THE MUDLINE

Surface Wave Frequency (Hz)	Phase difference between pressure pulses at the mudline and at 30 cm below the mudline (%)		
	Run 1	Run 2	Run 3
.71	7	8.4	5.8
.89	6	13.7	8
1.03	7	11.2	8
1.19	10	10.4	11.7
1.27	9	17.2	11.1
1.35	7	16.5	17.2

Run 1 - Loose Soil (γ_d = 1250 kg/m^3)

Run 2 & Run 3 - Dense Soil (γ_d = 1400 kg/m)

Note: Phase lag is defined as the difference in time between when the maximum pressure is felt on the mudline and when the maximum pressure is felt at 30 cm depth directly below. This time difference is divided by the wave period and multiplied by 100% to give phase lag in percent.

above. Further investigation and quantitative measurements are required to establish a mathematical relationship between the surface wave characteristics, soil properties and the porewater response at depth in the soil.

Tests were also conducted in which four pressure transducers were placed in the soil, one at the mudline, and one each at 7, 20 and 30 cm below the mudline and pressure readings were recorded using the data logging system. These tests were done for different soil densities and the behaviour under various soil and wave conditions are discussed below.

Figure 52 is the record of porewater pressure change inside the soil for a 9 cm high wave at a frequency of 0.89 Hz in 42 cm deep water. The dry density of the soil was 1500 kg/m^3. It is seen that there is a cyclic variation in the excess porewater pressure which varies over a constant range at each of the four depths with no residual porewater pressure. Theoretical values of wave induced porewater pressure inside soil have been given by Liu et al (1979). The porewater pressure measured and recorded in Figure 52 was compared with the above theory and the comparison is shown in Figure 53 as a normalized pressure with reference to pressure at the mudline. Similar results for loose soil (ρ_d = 1300 kg/m^3) are shown in Figures 54 and 55. It may be seen from Figures 52 to 55 that there is a reasonably good

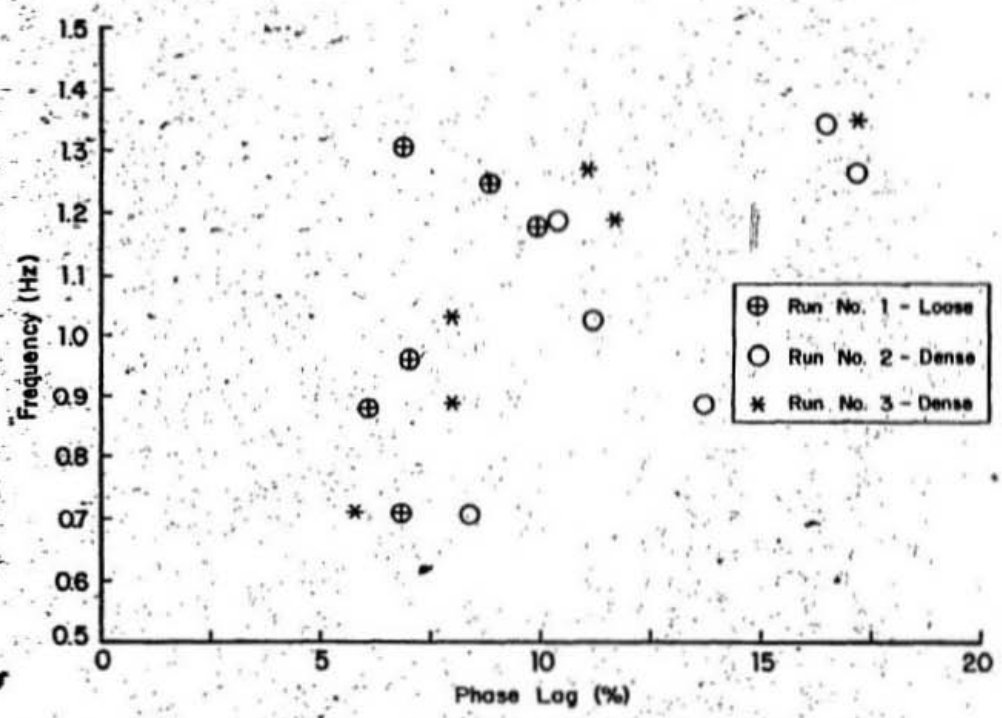


FIGURE 51 PHASE LAG BETWEEN PRESSURE AT MUDLINE AND PRESSURE AT Z = -30 CM

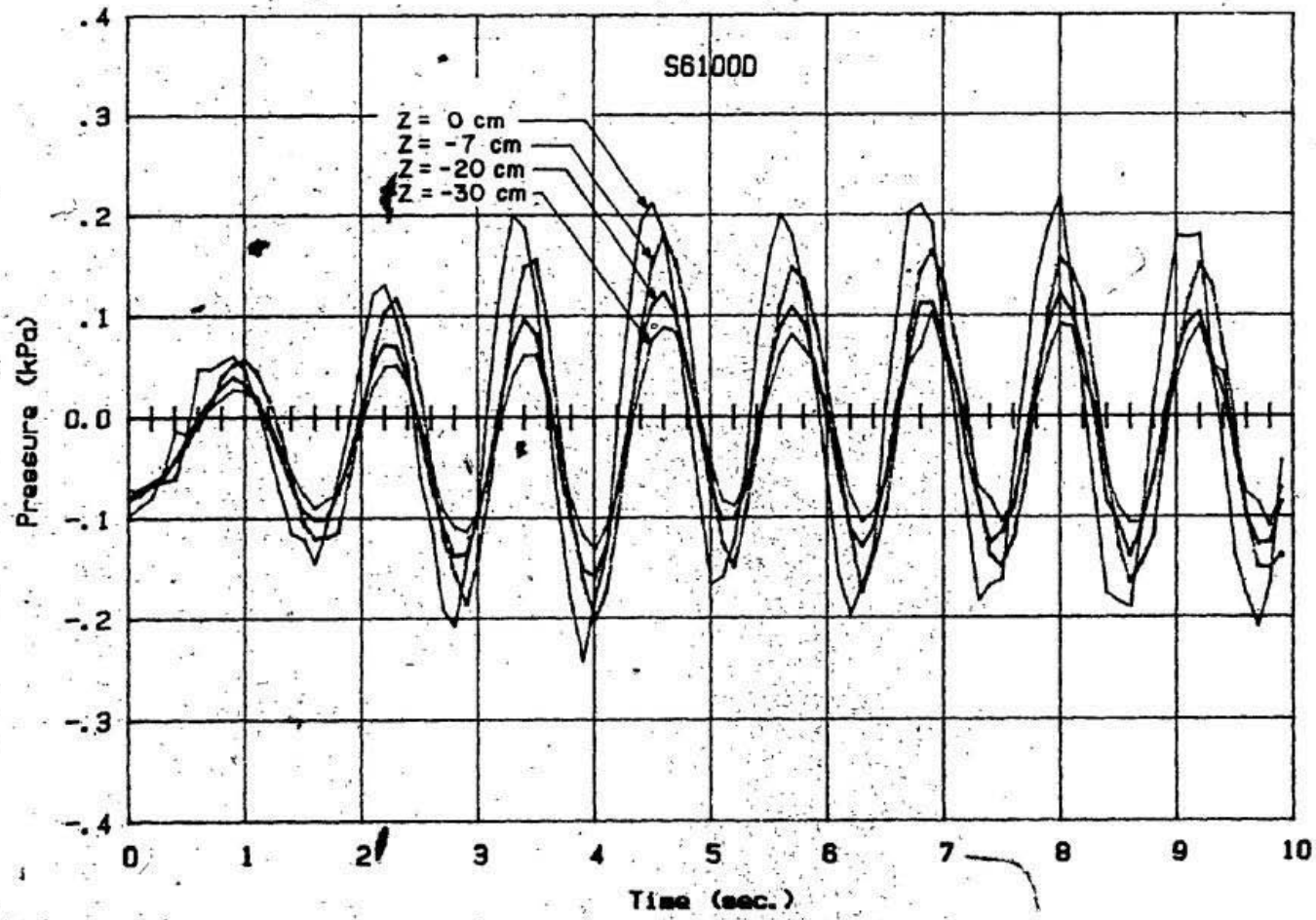


FIGURE 52 POREWATER PRESSURE RESPONSE (ρ_D = 1500 KG/M^3, NO FAILURE)

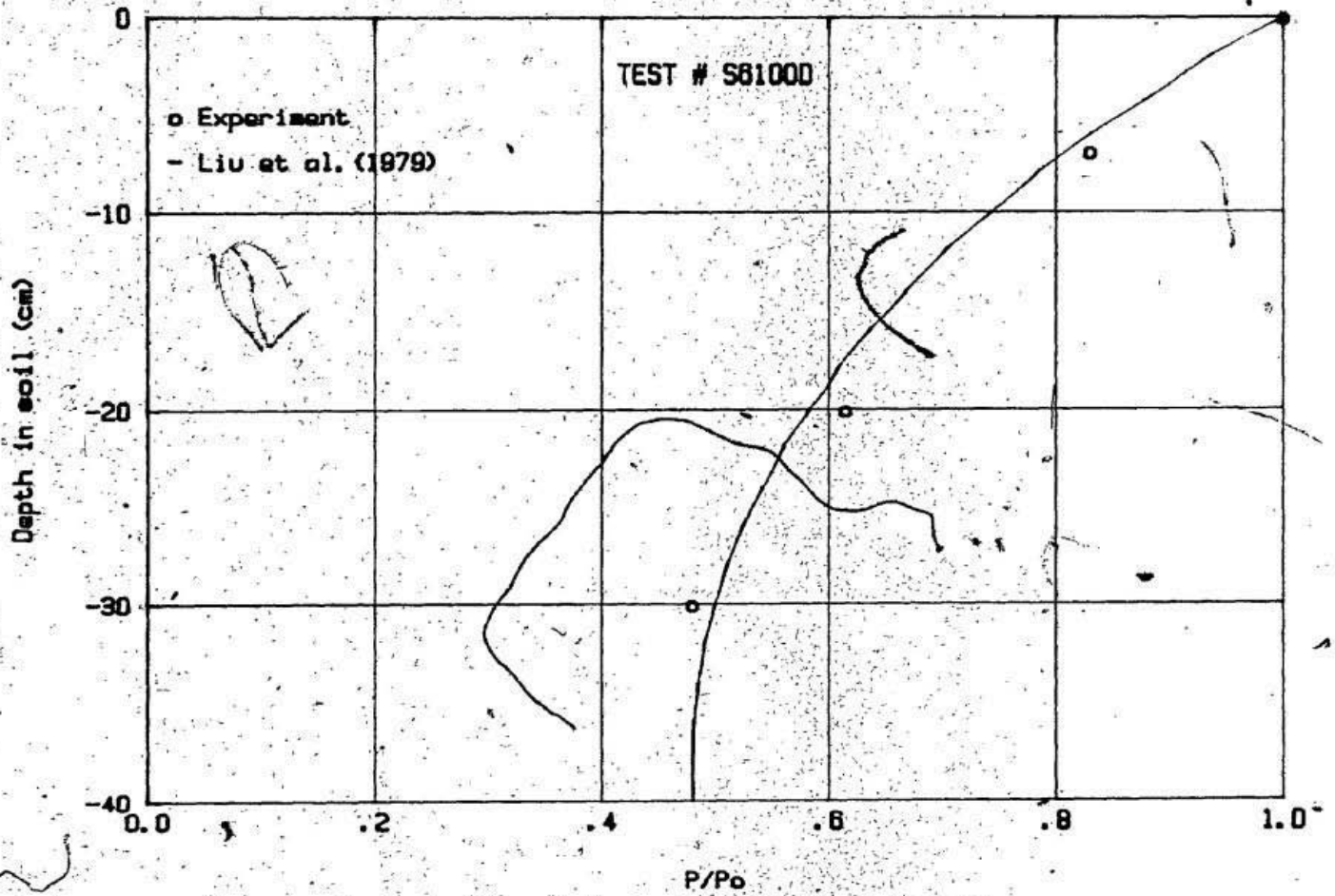


FIGURE 53 NORMALIZED POREWATER PRESSURE RESPONSE - COMPARISON OF THEORY AND EXPERIMENTS (ρ_D = 1500 KG/M^3, NO FAILURE)

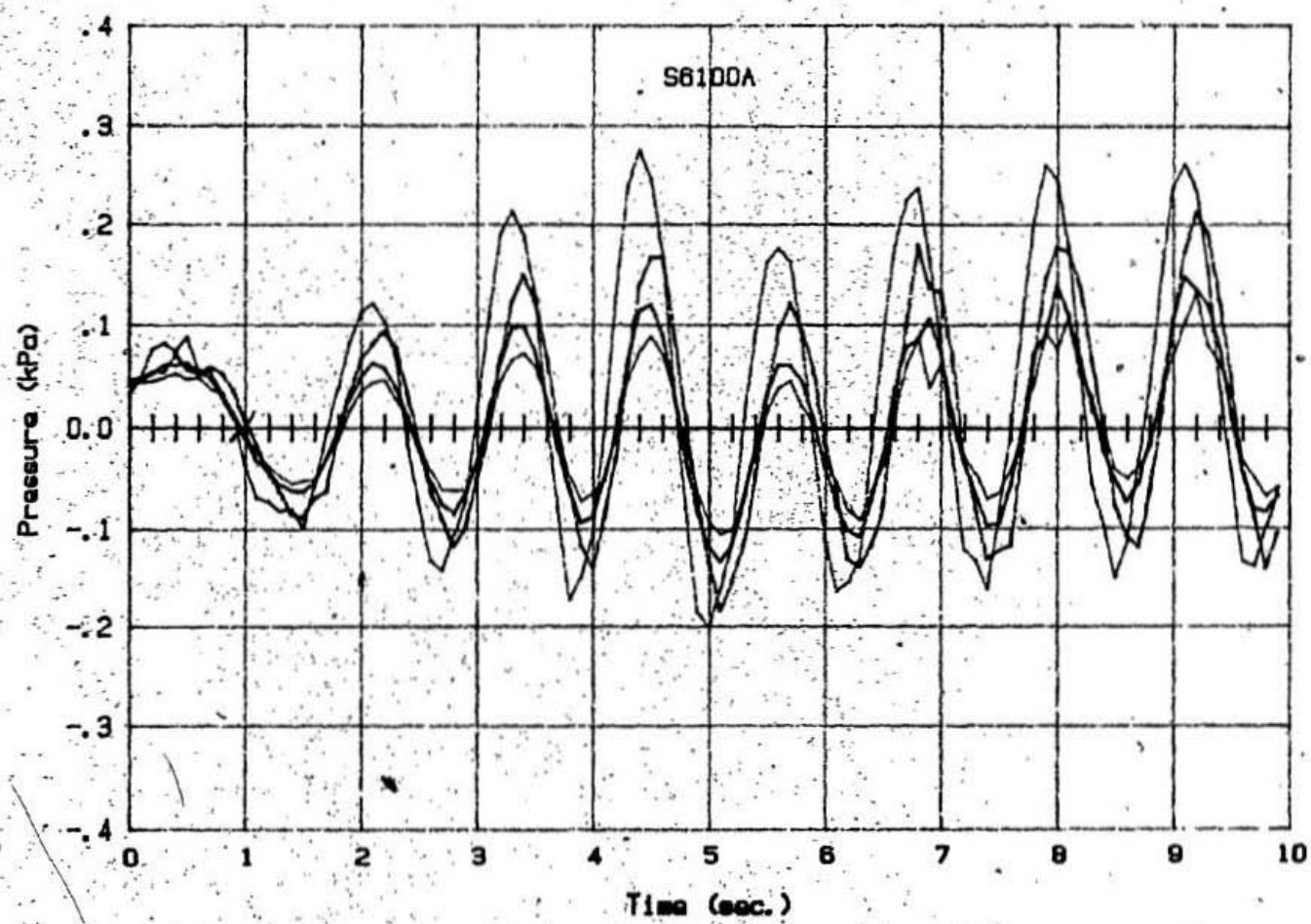


FIGURE 54 POREWATER PRESSURE RESPONSE (ρ_D = 1300 KG/M^3, NO FAILURE)

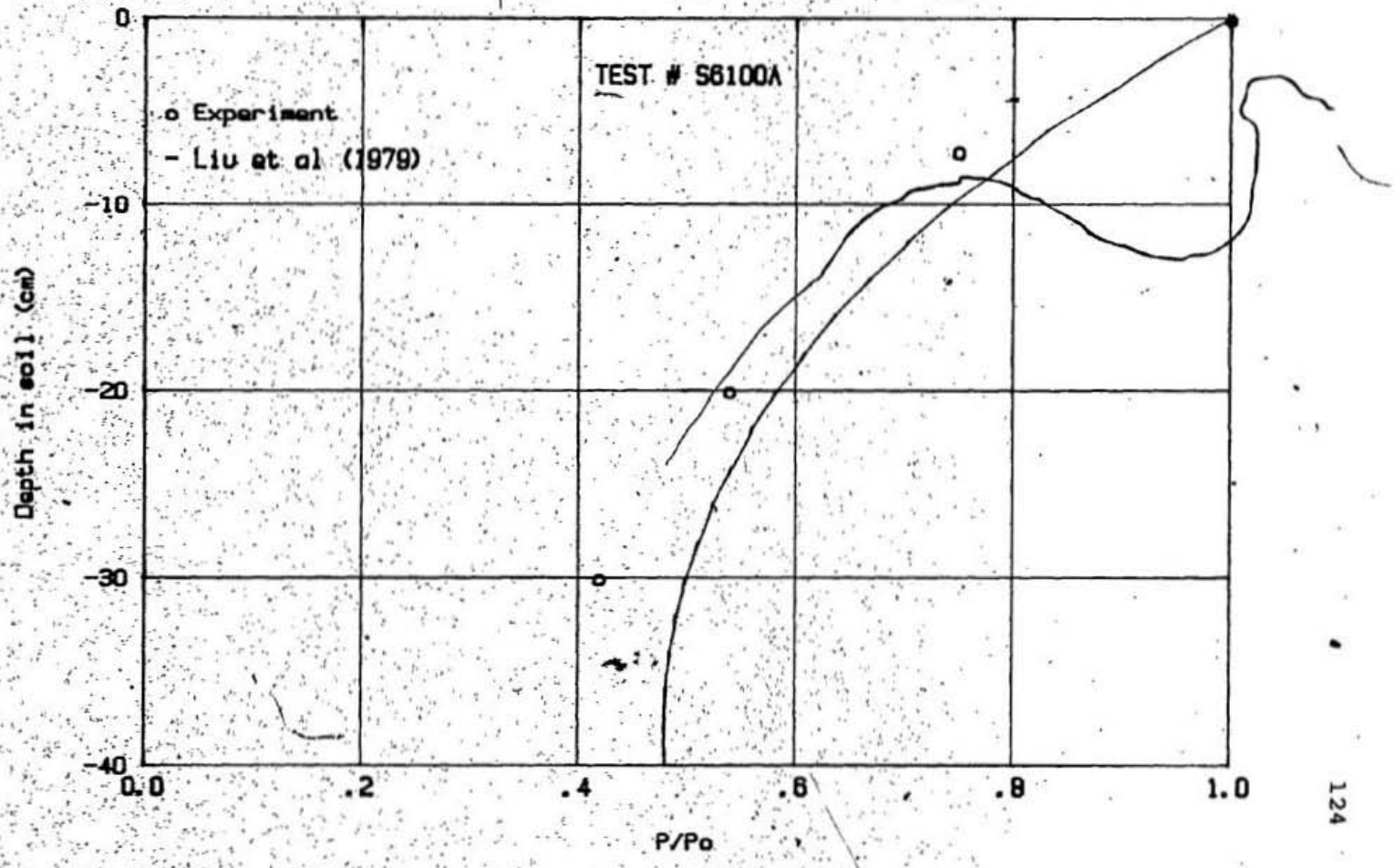


FIGURE 55 NORMALIZED POREWATER PRESSURE RESPONSE - COMPARISON OF THEORY AND EXPERIMENTS (ρ_D = 1300 KG/M^3, NO FAILURE)

correlation between theoretical and experimental results with the better correlation for the dense (ρ_d = 1500 kg/m^3) soil. Tests with a slightly different soil and wave periods between 0.74 sec. and 1.4 sec. have shown (Chari and Dawe, 1984) that the correlation between the theory and experiments was good only for the wave periods of about 1 second. The amplitude of the porewater pressure at depth z has been given by Liu, et al (1979) as

$$p_z = \Delta p_o \frac{\text{Cosh } k_o(d_s - z)}{\text{Cosh } k_o d_s} \qquad (38)$$

where

p_z = porewater pressure at depth z

Δp_o = amplitude of the wave pressure at the seafloor

k_o = wave number, $2\pi/L$

L = wavelength

d_s = thickness of the seabed overlying a rigid impermeable layer

z = depth below the mudline

One of the important properties which influences the porewater pressure response is the drainage characteristics of the soil. This in turn depends on the coefficient of permeability and the wave frequency. The relative significance of these two values was demonstrated experimentally in the qualitative tests already discussed. It would thus appear appropriate that any theory should incorporate the drainage behaviour of the soil. Although

some correlation has been shown between the equation of Liu et al (1979) and the experimental results, it would be necessary to modify Equation 38 to include the wave frequency and the coefficient of soil permeability.

The porewater pressure response for a loose sand (ρ_d = 1250 kg/m^3) is shown in Figure 56. While there is a cyclic porewater pressure variation for this type of soil also, the variation is not constant. There is a net increase in the porewater pressure during the first 8-10 waves after which the it reduces and the response stabilizes with the zero excess porewater pressure as the mean. The wave pressure at the mudline is transmitted to the soil as an increase in the neutral stress resulting in a transient increase in the porewater pressure. Any subsequent dissipation of the porewater pressure under continued wave pressure on the seabed is likely to result in a densification of the sand in a process somewhat similar to soil consolidation. This densification and an experimental verification thereof will be discussed later.

Figures 57, 58 and 59 are similar to Figure 56 in that these figures represent the typical porewater pressure response when there was no visible failure. Figure 60 represents the porewater pressure response when the depth of failure was observed to extend 1.5 cm below the mudline at the glass wall. Figures 61 to 67 show the porewater pressure

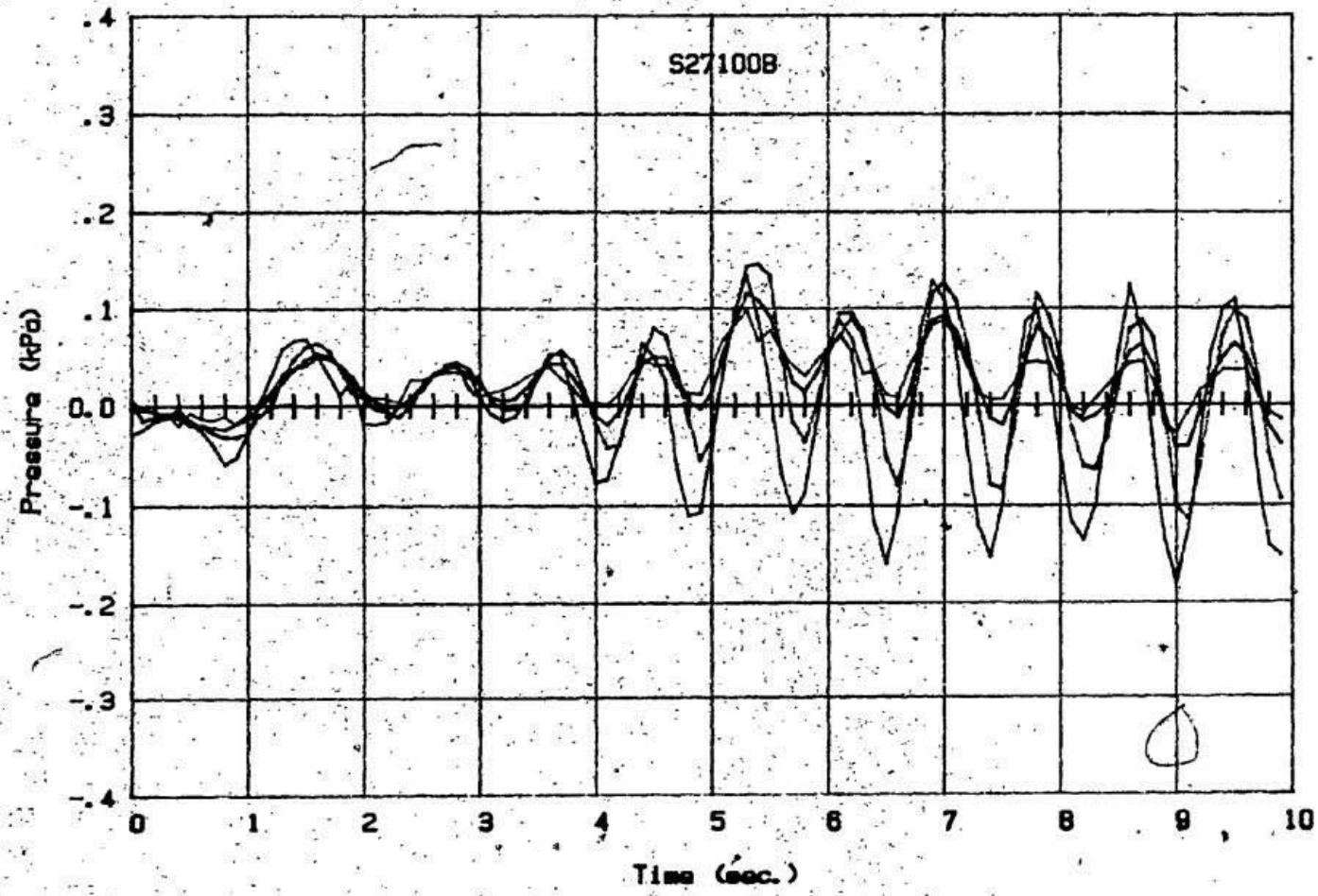


FIGURE 56 FOREWATER PRESSURE RESPONSE (ρ_D = 1250 KG/M^3, NO VISIBLE FAILURE)

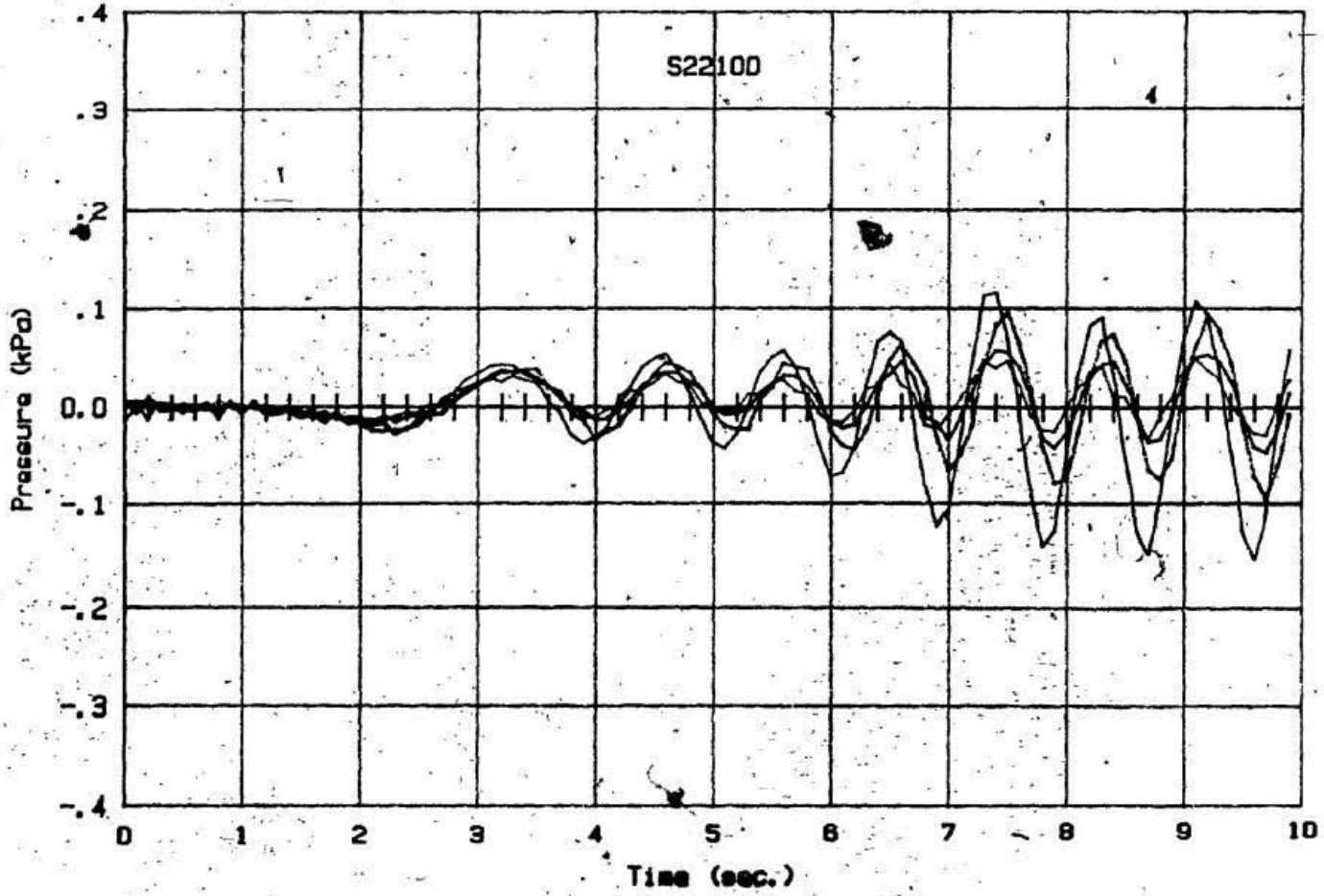


FIGURE 57 POREWATER PRESSURE RESPONSE (ρ_D = 1250 KG/M^3, NO VISIBLE FAILURE)

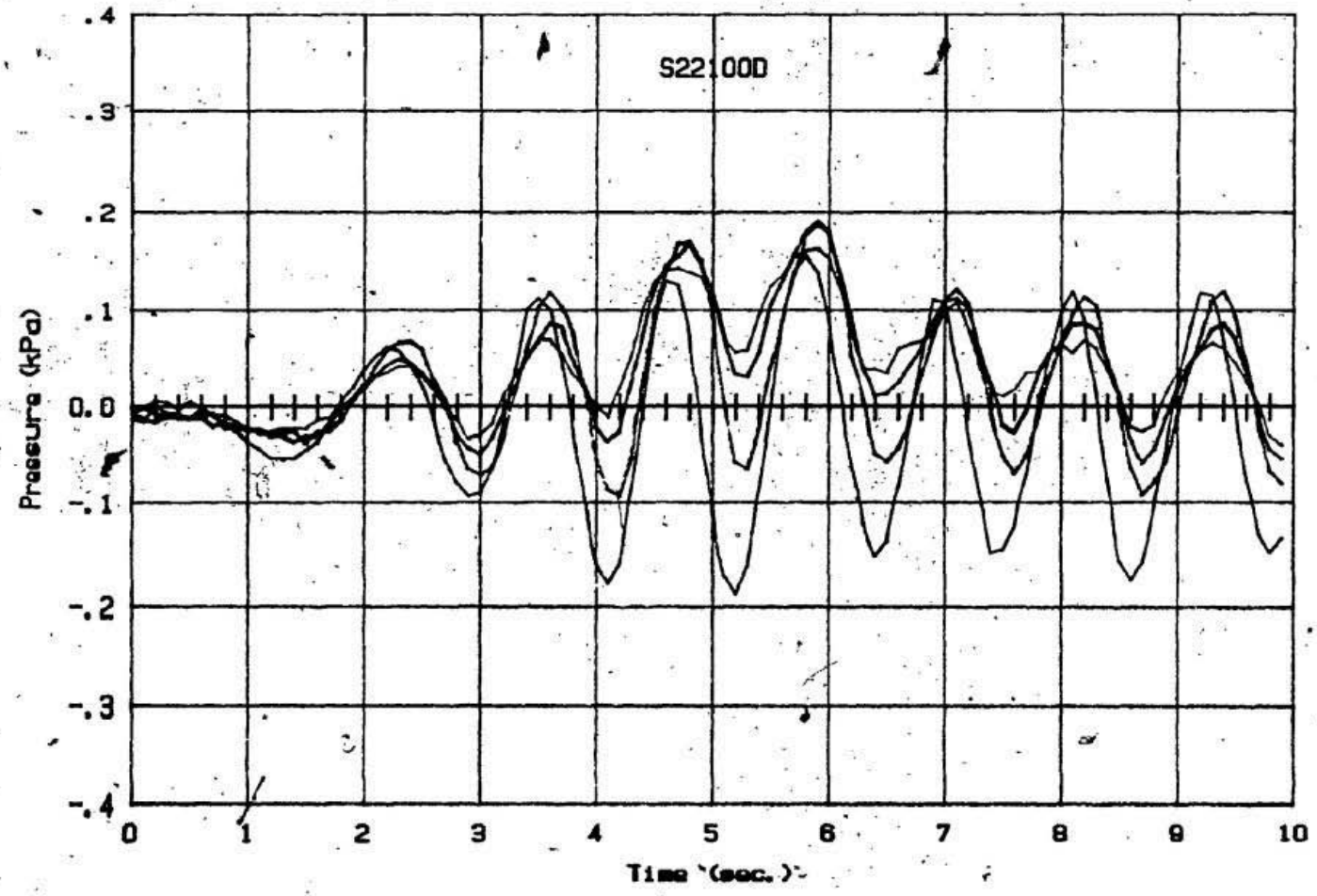


FIGURE 58 POREWATER PRESSURE RESPONSE (ρ_D = 1250 KG/M^3, NO VISIBLE FAILURE)

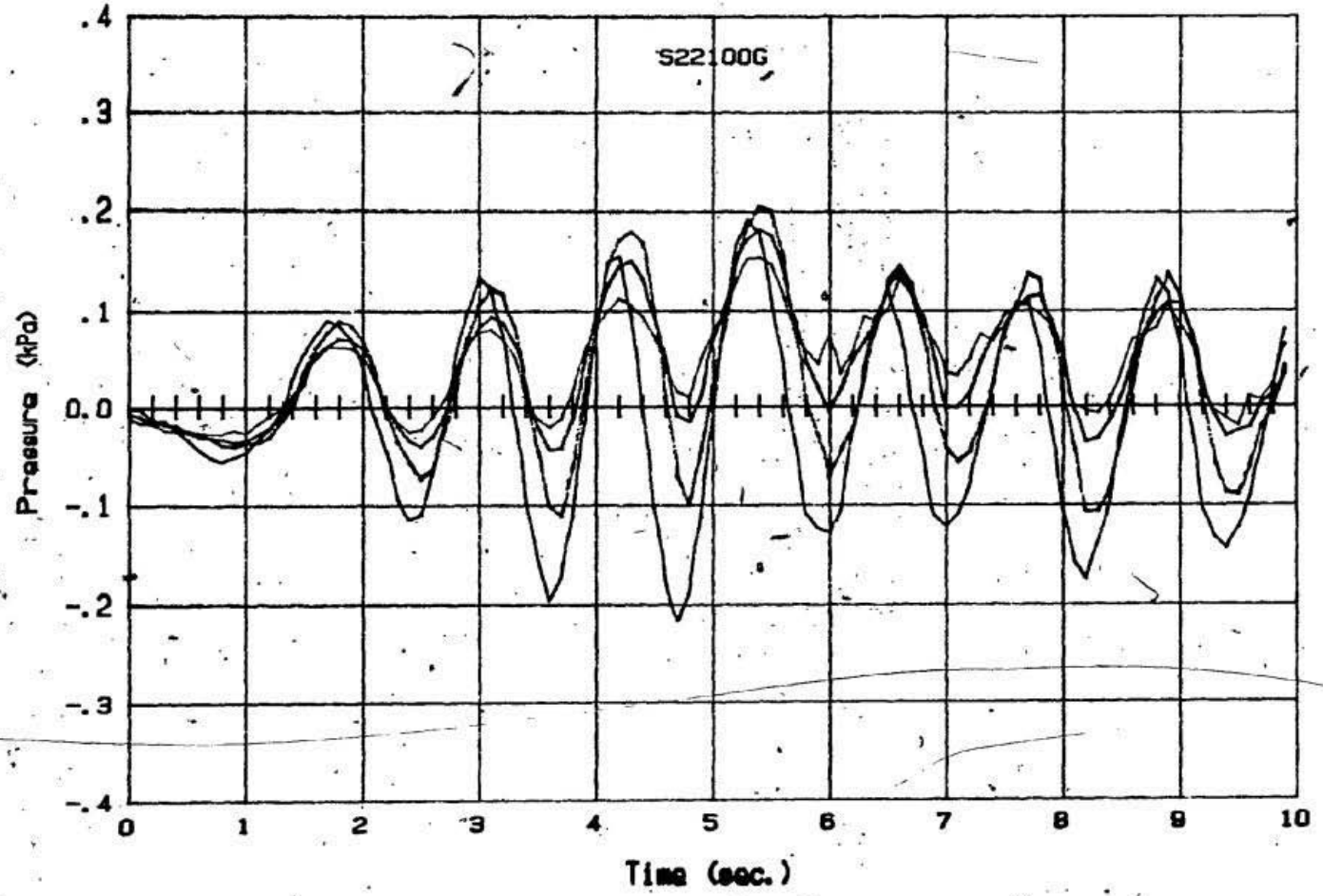


FIGURE 59 POREWATER PRESSURE RESPONSE (ρ_D = 1250 KG/M^3, NO VISIBLE FAILURE)

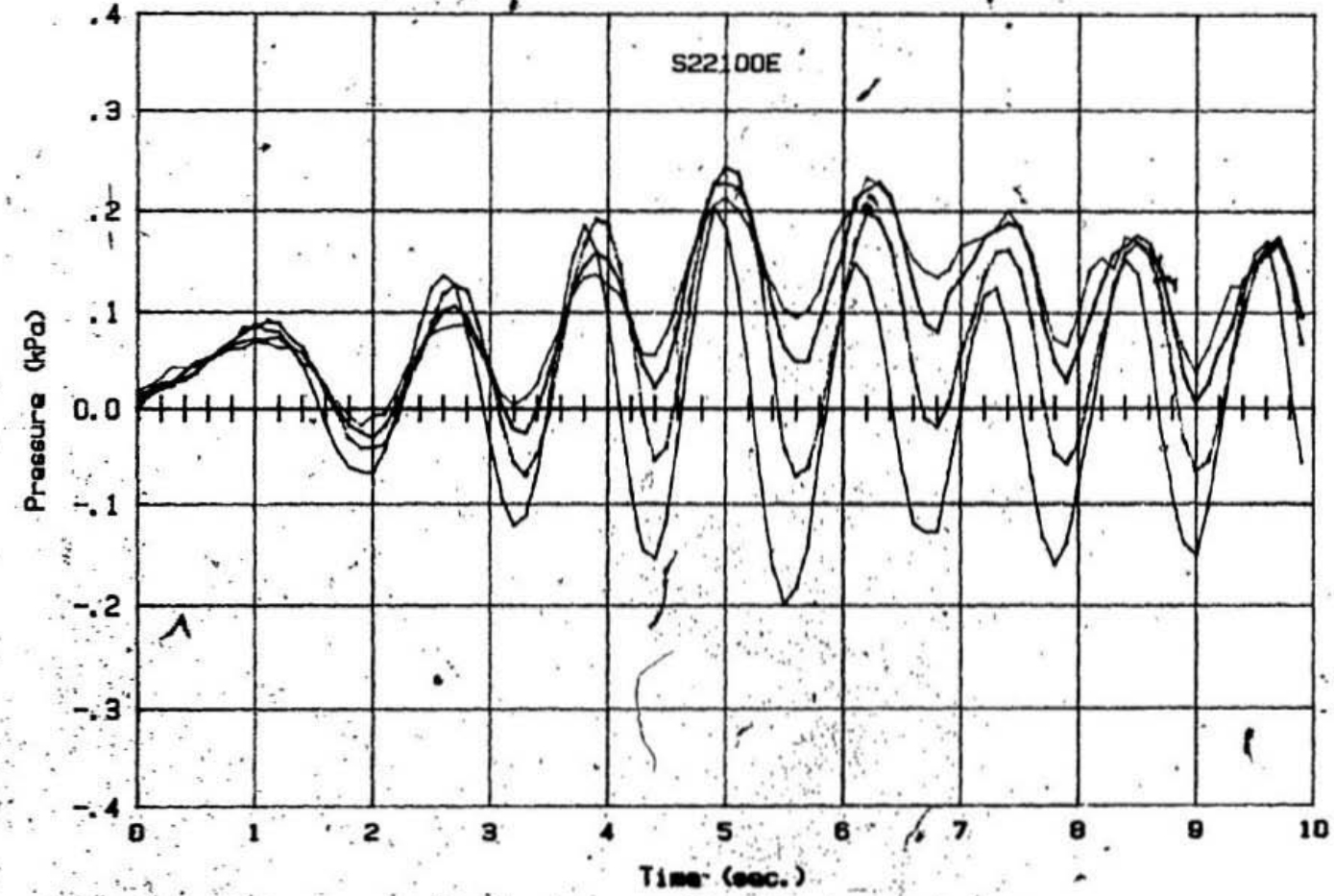


FIGURE 60 POREWATER PRESSURE RESPONSE (ρ_D = 1250 KG/M^3, VISIBLE FAILURE TO 1.5 CM DEPTH)

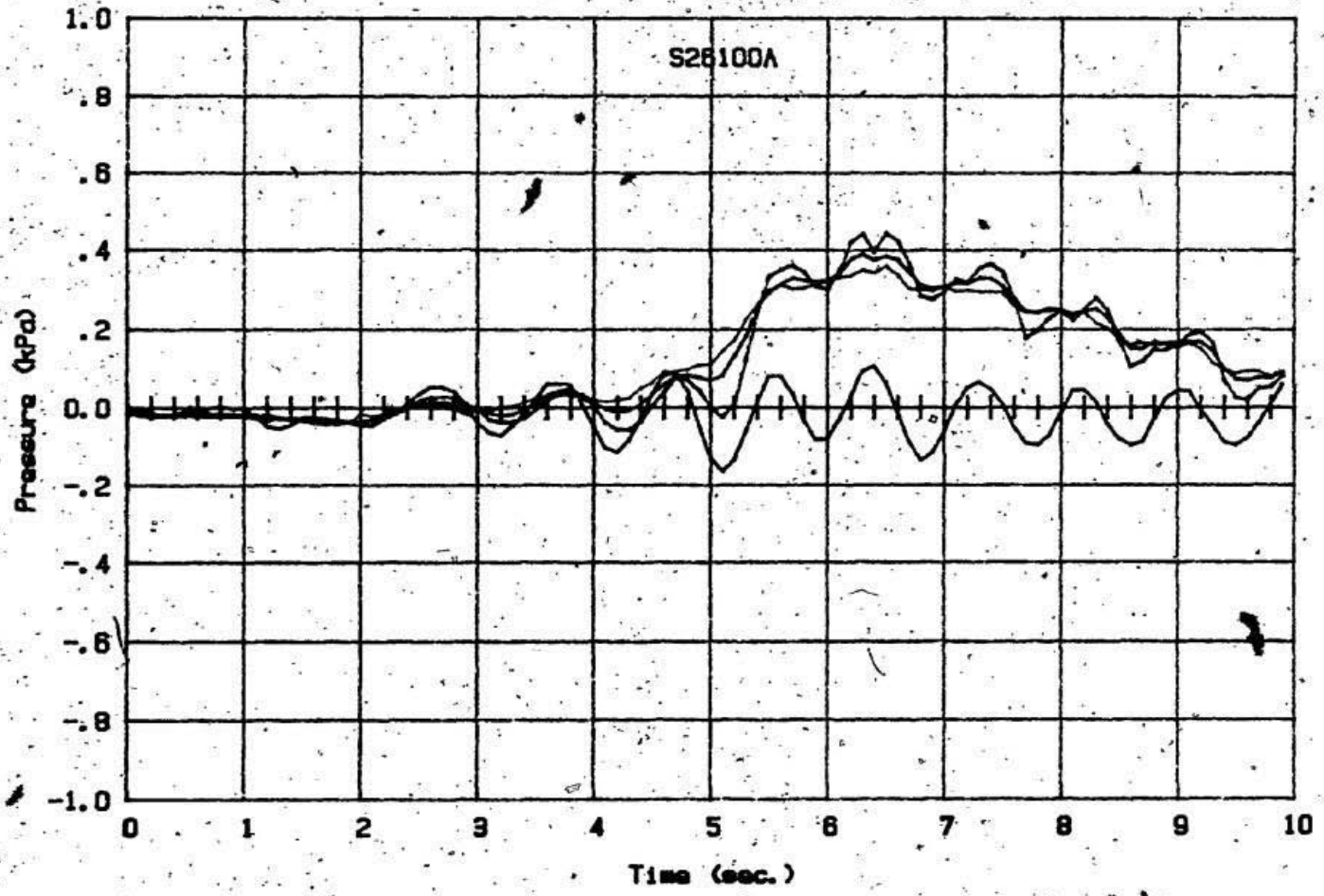


FIGURE 62 POREWATER PRESSURE RESPONSE (ρ_D = 1250 KG/M^3, VISIBLE FAILURE TO 3 CM DEPTH)

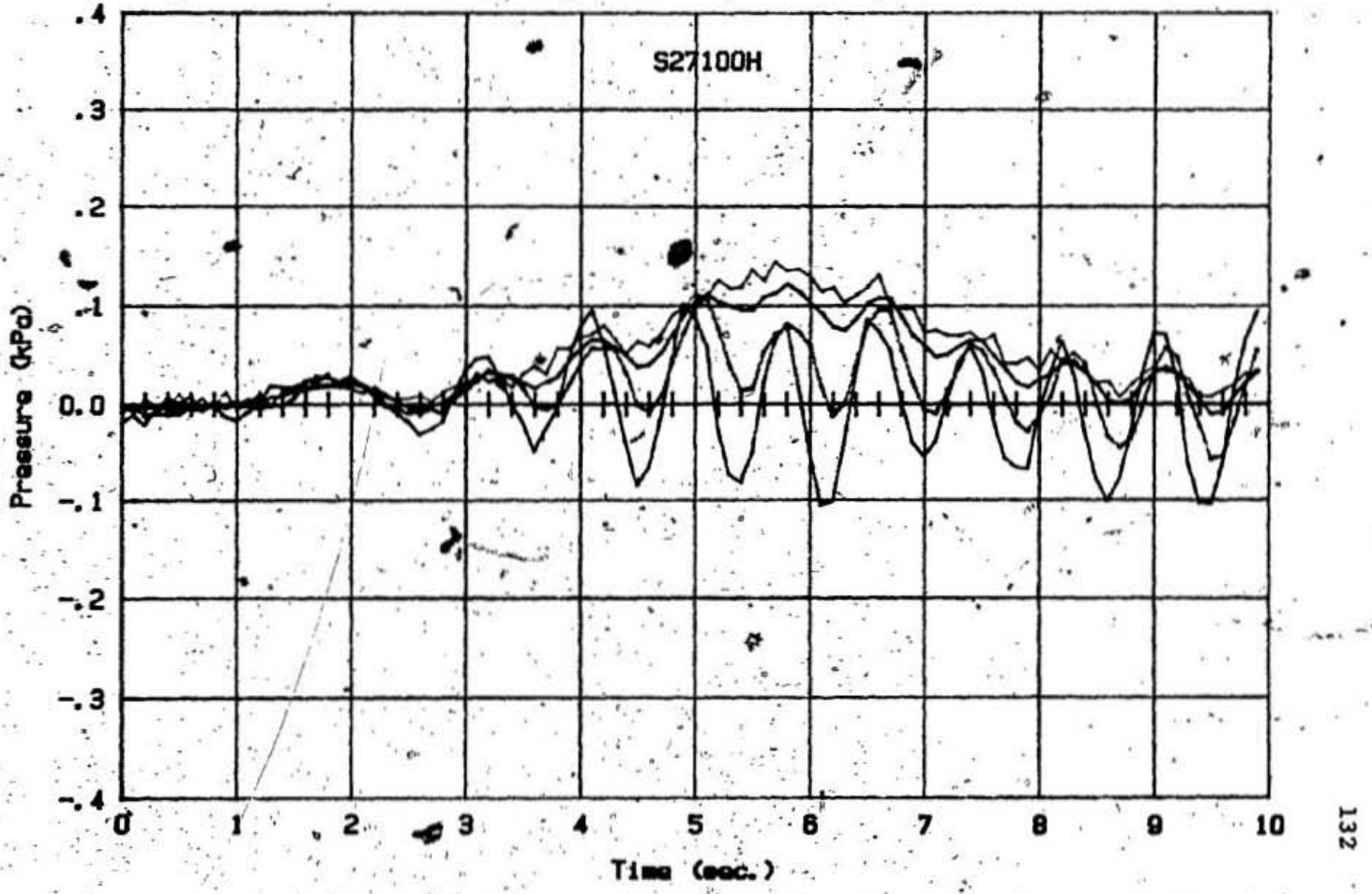


FIGURE 61 POREWATER PRESSURE RESPONSE (ρ_D = 1250 KG/M^3, VISIBLE FAILURE TO 2 CM DEPTH)

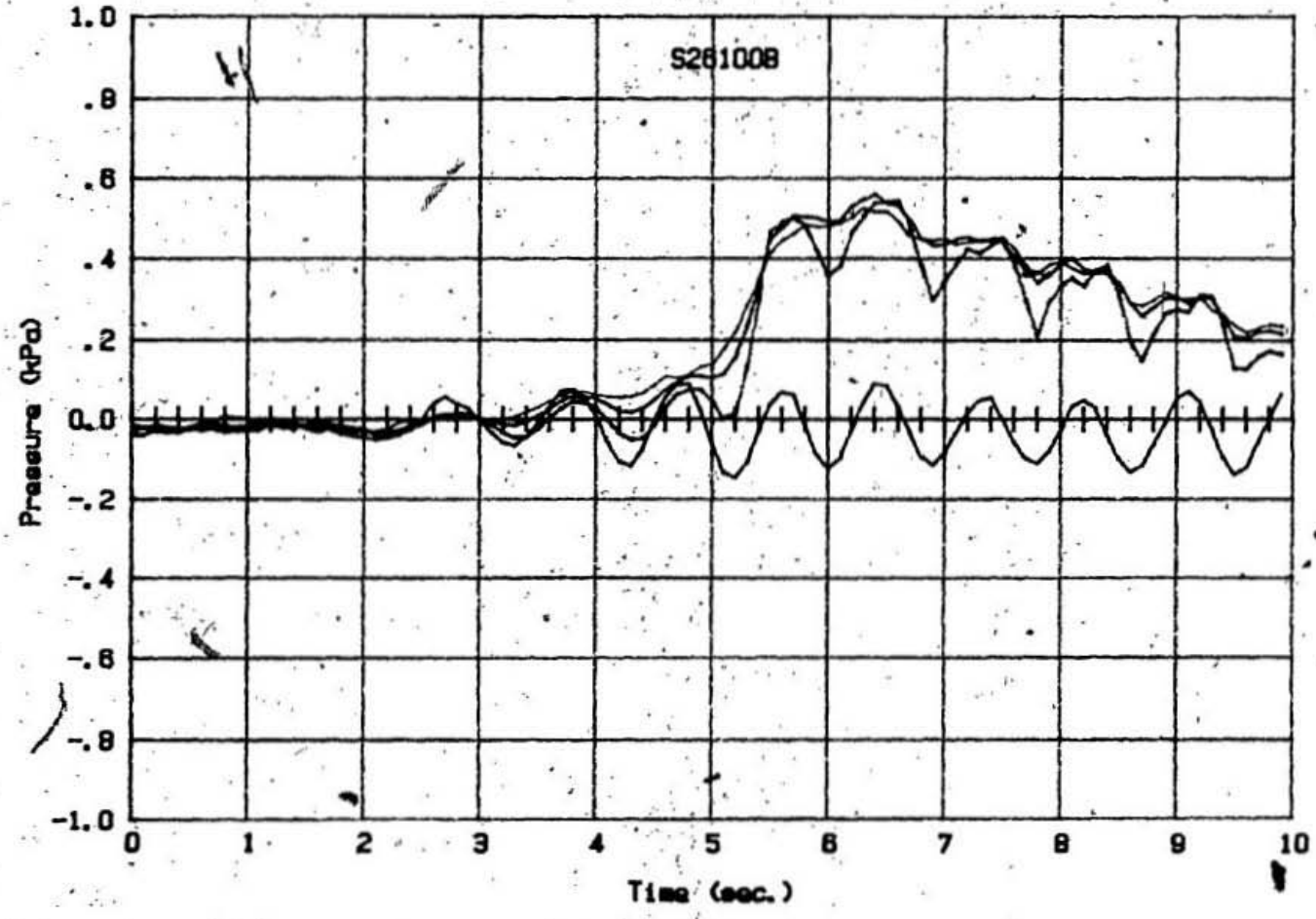


FIGURE 63 POREWATER PRESSURE RESPONSE (ρ_D = 1250 KG/M^3, VISIBLE FAILURE TO 5 CM DEPTH)

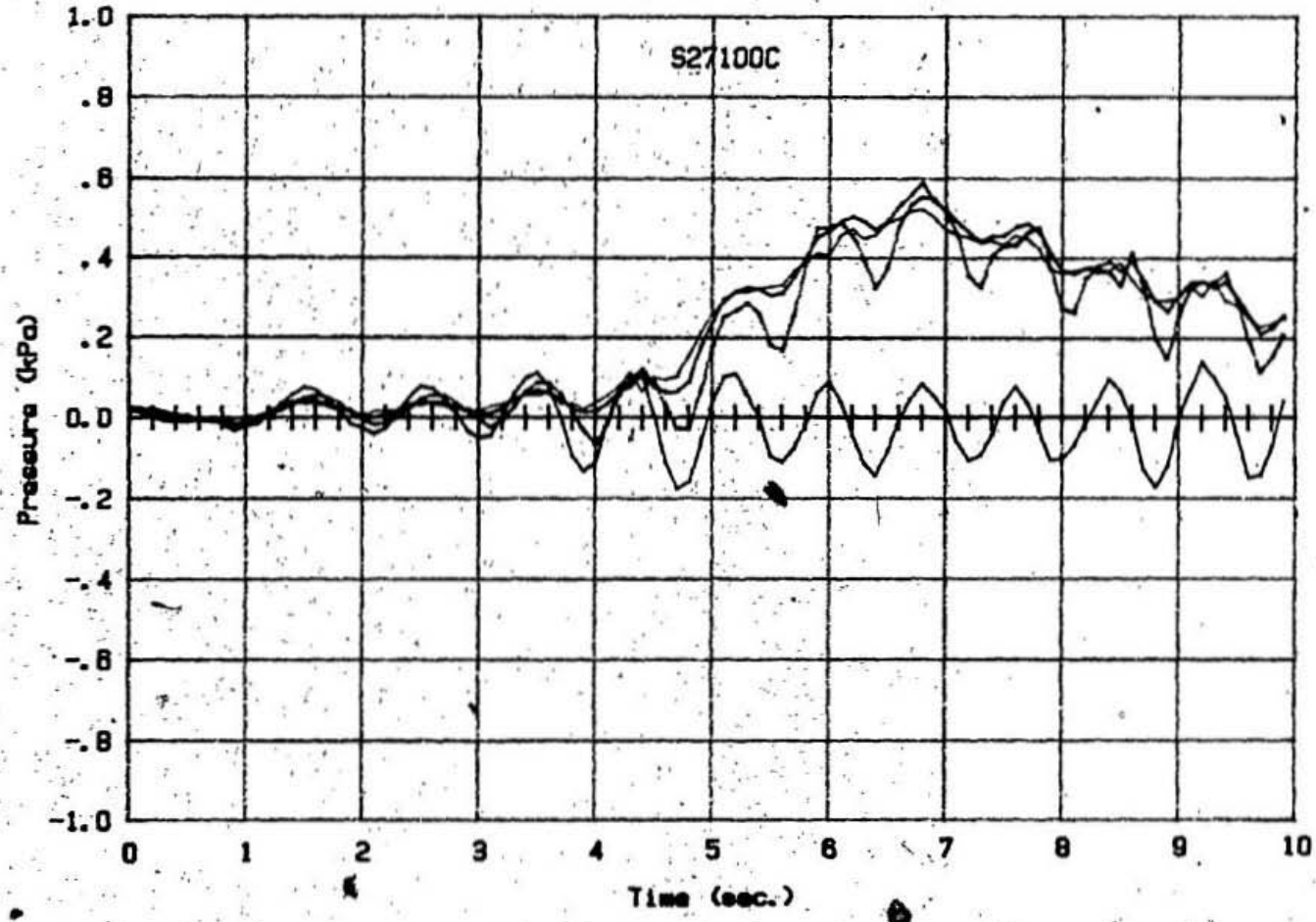


FIGURE 64 POREWATER PRESSURE RESPONSE (ρ_D = 1250 KG/M^3, VISIBLE FAILURE TO 5 CM DEPTH)

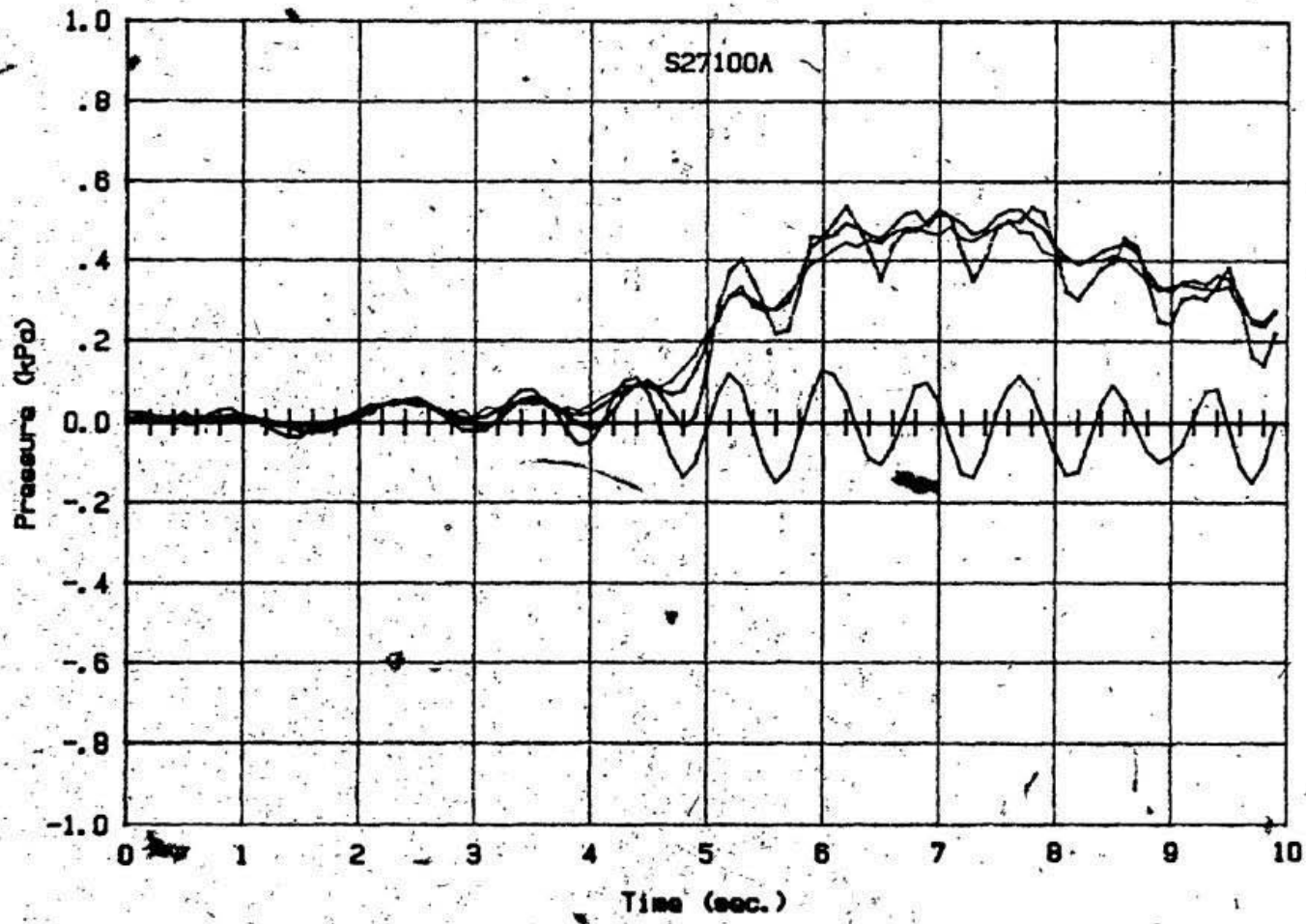


FIGURE 65 POREWATER PRESSURE RESPONSE (ρ_D = 1250 KG/M^3, VISIBLE FAILURE TO 5 CM DEPTH)

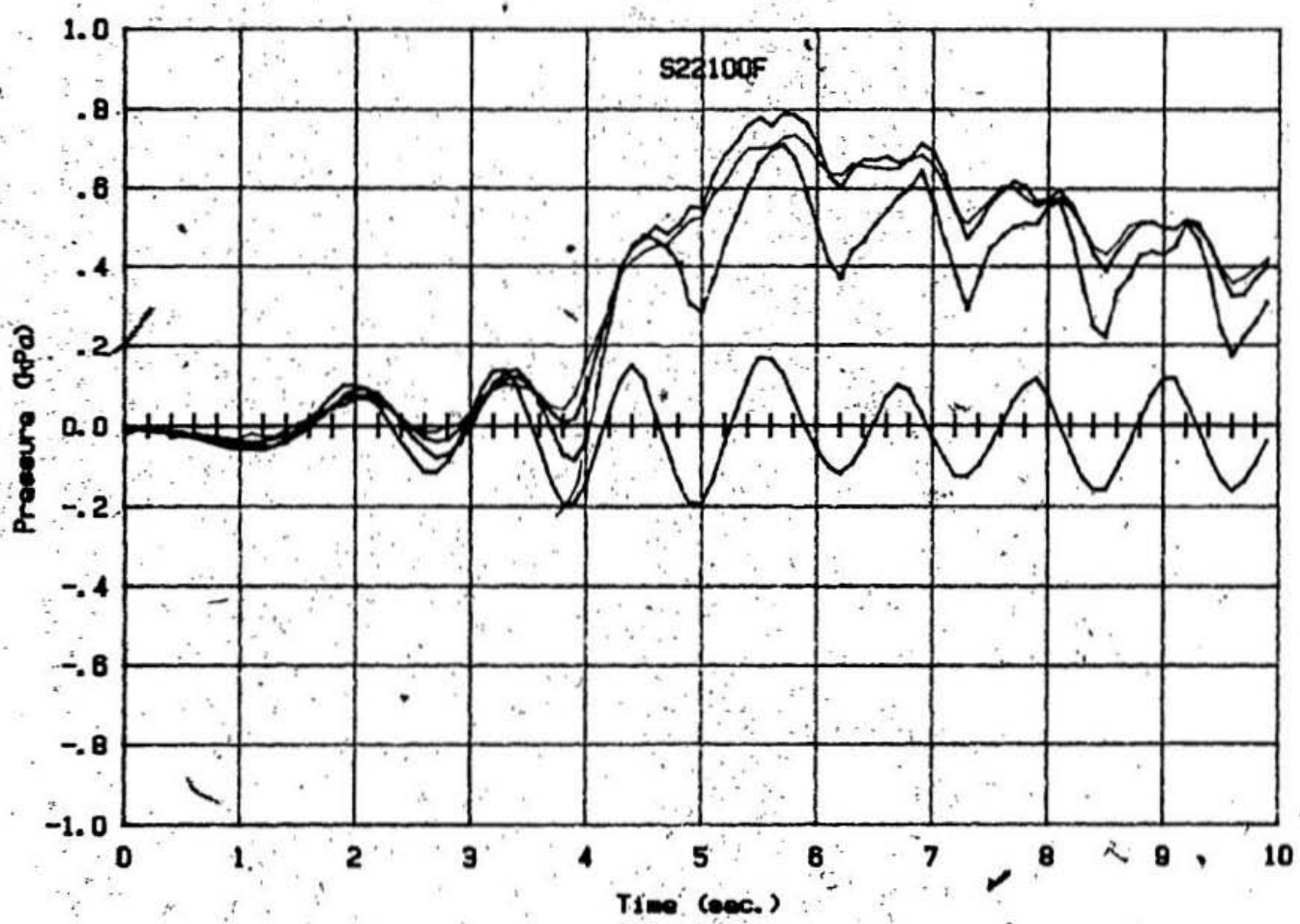


FIGURE 66 POREWATER PRESSURE RESPONSE (ρ_D = 1250 KG/M^3, VISIBLE FAILURE TO 7 CM DEPTH)

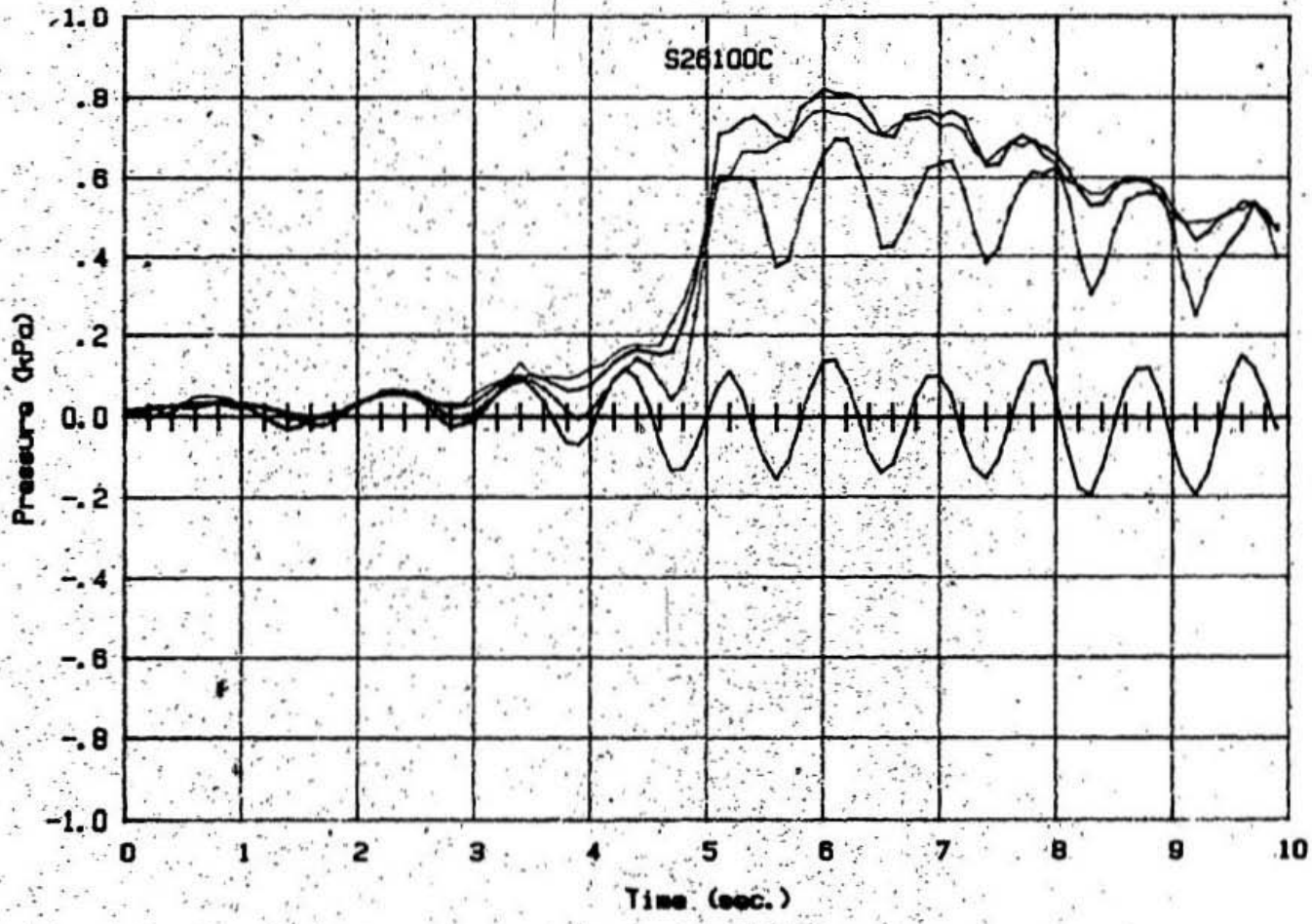


FIGURE 67 POREWATER PRESSURE RESPONSE (ρ_d = 1250 KG/M^3, VISIBLE FAILURE TO 10 CM DEPTH)

response during deeper failure. A simple explanation of what takes place is that when the wave characteristics reach a certain intensity the wave load directly causes soil failure. The depth of this failure appears to be related to wave characteristics as shown later. This failure allows a rearrangement of soil particles, during which time the soil behaves as a liquid and thus the high porewater pressures during deeper failure.

A summary of maximum excess porewater pressures developed during these tests is given in Table 6. The observed depth of failure, Z_L, and the soil overburden pressure corresponding to this depth are also given in the table. It can be seen that the measured net increase in porewater pressure is nearly equal to the overburden pressure in each case. The effective stress at the level of measurement must thus be approximately zero, indicating a correlation of the observed failure depth with the porewater pressure measurements and computations.

From visual observations through the glass wall, it was possible to delineate the soil movement under different wave conditions. The general pattern of soil failure observed was that the soil movement would begin at the mudline and progress deeper with each successive wave until the final depth was achieved. Once a maximum depth of failure was reached, the process would be reversed and the

TABLE 6

Measured and Computed Failure Depths and Corresponding Porewater Pressures

Fig. No.	Wave Characteristics		Observed depth of failure, Z_L (cm)	Raman-Nair liquefaction Depth (cm)	Raman-Nair depth of sliding (cm)	Net increase in pore water pressure at z = -30 cm (kPa)	
	Period (sec)	Water depth (cm)				Measured	Calculated, assuming liquefaction to Z_L
57	0.84	42	0	1.1	3.5	0.0	0.0
58	1.12	27	0	1.9	5.7	0.1	0.0
59	1.12	30	0	2.3	6.1	0.05	0.0
60	1.12	31	1.5	2.3	6.1	0.15	0.12
61	0.79	15	2	0.0	2.0	0.1	0.16
62	0.84	19	3	1.0	2.7	0.35	0.24
63	0.84	22	5	1.0	2.7	0.5	0.4
64	0.79	35	5	0.0	2.0	0.46	0.4
65	0.79	35	5	1.0	2.3	0.48	0.4
66	1.12	33	7	2.0	5.0	0.66	0.56
67	.84	30	10	1.0	4.0	0.75	0.8

soil movement would become progressively less with each wave and the soil layer was gradually densified. Figures 68(a,b) show the variation of failure depth with wavelength for wave heights of 10 cm and 6.5 cm respectively. Figure 68(c) shows the depth of failure for different wave heights when water depth and wavelength are kept constant. Obviously higher waves cause deeper soil failure. From the test results it was seen that soil failure occurs when wave steepness, H/L, is between 0.04 and 0.1. A comparison was made between the experimental results of failure depth and published theoretical computations (Raman-Nair, 1984). It can be seen in Figure 68 that there is no significant correlation. The computations involve soil parameters such as Poisson's ratio, permeability, dry unit weight, shear modulus and sand density. Of these variables, permeability, dry unit weight and sand density can be determined in the laboratory and can be used with some confidence, but parameters such as Poisson's ratio and shear modulus have been estimated by Raman-Nair (1984) from results published for equivalent soils.

It can be shown that the theoretical computations will be quite sensitive to variations in the above parameters. For example Figure 68(d) shows the effect of density on failure depth (Raman-Nair, 1984). It was also demonstrated that changes in other parameters have a similar effect.

As mentioned earlier, it was observed that after failure, the excess porewater pressure dissipated and the soil gradually densified. This process of densification was confirmed by two different types of observations. For example, when the depth of wave-induced failure extended about 8 cm below the mudline it was noticed that the original elevation of the mudline decreased by about 1.0 cm. Similarly when the depth of failure was 16 cm the mudline elevation dropped by about 2.0 cm. Thus it was observed that the entire zone of failure was densified after the dissipation of excess porewater pressure.

The phenomenon of soil densification was also verified by determining the soil densities at several depths before and after wave induced failure by sampling the soil with a thin wall sampler. The results are shown in Figure 69. Graphs #1 and #2 are the typical initial dry densities before the soil was subjected to wave action. Graph #3 is a typical profile of the soil density for a situation where the soil was subjected to wave action but did not liquefy. It may thus be concluded that under circumstances where there is no visible soil failure there is no change in density at depth. However, when inserting the thin wall sampler into the surface sand there appeared to be a thin denser crust just at the mudline which offered higher resistance to sampler penetration. This phenomenon was not quantified further.

In figure 69, it may appear that there is a considerable variation in the values of initial densities as represented by Graphs #1 and #2. This variation which is in the order of 4% is due to the practical limitation of sampling a loose soil of this type.

Density measurements were made of the loose sand after the soil was subjected to wave induced liquefaction and subsequent densification. Graphs #4 to #7 are the typical results of the measured density after failure. It is shown quantitatively that there is a change in density as a result of the wave effects. However, it has not been determined whether this phenomenon extends below the zone of failure. Further work is required to precisely delineate this densification zone.

4.2.3 Additional Triggering Forces Causing Soil Failure

In a previous section it was demonstrated that a sudden shock will increase the pore water pressure inside the soil which could then trigger a liquefaction failure of the entire soil bed. Such a sudden increase in pore water pressure could also happen in combination with wave induced pore water pressure. In order to demonstrate this in the laboratory, a loose sand (ρ_d = 1250 kg/m^3) was used with waves that would not by themselves cause liquefaction failure. The normal steady state response to waves is shown in the first part of Figure 70. After about 3 seconds a 260

gram lead mass was dropped from a height of 6 cm above the bottom onto the sand bed, at a horizontal distance of about 10 cm from the pressure transducer location. The porewater pressure response as recorded by the pressure transducers is shown in Figure 70.

The porewater pressures recorded are similar to wave induced porewater pressures measured when liquefaction occurred near the mudline. Soil liquefaction was also visually observed in this test where soil movement was seen to occur to a depth of about 2 cm and the mudline finally dropped in elevation by about 4 mm.

The above observations have practical significance in terms of seabed installations and the stability thereof. It is likely that the seabed may be stable under wave induced pressures, but a failure could be triggered by a localized phenomenon associated with construction activities. The extent to which this localized phenomenon will affect an extended zone of the seabed and the magnitude of the effect are topics which require further work.

4.2.4 Effects of Waves on a Sloping Bed of Sand

Two types of tests were done under this category in the laboratory. In one series, the sand bed was placed at a uniform slope in the test section of the tank. These tests were intended to simulate the wave-soil interaction for infinite slopes. However, one limitation in these tests was

that the maximum slope that could be obtained for the soil was about 1:10, which was dictated by the dimensions of the tank. The other series of tests involved finite slopes.

In the first series of tests on a sloped sand bed, gentle slopes of about 1:10 representing infinite slopes, were formed in both directions. Thus the effects of waves approaching shallower or deeper water were examined. Porewater pressures were recorded at about the middle of test section and are shown in Figures 71, 72, 73, 74, and 75. Visually recorded mudline elevations before and after soil failure are recorded in Figures 76, 77, 78, 79, and 80. The generated waves had a frequency of 1.03 Hz.

The slope failure in Figure 76 is an instantaneous slump that occurred during a period of about 1 second, and extended over a distance of 3.2 m. It was observed that the soil appeared to remain liquid in the middle portion of the slump, for a period of about 10 seconds. Figure 71 shows that the excess porewater pressure was mobilized in approximately 1 sec (between the 4th and 5th second), and corresponds to the failure time observed during the test. It is also seen from Figure 71 that the excess porewater pressure is dissipated in 10 seconds which corresponds to the period during which the soil was observed to be in a liquid state during the densification process.

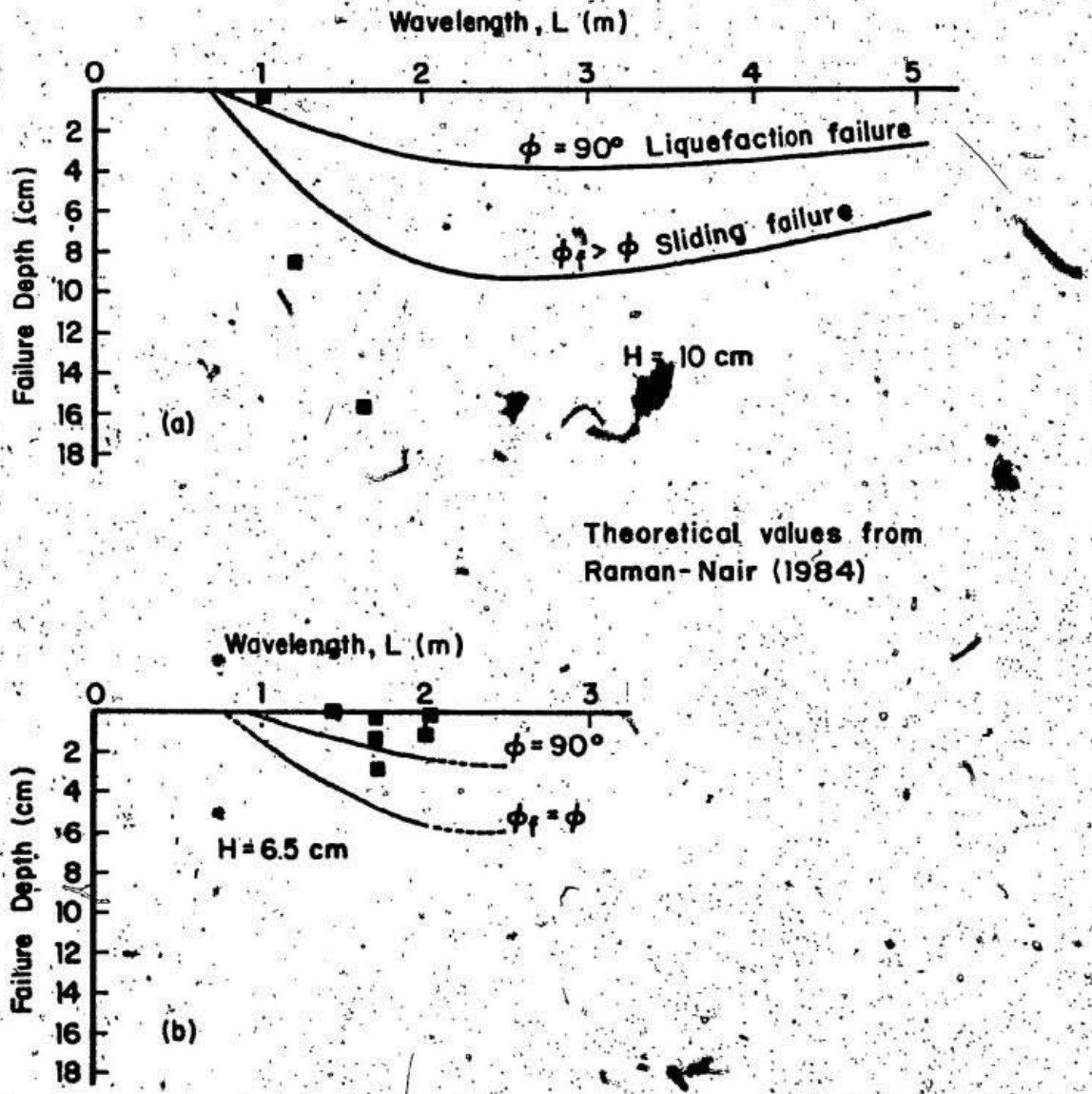


FIGURE 68 COMPUTER AND MEASURED DEPTHS OF WAVE INDUCED FAILURE FOR A FLAT BED OF LOOSE SAND

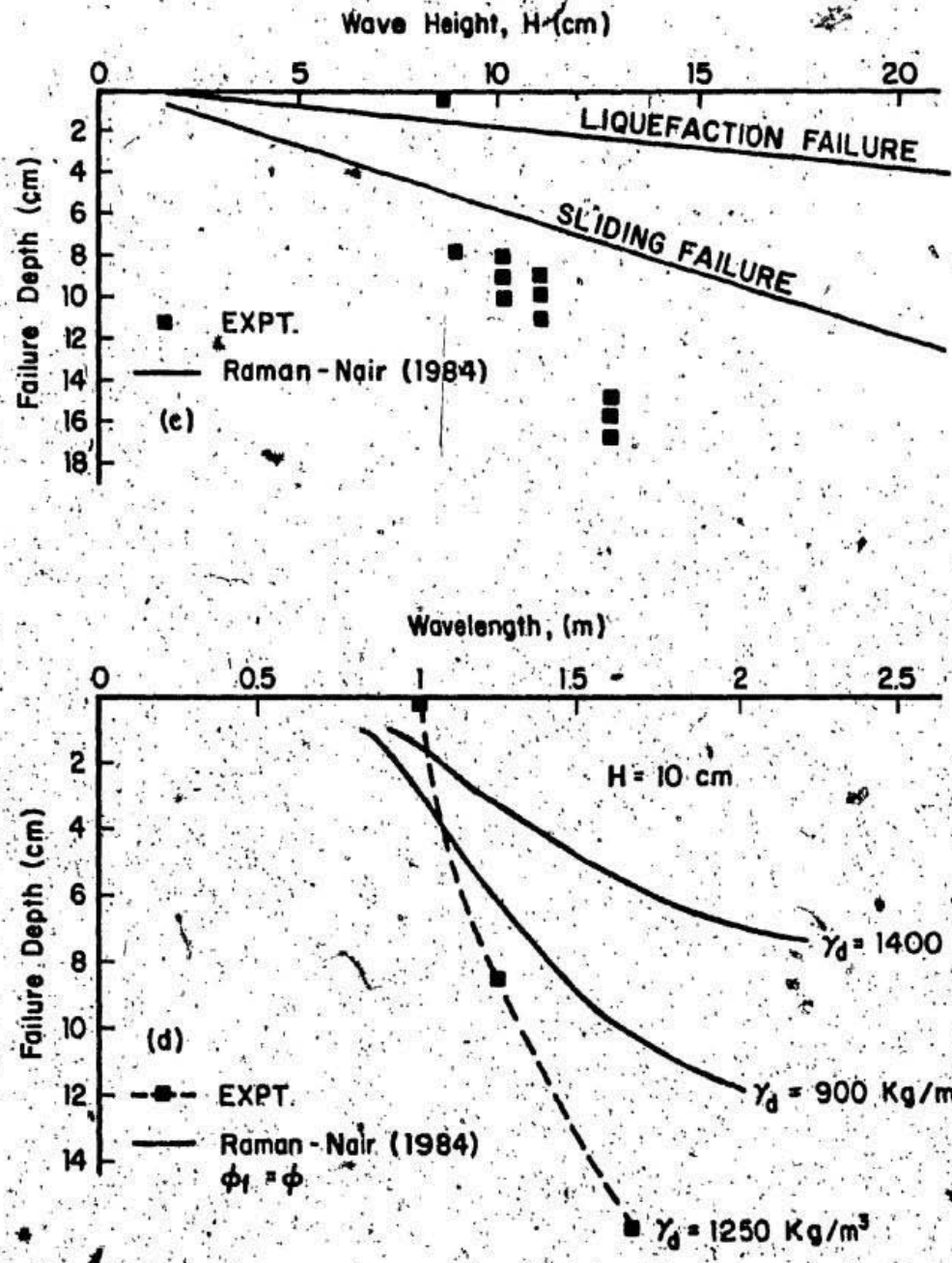


FIGURE 68 COMPUTED AND MEASURED DEPTHS OF WAVE INDUCED FAILURE FOR A FLAT BED OF LOOSE SAND

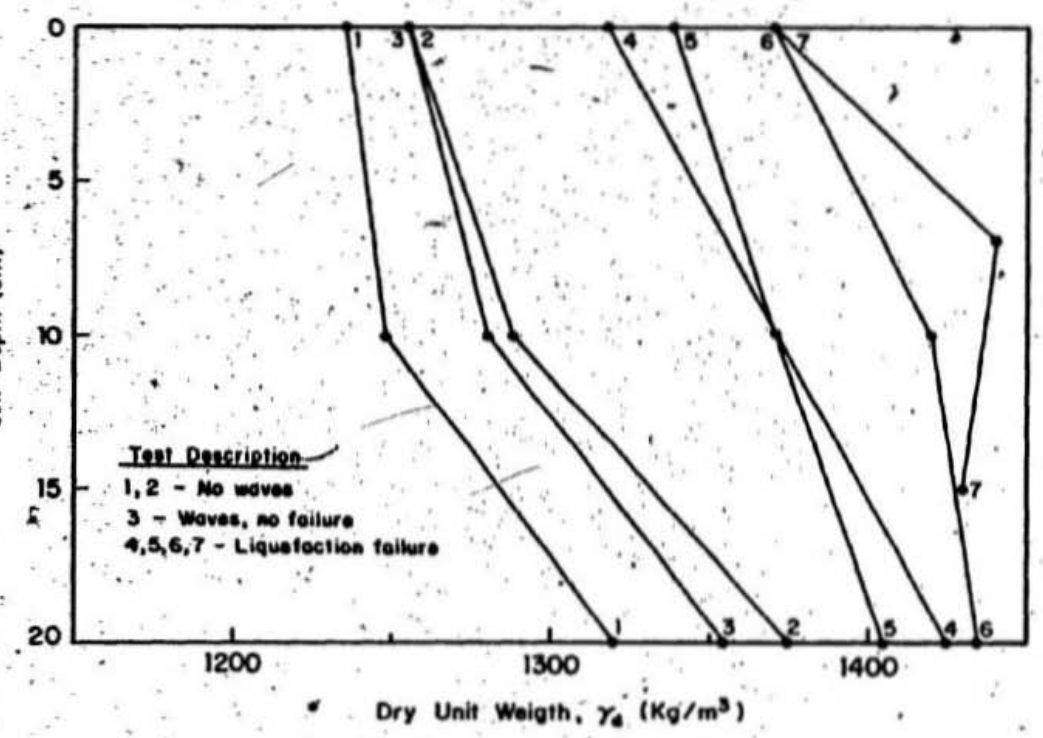


FIGURE 69 SOIL DENSIFICATION AFTER LIQUEFACTION

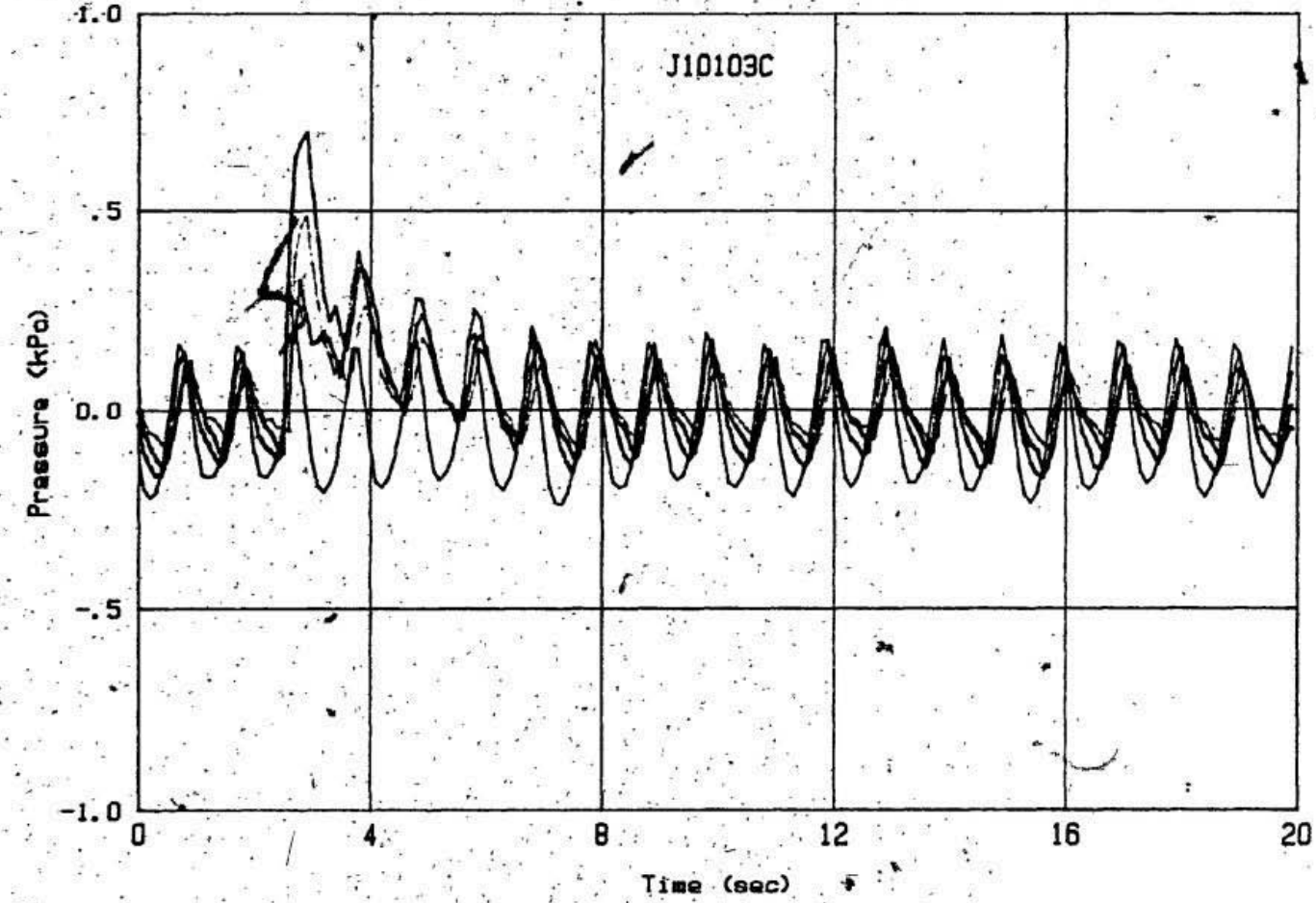


FIGURE 70 POREWATER PRESSURE RESPONSE TO COMBINED WAVES AND SHOCK LOADING

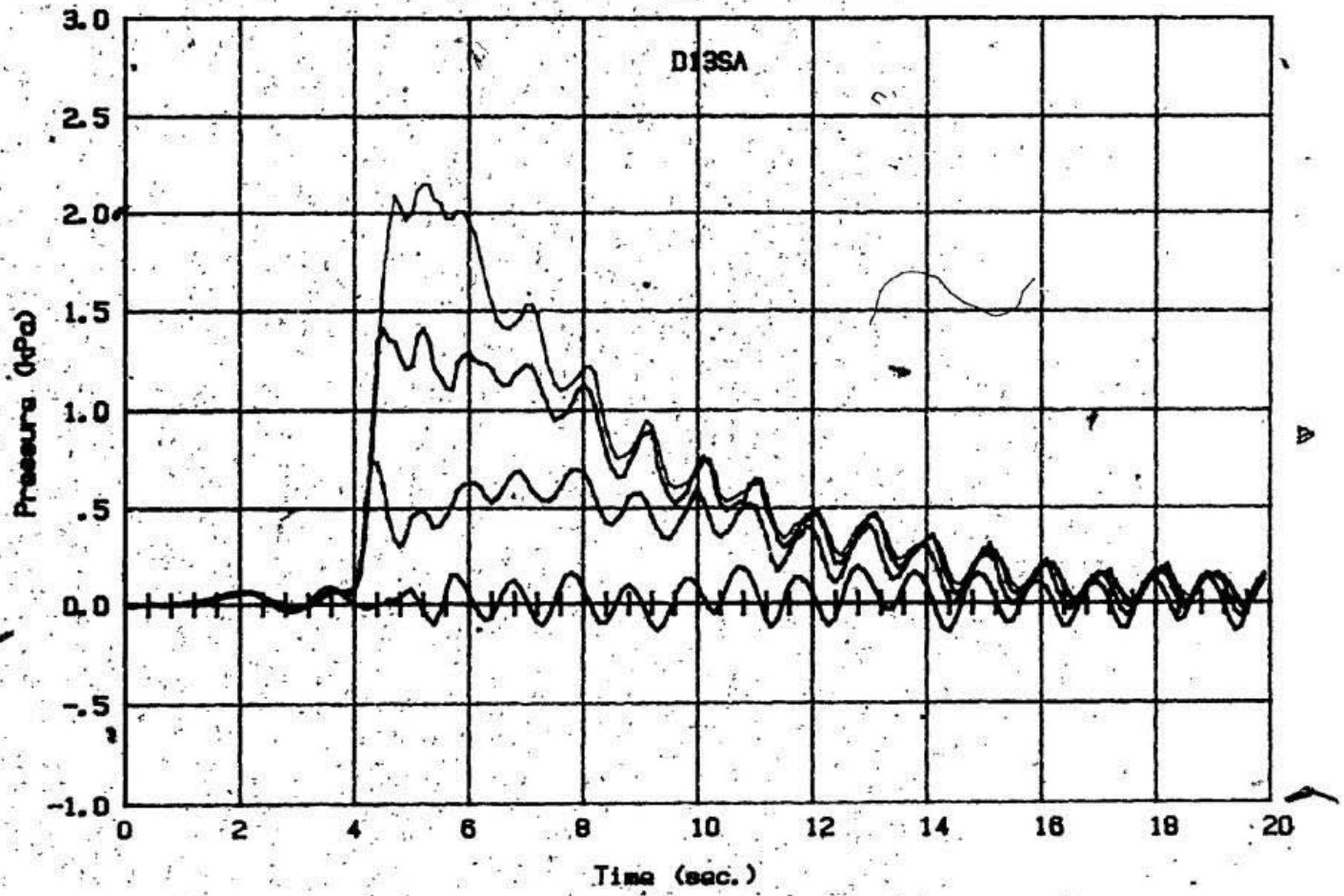


FIGURE 71 EXCESS PORE-WATER PRESSURE DURING WAVE INDUCED SLOPE FAILURE

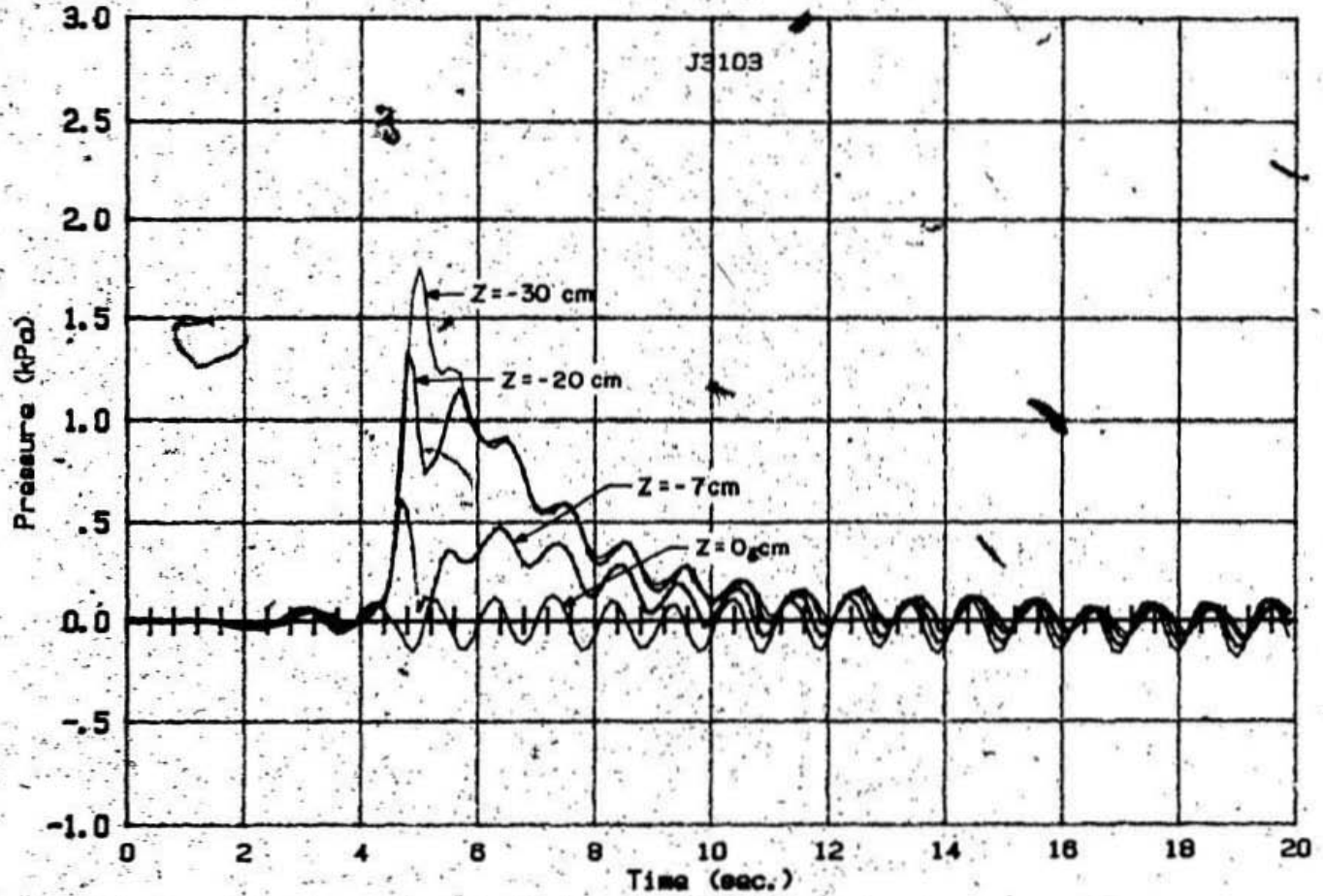


FIGURE 72 EXCESS PORE-WATER PRESSURE DURING WAVE INDUCED SLOPE FAILURE

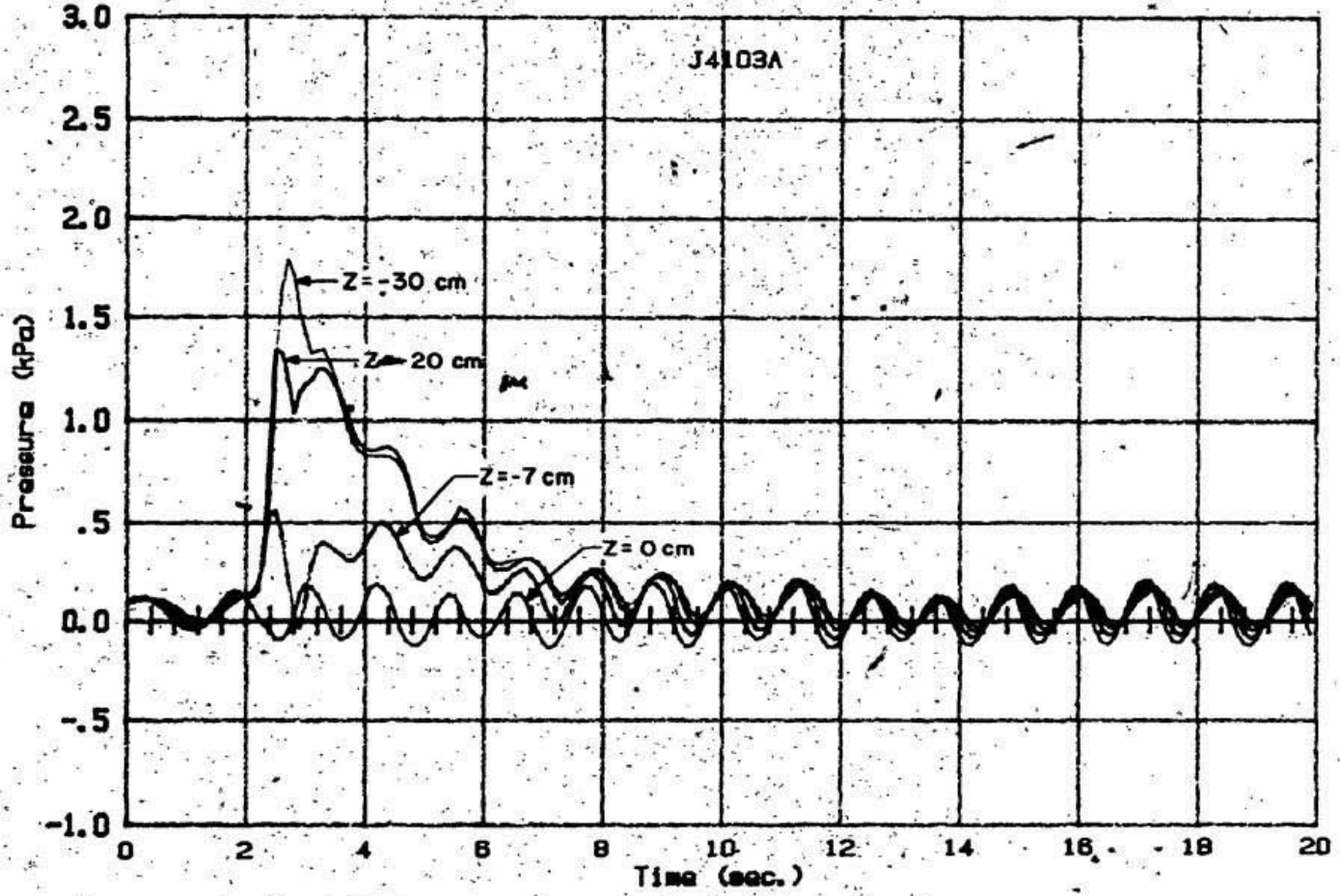


FIGURE 73 EXCESS PORE-WATER PRESSURE DURING WAVE INDUCED SLOPE FAILURE

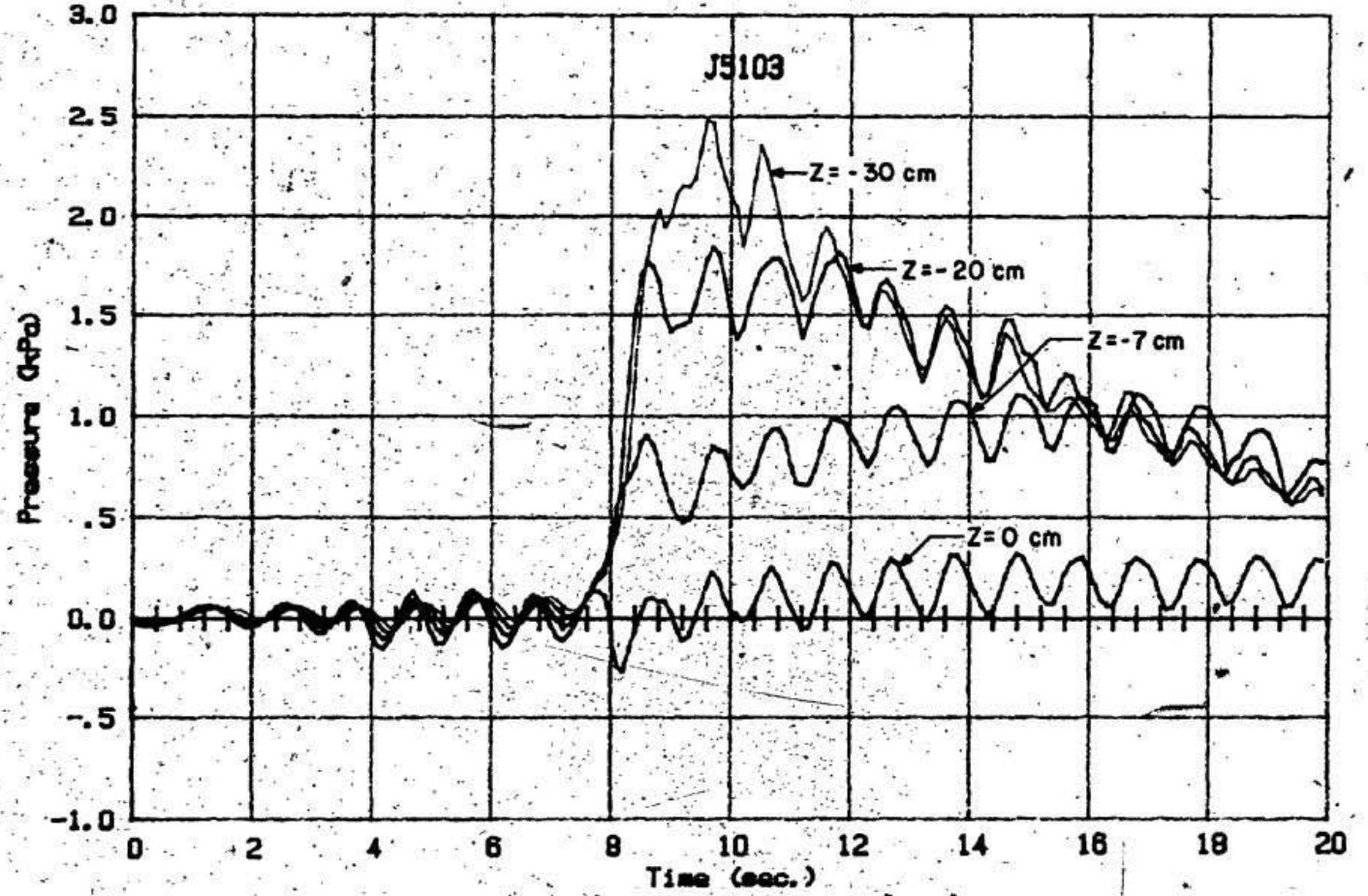


FIGURE 74 EXCESS PORE-WATER PRESSURE DURING WAVE INDUCED SLOPE FAILURE

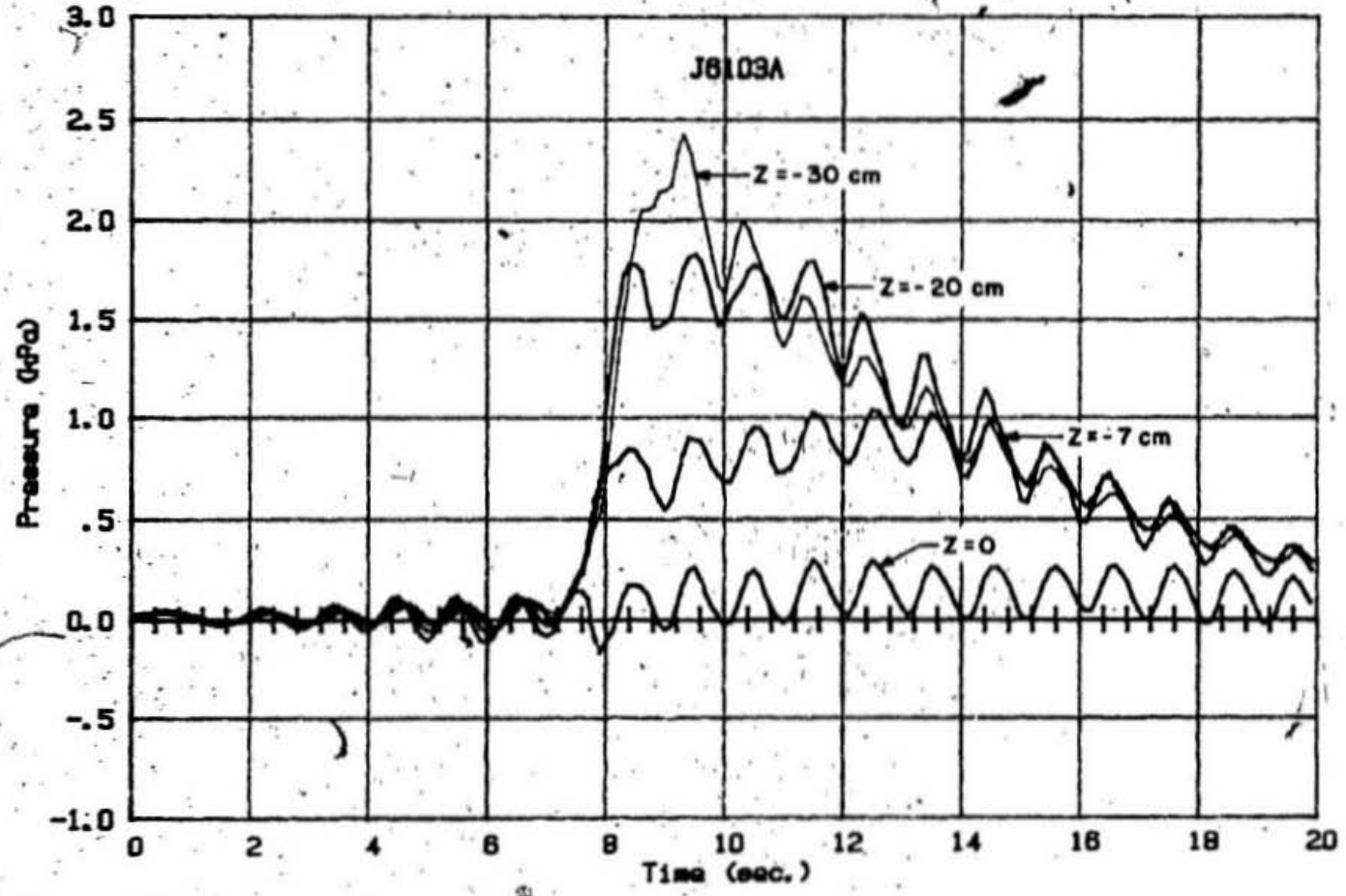


FIGURE 75 EXCESS PORE-WATER PRESSURES DURING WAVE INDUCED SLOPE FAILURE

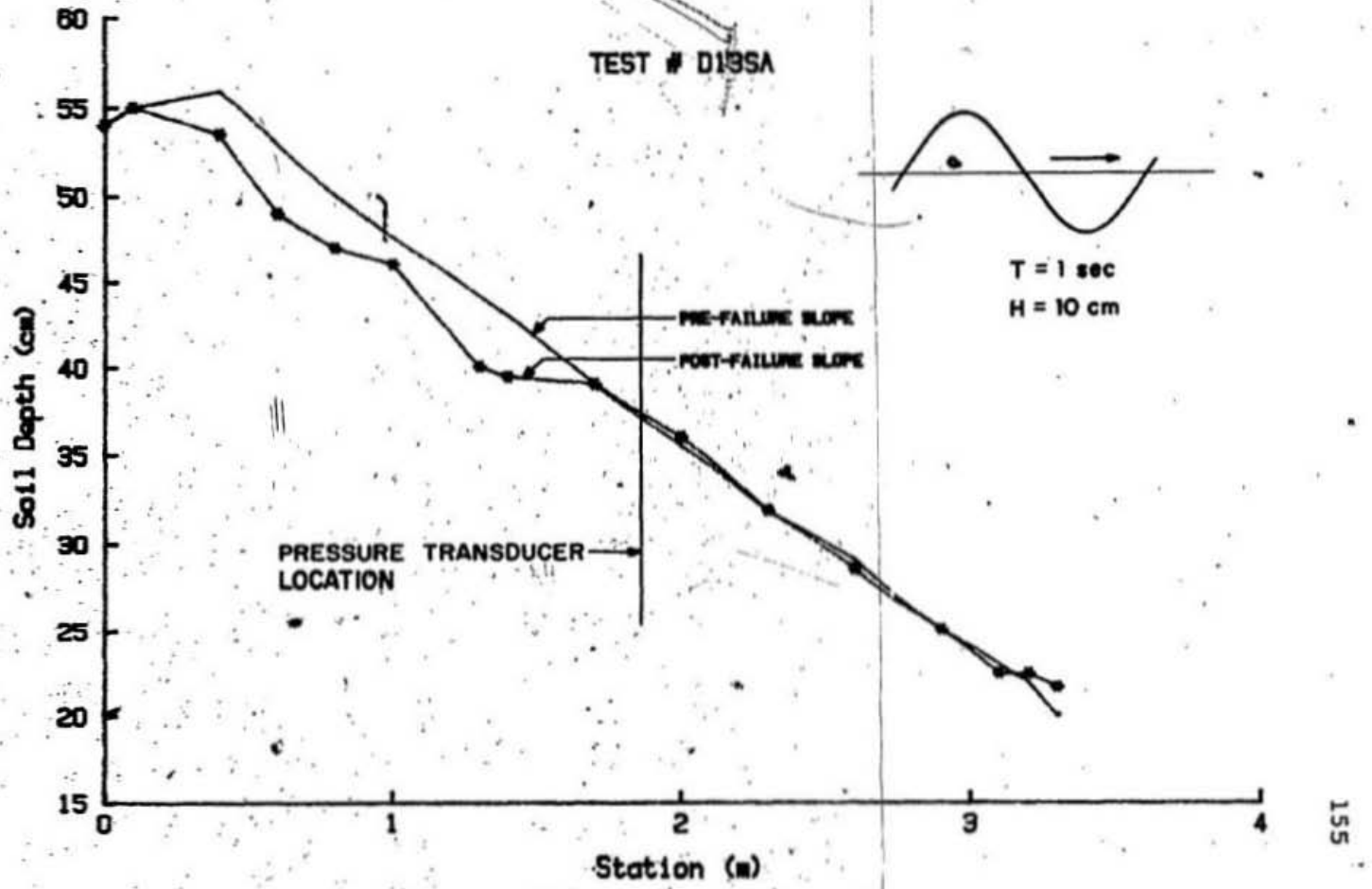


FIGURE 76 WAVE INDUCED SLOPE FAILURE

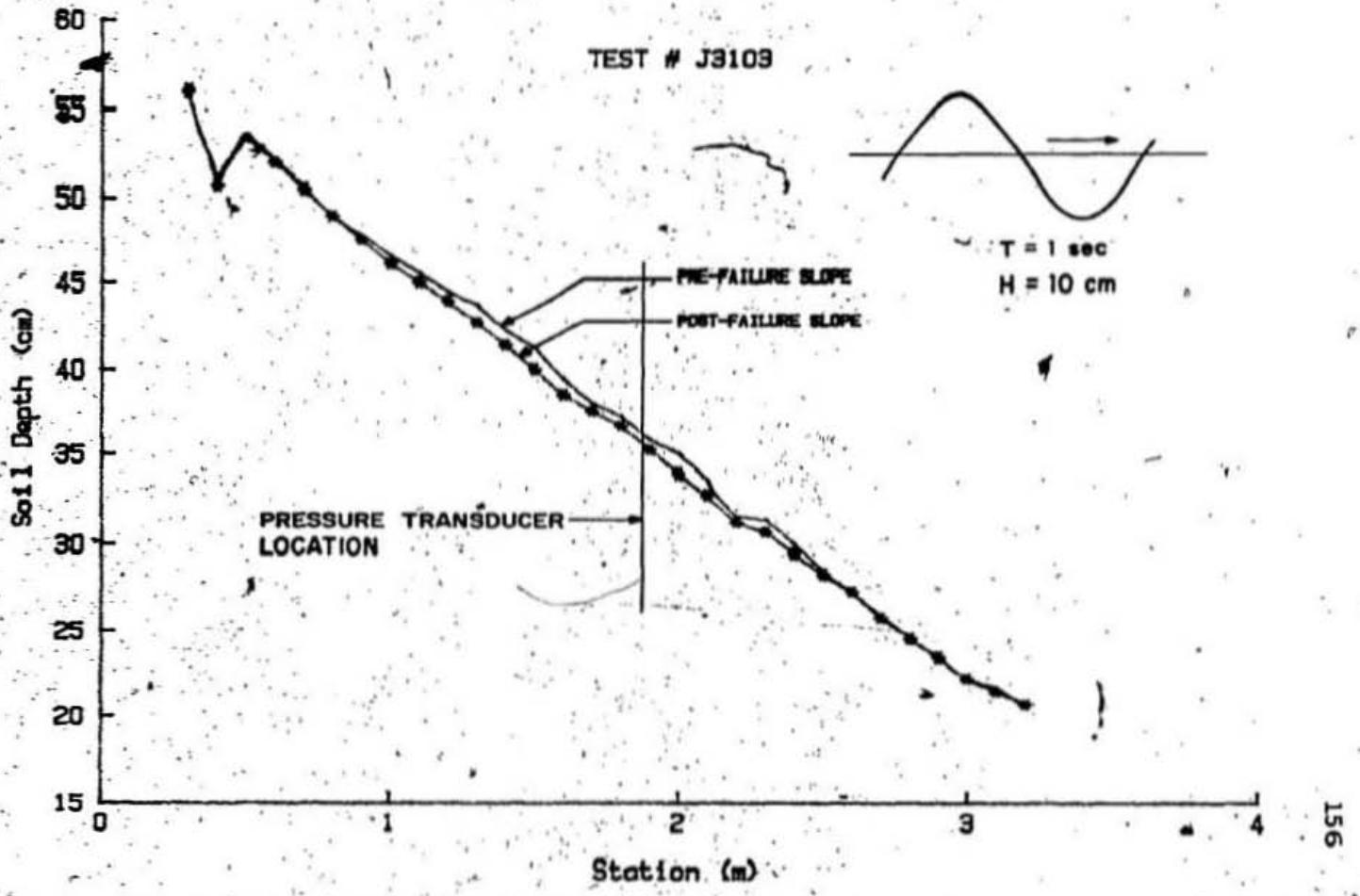


FIGURE 77. WAVE INDUCED SLOPE FAILURE

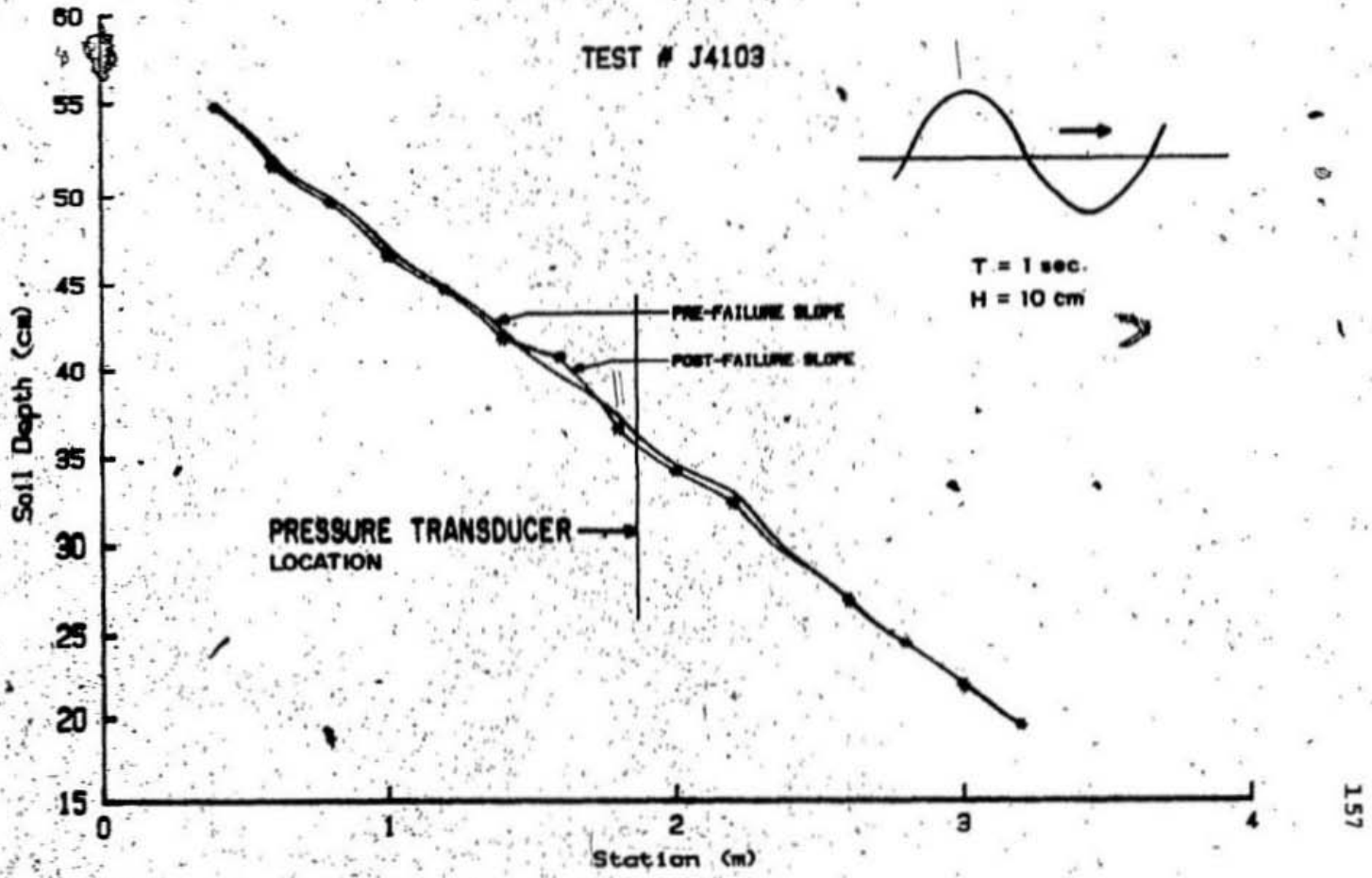


FIGURE 78 WAVE INDUCED SLOPE FAILURE

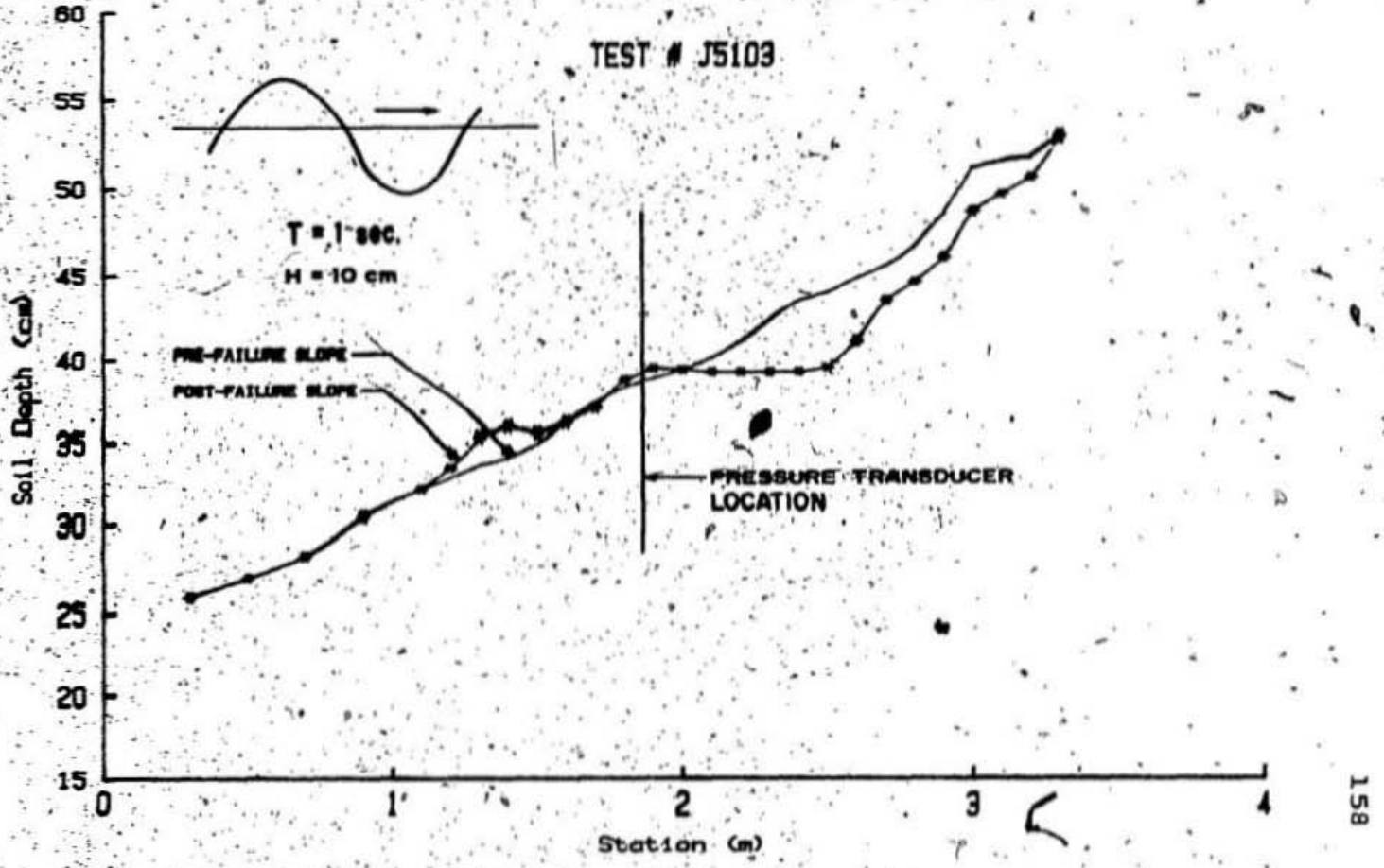


FIGURE 79 WAVE INDUCED SLOPE FAILURE

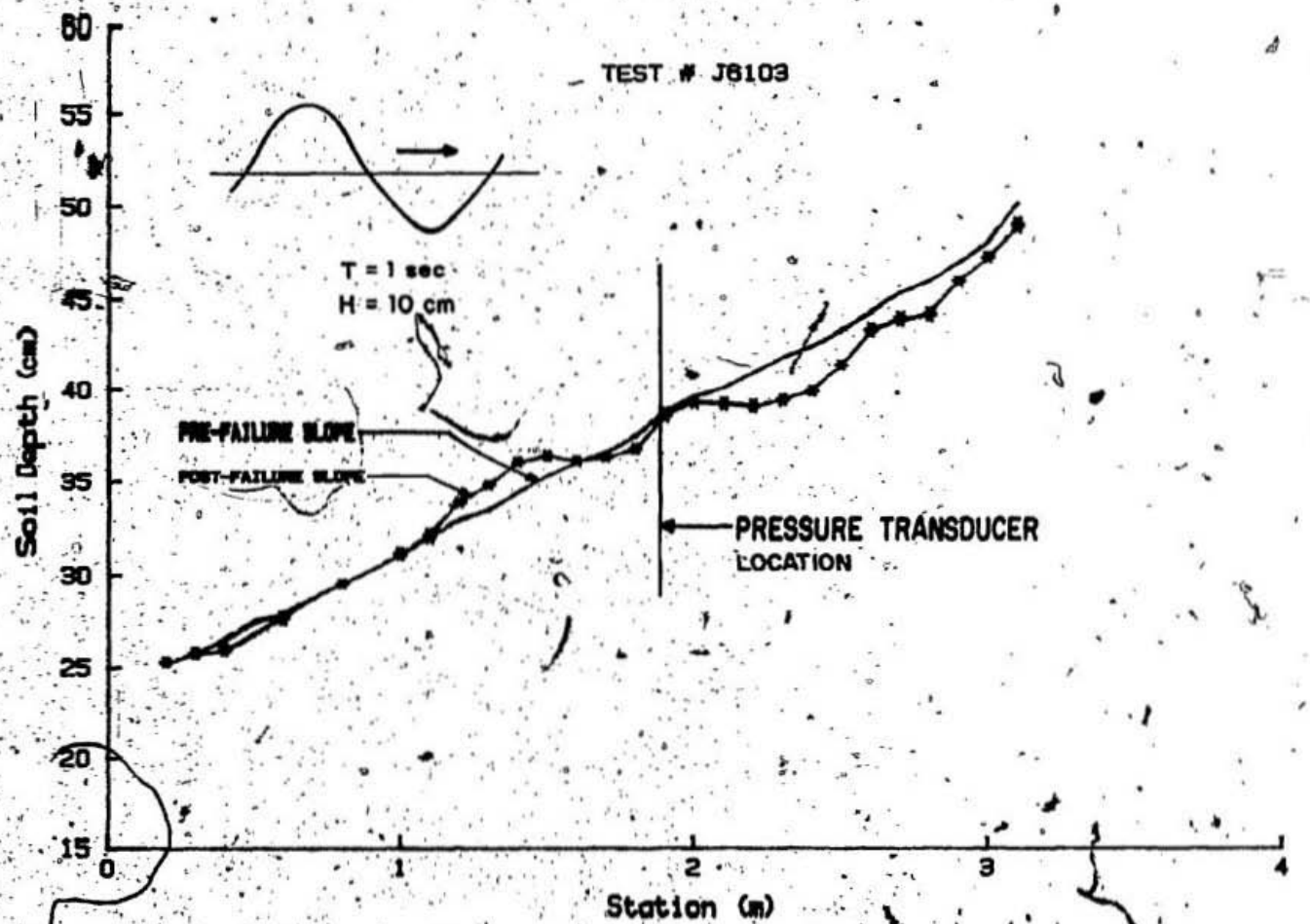


FIGURE 80 WAVE INDUCED SLOPE FAILURE

It was seen from visual observations and from an interpretation of the porewater pressure measurements in the above records, that the failure of the sloping bed of sand is sudden, unlike the failure in the tests with a flat bed (Figure 65) where failure began at the surface and progressed deeper gradually. Comparison of Figures 71 and 65 clearly shows that the pressure buildup is relatively sudden in the case of a sloped soil, which is followed by mass slumping. The excess porewater pressure is dissipated slowly in both cases, after failure.

There are some differences in the extent and type of failure when the waves travelled down the slope and up the slope. When the waves progressed toward shallower water, the excess porewater pressure developed during the slump was approximately 25% more than when the waves progressed toward deeper water. The change in soil profile was also noticeably more and the duration of the instability was longer. It was also noticed that when waves progressed toward shallower water a relatively larger number of waves was required to cause failure. However, the types of sudden failure and rapid development of excess porewater pressure were similar.

The drainage characteristics of a sloping seabed are different from those of a flat seabed because of the

slope and these differences are seen in the pressure records. One example is the phase lag discussed earlier between the wave induced pressure at the mudline and the porewater pressures inside the soil. This difference can be seen in Figures 71 and 74. In both cases, before failure there was a phase lag between the pressure changes at the mudline and the pressure change at depth. In the case of waves approaching deeper water this lag was similar to a flat seabed in that the pressure change at depth always lagged behind the pressure change at the mudline. However, in the case of waves approaching shallower water, after the initial failure the pressure change at the mudline lagged behind the pressure change at depth.

Tests with a slightly different soil and a range of wave frequencies, have shown that phase lag is dependent on the slope but that the pressure pulse at depth generally lagged the pressure pulse at the mudline (Chari and Dawe, 1984). This is probably due to the fact that drainage is influenced by the direction of the waves.

The densification time for the soil when it failed due to waves approaching shallower water appears to be generally longer than the time required when it failed due to waves approaching deeper water. The factors affecting this process are not examined here and the observations at present are only qualitative.

A second series of tests was done to verify the effect of waves in triggering the failure of a finite slope. A relatively steep slope was formed in the middle of the flat test bed by carefully excavating a "V" shaped cut across the width of the tank as shown in Figure 81. The angle of the slope was very nearly equal to the natural ahgle of repose for the sand.

The porewater pressures were recorded as 1.1 Hz waves were passed over the test soil. The results are shown in Figure 82. A sudden increase in porewater pressure was recorded after the first 4 waves; this coincides with a visually observed soil failure. The type of failure and infilling of the excavated trench are shown in Figure 81 from visual observations.

From an examination of the recorded pore water pressures and the visual observation of the failure it may be concluded that the soil failure initially is a failure of the slope and not the liquefaction type of failure that was observed in earlier tests with a flat sand bed. It is also likely that this slope failure induces a consequent sudden pore water pressure in the lower pressure transducers at 20 cm and 30 cm below the mudline. There was no sudden increase in pressure at 7 cm below the mudline since the transducers were located at the edge of the trench on the far side of the excavation and failure was confined to the opposite slope of

the excavation near the wavemaker. Just after the initial failure there is a slight increase in pore water pressure at 7 cm depth; this is probably due to the hydraulic gradient set up as porewater is escaping from the location of densification. It is also probable that densification occurred only below the 7 cm depth. The soil failure was confined only to the slope of the trench near the waveboard; the opposite slope of the trench (on the beach side) and the flat test section were not affected.

Additional experiments were conducted in which a 260 gram mass was dropped from a height of 6 cm above the mudline, as already described for similar tests for a flat sand bed. In these tests it was found that the sudden increase in porewater pressure caused soil liquefaction under the combined effect of the shock and wave induced porewater pressures. However in this case the trench which extended across the width of the tank acted as a damper and the remaining test portion of the tank beyond the trench remained stable as seen in Figure 83. Figure 84 shows the porewater response.

The above observation is consistent with the conclusions of Vaid and Finn (1979) an Finn et al (1983) that the drainage from a sloping seafloor is faster than from a level one and that static shear stresses induced in a sloping seafloor tend to retard the rate of development of porewater

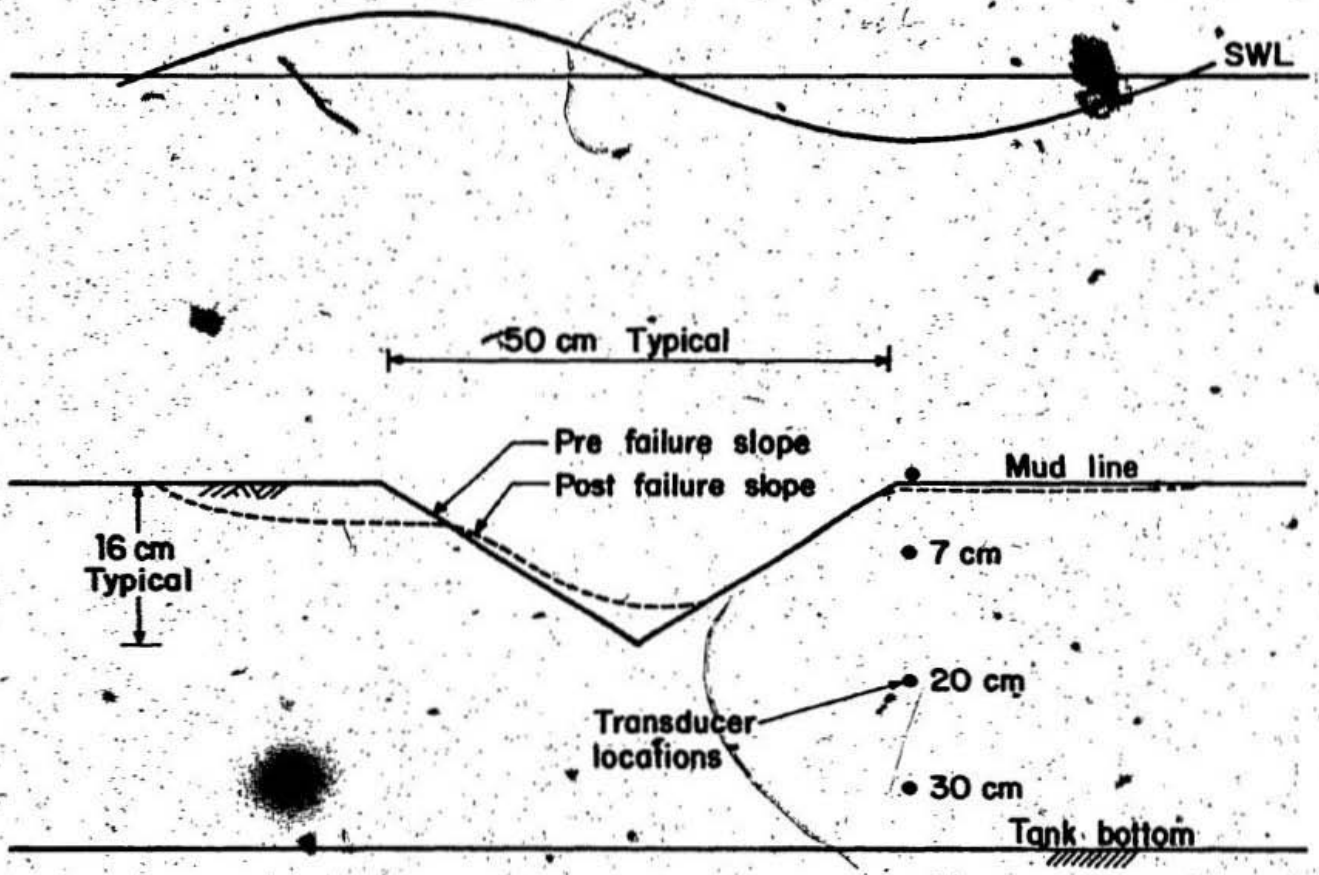


FIGURE 81 TYPICAL EXCAVATED TRENCH

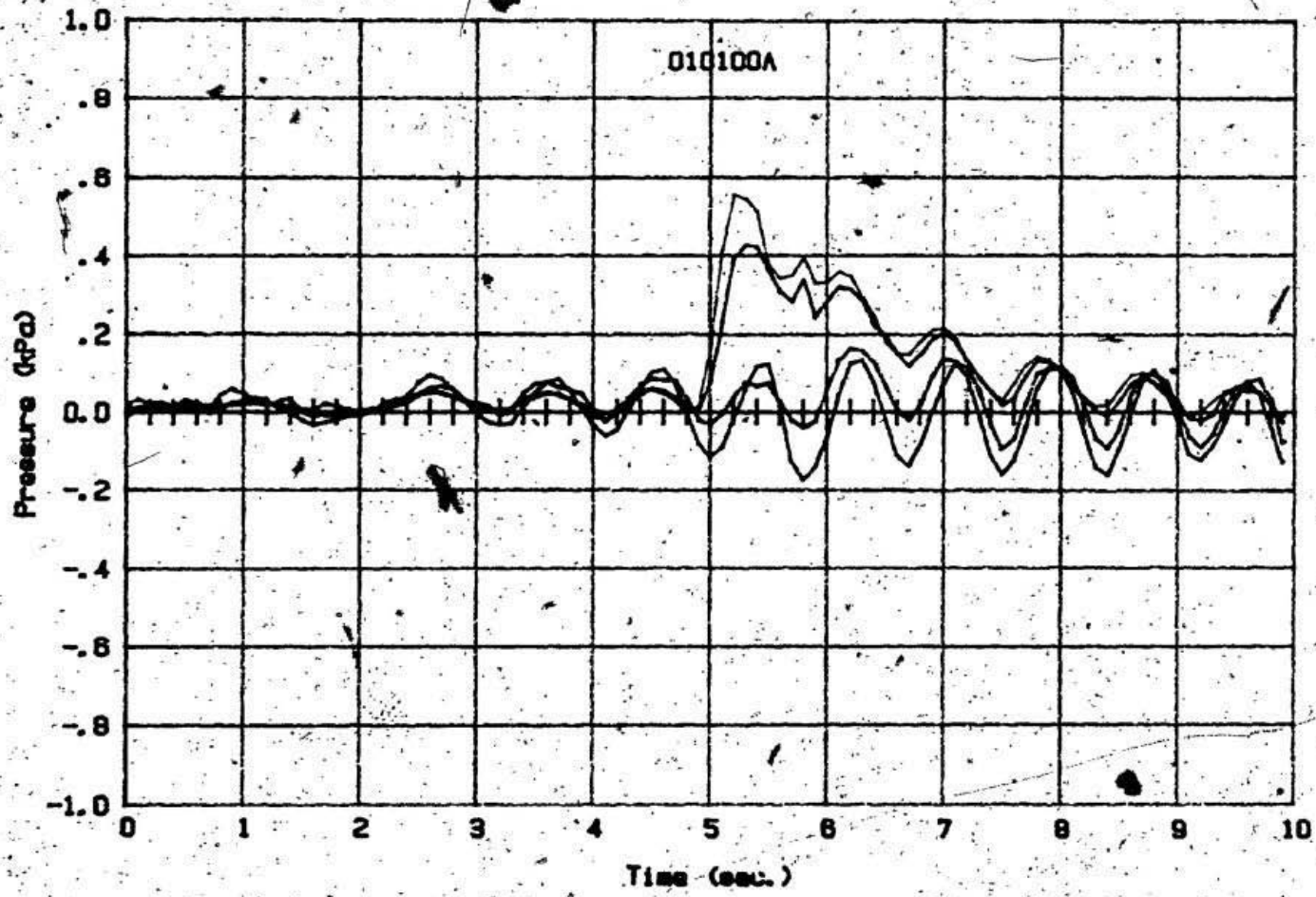


FIGURE 82 POREWATER PRESSURE RESPONSE AS WAVES TRIGGER FAILURE OF A FINITE SLOPE

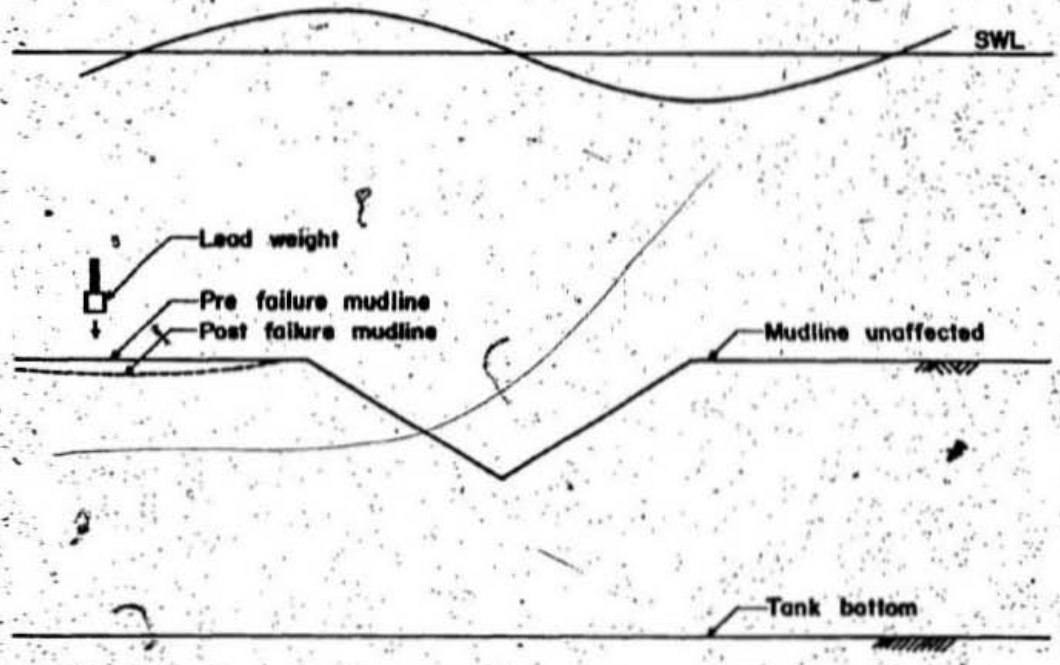


FIGURE 83 EXCAVATED TRENCH ACTING AS A DAMPER

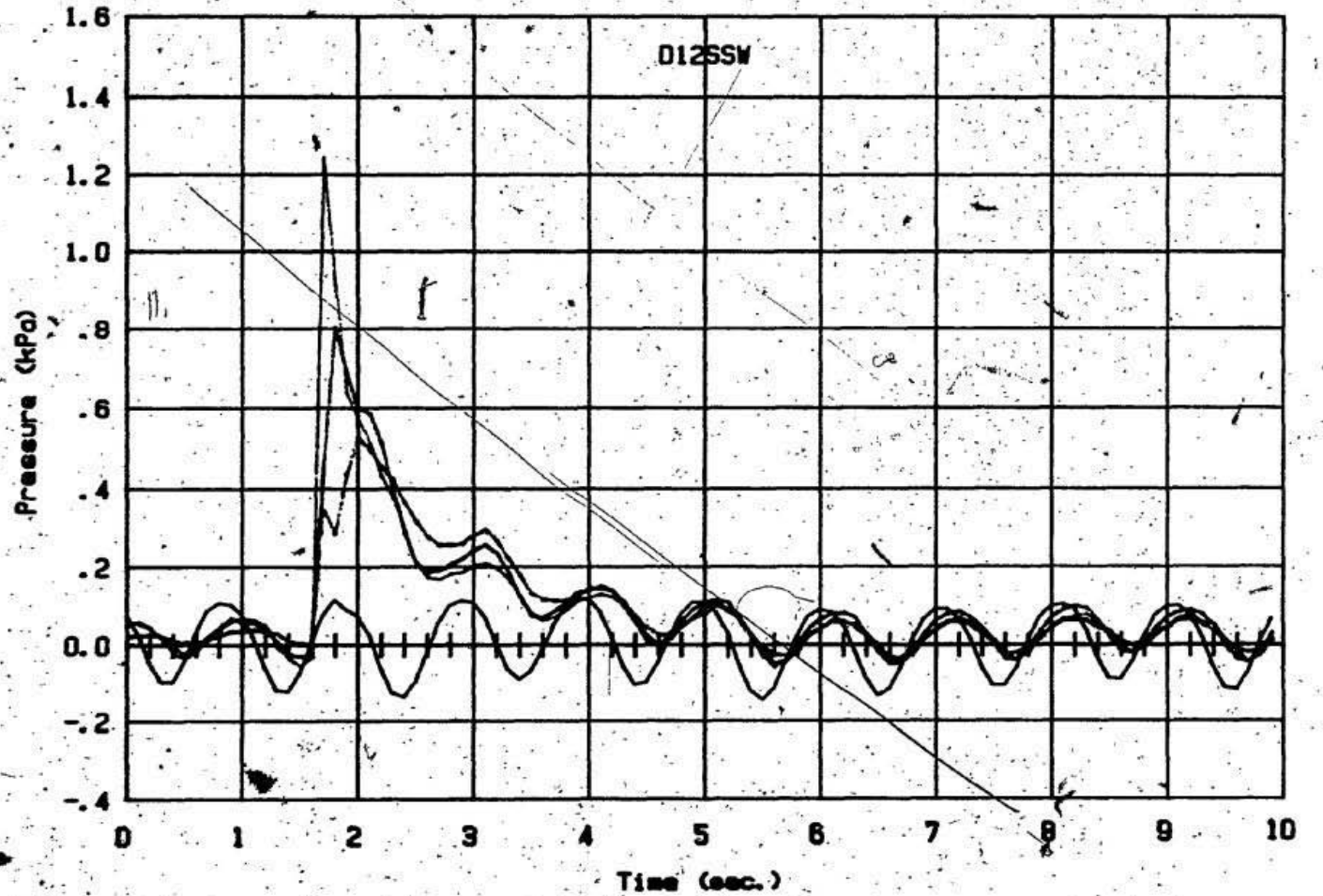


FIGURE 84 POREWATER PRESSURE RESPONSE AS SOIL FAILURE IS TRIGGERED BY COMBINED WAVES AND SHOCK

pressures. The tests with infinite and finite slopes were mostly qualitative. But the results are in general agreement with earlier published theoretical results. Further work with several strings of pressure measurements along the length of the tank is recommended.

CHAPTER V

SUMMARY AND CONCLUSIONS

Laboratory model studies were conducted of the interaction of ocean waves with the seafloor and the results were compared with published theories. A summary of the results of this research and some suggestions for further investigation are given in this chapter.

A substantial part of the work was devoted to the design and fabrication of a wave-soil tank and its calibration. The test tank which is 8.5 m long, can be tilted to maximum inclinations of ± 1:10 and contains a wave maker, a main test section with a glass side in which the soil is placed, and a beach suitably designed to minimize wave reflection. The performance of the flap type wave generator was in general agreement with theoretical results expected of such wavemakers. Maximum wave heights of 120 mm can be generated in the tank in water depths of 500 mm. For the range of waves generated during the calibration, Stokes 2^{hd} and 3rd order theories are found to be applicable.

Laboratory wave tanks are not of standardized sizes and so the performance generally tends to be individualistic and unique. Each wave tank requires a beach of individual design to suit its performance requirements. For the wave tank used in this investigation, an impermeable beach of

parabolic shape was found to give reflection coefficients below 10%. While this was treated as satisfactory within the time constraints of this research, it may be possible to get a better performance by further refinement of the beach design.

A cohesionless soil, somewhat similar to the surficial sediments in the Hibernia region of the Grand Banks of Newfoundland, was used as the test soil. Qualitative tests and quantitative measurements were carried out to determine the wave induced pressures at the mudline and inside the soil. These tests were correlated with the conditions required to cause soil failure. Tests were conducted at different soil densities and under different wave loading.

The pressure measurements at the mudline were found to be in general agreement with the computations of Weigel (1965) using Stokes 2nd order wave equation. However, the theoretical predictions are based on the assumption of an impermeable seabed. A better fit between the measured and theoretical results is likely by considering the soil permeability in the theoretial formulation. Porewater pressures inside the soil were found to be out of phase with the surface waves at all frequenties used. This phase difference was shown to depend on wave frequency. The lag or lead of the pressure wave inside the soil will also be dependent on the drainage properties of the soil.

For a flat bed of loose sand, soil liquefaction was found to occur for certain surface waves. The extent of soil failure was visually observed and correlated with the measured pressures and effective weight computations of the soil. There is a good correlation among the results. Whenever there was liquefaction, the soil restabilized and finally reached a denser state. Even when there was no soil failure, a thin dense crust at the mudline was always formed under wave induced pressures. This phenomenon may require further investigation and is likely to be related to ripple formation on the seabed.

The transient and cyclic pressures developed inside the soil were compared with the theoretical computations of Liu et al (1979). While there is an agreement with the theoretical values at specific wave frequencies, a general correlation is not found. It is concluded that the theoretical formulation may require further refinement to include the soil permeability and the wave frequency.

The measured depths of failure were compared with the calculations of Raman-Nair (1984) based on Biot's (1941) theory. The theoretical computation includes variables such as the elastic constants for the soil and its density. A realistic comparison is possible only if the elastic constants can be determined accurately.

Tests were conducted in which a local shock load was induced on a flat sand bed which was otherwise stable under the wave loads. The resulting porewater pressure rise was sudden, with soil failure and densification similar to the wave induced failure. The practical implication of this observation is the possibility that the seafloor which may be stable under wave loads may suddenly fail due to local shocks that may occur during the construction phase of a seabed installation.

Wave interaction with an infinite slope of the seafloor was examined by running waves up-slope and down-slope. The phase lag of the pressure wave inside the soil is different in these tests compared with those using a flat seabed because of the sloping surface and the change in drainage characteristics. The slope failure is a sudden mass slumping and is different from the gradual progressive failure of a flat seabed. Similar observations were made for a finite slope. Soil failure was always accompanied by densification similar to the behaviour of a flat mudline. Further measurements are recommended for the slope studies with several rows of pressure transducers.

The stability of seabed sediments can be influenced by a suitable combination of storm wave conditions. The drainage characteristics of the soil, its density, the bathymetry and slope of the seafloor, and the type of surface

waves are the primary factors to be considered in evaluating the seabed stability. Even a stable seafloor may fail due to local shock loads. Although the existing theoretical formulations are satisfactory for some specific conditions, further efforts are required to refine these methods for general application. Bottom currents are to be considered in addition to wave effects wherever such currents are significant. An evaluation of the combined effect of the bottom currents and waves is a challenging problem for further studies.

REFERENCES

Andresen, A. and L. Bjerrum (1967). Slides in subaqueous slopes in loose sand and silt. Marine Geotechnique.

Aviero, P. (1982). A work report done for the Faculty of Engineering, Memorial University of Newfoundland.

Bea, R.G. (1971). How sea-floor slides affect offshore structures. The Oil and Gas Journal, November 29, 1971.

Bea, R.G. and R.P. Aurora, (1981). A simplified evaluation of seafloor stability. Thirteenth Annual Offshore Technology Conference, OTC 3975.

Biot, M.A. (1941). General theory of three-dimensional consolidation, Journal of Applied Physics, Vol. 12, February.

Bishop, A.W. (1955). The use of the slip circle in the stability analysis of slopes. Geotechnique, 5(1), pp. 7-17.

Bowles, J.E. (1979). Physical and Geotechnical Properties of Soils. McGraw-Hill Book Company.

Chari, T.R. and C.R. Dawe (1984). Holocene Development and Sediment Stability of the Northern Grand Banks of Newfoundland; Cyclic Loading Tests and Wave Tank Studies; Part II - Wave Tank Studies. Report submitted to C-CORE as part of the DSS Contract, September, 1984.

Christian, J.T., P.K. Taylor, J.K.C. Yen and D.R. Erali (1974). Large diameter underwater pipeline for nuclear power plant designed against soil liquefaction. OTC 2094 presented at the Sixth Annual Offshore Technology Conference in Houston, Texas, May 1974.

Cross, R., S.R. Huntsman, D.D. Treadwell, V.A. Baker (1979). Attenuation of wave induced pore pressures in sand. Proceedings 4th International Conference on Civil Engineering in the Oceans. San Francisco, California, pp. 745-757.

Demars, K.R. (1983). Transient stresses induced on sandbed by wave loading. ASCE Journal of Geotechnical Engineering, Vol. 109, NO. 4, April, 1983.

Doyle, E.H. (1973). Soil-wave tank studies of marine soil instability. Fifth Offshore Technology Conference, Houston, Texas, Vol. 2, pp. 753-766.

Dunn, I.S., L.R. Anderson, F.W. Kiefer, (1980). Fundamentals of geotechnical analysis. John Wiley and Sons, New York.

Fellenius, W. (1936). Calculation of the stability of earth dams. Transactions Second Conference on Large Dams, 4, Washington, D.C.

Finn, W.D., Liam, R. Siddharthan, G.R. Martin (1983). Response of seafloor to ocean waves. Journal of Geotechnical Engineering, Vol. 109, No. 4, April, 1983, ASCE Paper #17880.

Florin, V.A. and Ivanor, P.L. (1961). Liquefaction of saturated sandy soils. Proc. Fifth International Conference on Soil Mechanics and Foundation Engineering, Paris, Vol. 1, pp. 107-111.

Flugge, W. (1962). Handbook of Engineering Mechanics. McGraw-Hill Book Company Inc., Chap. 55.

Gilbert, G., D.M. Thompson and A.J. Brewer (1971). Design curves for regular and random wave generators. Journal of Hydraulic Research, 9(2), pp. 163-196.

Goda, Y. and Y. Suzuki (1976). Estimation of incident and reflected waves in random wave experiments, Chapter 48, Coastal Engineering, 1976.

Grace, R.A. (1970). How to measure waves. Ocean Industry, Feb. 1970, pp. 65-69.

Hamill, P.A. (1963). Experimental development of a perforated wave absorber of simple construction and minimum length. National Research Council of Canada, Mechanical Engineering Report MB-252. NRC No. 7472.

Hansen, J. Buhr, and Ib A. Svendsen (1974). Regular waves in laboratory facilities. Fourteenth International Conference of Coastal Engineering, Copenhagen, June 1974.

Heezen, B.C. and Menard, H.W. (1963). Topography of the deep-sea floor, The Sea, Vol. 3, Hill, M.H., ed. New York, Interscience Publishers, pp. 233-280.

Henkel, D.J. (1970): The role of waves in causing submarine landslides. Geotechnique 20, No. 1, 75-80.

Hull, J.A. (1973), Wave induced submarine slope instabilities, M.Sc. Thesis, Queen's University of Kingston, Ontario, Canada.

Janbu, N. (1973). Slope stability computions. Embankment-Dam Engineering, Casagrande Volume, edited by R.C. Hirschfield and S.J. Poulos, pp. 47-86, John Wiley & Sons, New York.

Keating, T. and N.B. Webber (1977). The generation of periodic waves in a laboratory channel: a comparison between theory and experiment. Proc. Instn. Civ. Engrs., Part 2, 1977, 63, Dec. 819-832.

Kraft, L.M. and D.J. Watkins (1976). Predication of wave-induced seafloor movements, Proceedings, Fifteenth International Conference on Coastal Engineering, ASCE, Vol. II, Chap. 49, pp. 1605-1623.

Lambe, T.W. and R.V. Whitman (1969). Soil Mechanics, John Wiley and Sons, New York.

Liu, P.L.F., P. Timothy, and O'Donnell (1979). Wave induced forces on buried pipelines in permeable seabeds. Fourth Conference on Civil Engineering in the Oceans. San Francisco, Calif., pp. 111-121.

Mitchell, R.J. and J.A. Hull (1973). Stability and bearing capacity of bottom sediments. Fourteenth Int. Coastal Eng. Conf., pp. 1252-1273.

Mitchell, R.J., K.K. Tsui and D.A. Sangrey (1972). Failure of submarine slopes under wave action. Thirteenth Int. Coastal Eng. Conf., Vancouver, July 1972, Vol. 11, pp. 1515-1539.

Morgenstern, N.R. (1967). Submarine slumping and the initiation of turbidity currents. Marine Geotechnique.

Morgenstern, N.R. and V.E. Price (1965). The analysis of the stability of general ship surfaces, Geotechnique, Vol. 15, pp. 79-93.

Muggeridge, D.B. and J.J. Murray (1981). Calibration of a 58 m wave flume. Canada Journal of Civil Engineering, Vol. 8, No. 4, pp. 449-455.

Nataraja, M.S. and H.S. Gill (1983). Ocean wave-induced liquefaction analysis. ASCE Journal of Geotechnical Engineering. Vol. No. 4, April 1983.

Raman-Nair, W.W. (1984). Stress analysis of a porous deformable seabed under wave loading. M.Eng. Thesis, Memorial University of Newfoundland.

Sangrey, D.A., J.D. Henkel, and M.J. Esrig (1964). The effective stress response of a saturated clay soil to repeated loading. Canadian Geotechnical Journal. Vol. 6, No. 2, pp. 241-252.

Scott, R.F. and K.A. Zuckerman (1970). Study of slope instability in the ocean floor.

Seed, H.B., I. Arango, C.K. Chan and R.C. Ascoli (1981). Earthquake-induced liquefcation near Lake Amatitlan, Guatemala. Journal of the Geotechnical Engineering Division, ASCE, Vol. 107, GT4, April.

Seed, H.B., and I.M. Idriss (1971). Simplified procedure for evaluating soil liquefaction potential. Journal of the Soil Mechanics and Foundations Division. ASCE. Vol. 97, No. SM9, pp. 1249-1273.

Seed, H.B., P.P. Martin and J. Lysmer (1976). Porewater pressure changes during soil liquefaction. Journal of the Geotechnical Engineering Division, ASCE, Vol. 102, No. GT4, April.

Seed, H.B. and M.S. Rahman (1978). Wave induced pore pressure in relation to ocean floor stability of cohesionless soils. Marine Geotechnology, Vol. 3, No. 2.

Sevaldson, R.A. (1956). The slide in Lodalen, Oct. 6, 1954, Geotechnique, 6, pp. 167-182.

Shapery, R.A. and W.A. Dunlap (1978). Prediction of storm-induced sea bottom movement and platform forces. Tenth Annual Offshore Technology Conference, Houston, Texas, May, 1978, OTC-3259.

Sharp, J.J. and Allen, J.H., 1973. Ocean engineering- fluid mechanics laboratory, Engineering Journal, 56, pp. 23-25.

Shepard, F.P. (1955). Delta-front valleys bordering the Mississippi distributaries. Bull. Geol. Soc. Am. 66, 1489-1498.

Singh, H. (1971). The behaviour of normally consolidated and heavily overconsolidated clays at low effective stress. Ph.D. Thesis, Cornell University, Ithaca, New York.

Shore Protection Manual, U.S. Army Coastal Engineering Research Centre, U.S. Government Printing Office, Washington, D.C., 1975.

Sleath, J.F.A. (1970). Wave-induced pressures in beds of sand, Journal of the Hydraulics Division, ASCE, Vol. 96, NO. HY2, Feb, 1970.

Sterling, G.H., E.E. Strohbeck (1973). The failure of the South Pass 70 "B" platform in Hurricane Camille, Fifth Annual Offshore Technology Conference, OTC 1898.

Terzaghi, K. (1956). Varieties of submarine slope failures. Proceedings of the Eight Texas Conference on Soil Mechanics and Foundation Engineering. 41 pp. Reprint, Harvard Soil Mechanics Series, No. 52.

Tsui, K.K. (1972). Stability of submarine slopes, Ph.D. Thesis, Queen's University of Kingston, Ontario, Canada.

Tsui, y. and S.C. Helfrich (1983). Wave-induced pore pressures in submerged sand layer. Journal of Geotechnical Engineering, ASCE, Vol. 109, No. 4, April.

Ursell, F., R.G. Dean and Y.S. Yu (1960). Forced small amplitude water waves: a comparison of theory and experiment, J. Fluid Mech., 1960, 7, 33-52.

Vaid, Y.P. and W.D. Liam Finn (1979). Effect of static shear on liquifaction potential, Journal of Geotechnical Engineering Div., ASCE, Vol. 105, No. GT10, Proc. paper 14909, 1979, pp. 1233-1246.

VanLammeren, W.P.A. and A.J.W. Lap (1964). The combined wave and current laboratory of the Netherlands Ship Model Basin. Publication 244 of the N.S.M.B. (Reprint). Also published in International Ship Building Progress, Vol. 2, #118, June 1964.

Whitman, R.V. and W.A. Bailey (1967). Use of computers for slope stability analysis. Journal ASCE, Vol. 93, No. SM4.

Wiegel, R.L. (1964). Oceanographical Engineering, Prentice-Hall, Englewood Cliffs, N.J.

Wright, S.G. (1976). Analyses for wave induced sea-floor movements. Eight Annual Offshore Technology Conference, Houston, Texas, May 1976, OTC 2427.

Wright, S.G. and R.S. Dunham (1972). Bottom stability under wave induced loading. Paper presented at the Fourth Annual Offshore Technology Conference, Houston, Texas, May 1972, OTC 1603.

Yamamoto, T. (1978). Sea bed instability from waves. Paper OTC 3262 presented at the 10th Annual Offshore Technology Conference, Houston, Texas, May, 1978.

Yamamoto, Tokyo, H.L. Koning, H. Sellmeijer and E.V. Hijum (1978). On the response of a pore-elastic bed to water waves. J. Fluid Mechanics. Vol. 87, part 1, pp. 193-206.

The Ship That Sank Twice (1984). "Experiment". A video presentation by MUN Educational Television. Guest Roy Dawe, Host Rob Pitt.

APPENDIX

```
10 **************ROYMAY 1984*******************************
20 This Program is used to collect data using an H.P. Data
...Acquisition Unit and to recall data stored on disk.
...Pressures are given in cm of water.
30 Printer is 701
40 Check = 0
50 ON KEY# 1,"DATA" GOSUB 380
60 ON KEY# 3,"RECALL" GOSUB 2180
70 CLEAR
80 GCLEAR
90 DISP "HOW MANY DATA POINTS PER SENSOR,20,100, OR 200"
100 INPUT NP
110 IF NP = 20 THEN GOTO 140
120 IF NP = 100 THEN GOTO 170
130 GOTO 200
140 DIM BDATA$[248],PT2(20),PT3(20),PT4(20),PT5(20),
....PT6(20), A$[999], MULTPLX(900)
150 RC = 3
160 GOTO 220
170 DIM BDATA$[1208],PT2(100),PT3(100),PT4(100),PT5(100),
....PT6(100), A$[999], MULTPLX(900)
180 RC = 13
190 GOTO 220
200 DIM BDATA$[2408],PT2(200),PT3(200),PT4(200),PT5(200),
....PT6(200), A$[999], MULTPLX(900)
210 RC = 23
220 NDP = NP
230 CAL2=10065 @ CAL3= 9758 @ CAL4=9922 @ CAL5=9884
240 KEY LABEL
250 PAGESIZE 24
260 J = 0
270 K = 0
280 BLOCK = 0
300 CLEAR @ KEY LABEL
310 DISP "ENTER PLOTTER ADDRESS",
320 INPUT PL
330 DISP "PRESS DATA OR RECALL"
340 PLOTTER IS PL @ CSIZE 3
350 DEG
370 GOTO 370
380 DISP "READING DATA FROM 3497A"
390 IOBUFFER BDATA$
400 CLEAR 509
410 OUTPUT 509 ; "VF2VAOVR1VT2SD0"
420 OUTPUT 509 ; "SO1VN1AF2AL5AE1TO100VD5AC2"
430 DISP " DATA GOING IN HANG ON"
440 TRANSFER 509 TO BDATA$ FHS
460 DISP "DATA TRANSFER COMPLETE"
470 DISP "# OF DATA POINTS PER SENSOR= ";NDP
480 IF K = 0 THEN GOTO 500
490 IF K > 0 THEN GOTO 510
500 NDP = 10 @ GOTO 520
510 DISP "UNPACKING DATA, PLEASE WAIT" @ NDP = NP
520 FOR I = 3 TO 12 STEP 3
```

```
530 A$ = DTB$ (NUM (BDATA$[I-2,I-2]))
540 D$ = A$
550 A2 = BINAND (BTD (A$[9,10],3)
560 M = 10↑(-6+A2) @ !  RANGE MULTIPLIER
570 IF BINAND ( BTD ( A$[11,11]),1) = THEN SIGN=-1
....ELSE SIGN = 1 @ ! SIGN BIT
580 ORNG = BINAND (BTD (A$12,12]),1)  !  OVERANGE BIT
590 MSD = BINAND ( BTD (A$[13,16]),15)
600 A$ = DTB$ (NUM ( BDATA$[I-1,I-1]))
610 B$ = A$
620 SSD = BINAND (BTD (A$[9,12]),15)
630 TSD = BINAND (BTD (A$[13,16]),15)
640 A$ = DTB$ (NUM ( BDATA$[I,I]))
650 C$ = DTB$ (NUM ( BDATA$[I,I]))
660 FSD = BINAND (BTD (A$[9,12]),15)
670 LSD = BINAND (BTD (A$[13,16]),15)
680 MULTPLX(I/3)=(ORNG*10↑5+MSD*10↑4+SSD*10↑3+
....TSD*100+FSD*10+LSD)*M*SIGN
690 NEXT I
700 C1 = 1 @ N = NDP
710 FOR I = 1 TO NDP
720 IF K > 0 THEN GOTO 1970
730 PT2(I) = MULTPLX(C1)*CAL2 @ C1 = C1+1
740 PT3(I) = MULTPLX(C1)*CAL3 @ C1 = C1+1
750 PT4(I) = MULTPLX(C1)*CAL4 @ C1 = C1+1
760 PT5(I) = MILTPLX(C1)*CAL5 @ C1 = C1+1
770 NEXT I
780 GOTO 890
790 K = K+1
800 IF BLOCK > 0 THEN GOTO 2030
810 DISP " START WAVES AND PRESS CONTINUE"
820 GOTO 380
830 FOR I = 1 TO NDP
840 DISP PT2(I);PT3(I);PT4(I);PT5(I)
850 NEXT I
860 GOSUB 1110
870 P0(0)= 0 @ P1(0)= 0 @ PT2(0)= 0 @ PT3(0)= 0 @ PT4(0) =
....0 @ PT5(0)= 0 @ PT6(0)= 0 @ PT7(0)= 0 @ PT8(0)= 0
880 ALPHA @ GOTO 2030
890 FOR I = 1 TO NDP
900 PT2(0) = 0
910 PT3(0) = 0
920 PT4(0) = 0
930 PT5(0) = 0
940 PT2(I) = PT2(I-1)+PT2(I)
950 PT3(I) = PT3(I-1)+PT3(I)
960 PT4(I) = PT4(I-1)+PT4(I)
970 PT5(I) = PT5(I-1)+PT5(I)
980 NEXT I
990 PT2AVG = PT2(NDP)/NDP
1000 PT3AVG = PT3(NDP)/NDP
1010 PT4AVG = PT4(NDP)/NDP
1020 PT5AVG = PT5(NDP)/NDP
1030 NDP = NP @ FOR I = 1 TO NDP
```

```
1040 PT2(I) = PT2AVG
1050 PT3(I) = PT3AVG
1060 PT4(I) = PT4AVG
1070 PT5(I) = PT5AVG
1080 NEXT I
1090 GOTO 790
1110 MINVAL = 9999
1120 MAXVAL = -9999
1130 DISP "HOW MANY SIGNALS TO BE PLOTTED " @ INPUT SIGNUM
1140 FOR I = 2 TO SIGNUM+1 @ DISP "PT";I;" () PLOTTED
(Y/N)" @ INPUT SIG$(I-1)
1150 NEXT I
1160 FOR J = 1 TO 4
1170 FOR I = 1 TO NDP
1180 ON J GOTO 1190, 1230, 1270, 1310
1190 IF SIG$(J) = "N" THEN 1350
1200 IF MINVAL > PT2(I) THEN MINVAL = PT2(I)
1210 IF MAXVAL < PT2(I) THEN MAXVAL = PT2(I)
1220 GOTO 1340
1230 IF SIG$(J) = "N" THEN 1350
1240 IF MINVAL > PT3(I) THEN MINVAL = PT3(I)
1250 IF MAXVAL < PT3(I) THEN MAXVAL = PT3(I)
1260 GOTO 1340
1270 IF SIG$(J) = "N" THEN 1350
1280 IF MINVAL > PT4(I) THEN MINVAL = PT4(I)
1290 IF MAXVAL < PT4(I) THEN MAXVAL = PT4(I)
1300 GOTO 1340
1310 IF SIG$(J) = "N" THEN 1350
1320 IF MINVAL > PT5(I) THEN MINVAL = PT5(I)
1330 IF MAXVAL < PT5(I) THEN MAXVAL = PT5(I)
1340 NEXT I
1350 NEXT J
1360 MAXVAL = CEIL (MAXVAL)  IF MINVAL < 0 THEN MINVAL =
.....-(1*CEIL (ABS (MINVAL))) ELSE MINVAL = INT (MINVAL)
1370 GCLEAR
1390 LOCATE 20,120,20,90
1400 SCALE 0,NDP,MINVAL,MAXVAL
1410 FXD 0,1 @ LGRID -4,-(MINVAL/2),0,0,5,1
1420 FOR J = 1 TO 4
1430 PAUSE
1440 FOR I = 1 TO NDP
1450 ON J GOTO 1460,1490,1520,1550
1460 IF SIG$(J) = "N" THEN 1590
1470 IF I = 1 THEN PEN UP @ MOVE I-1,PT2(I)
1480 DRAW I-1 , PT2(I) @ GOTO 1580
1490 IF SIG$(J) = "N" THEN 1590
1500 IF I = 1 THEN PEN UP @ MOVE I-1,PT3(I)
1510 DRAW I-1 , PT3(I) @ GOTO 1580
1520 IF SIG$(J) = "N" THEN 1590
1530 IF I = 1 THEN PEN UP @ MOVE I-1,PT4(I)
1540 DRAW I-1 , PT4(I) @ GOTO 1580
1550 IF SIG$(J) = "N" THEN 1590
1560 IF I = 1 THEN PEN UP @ MOVE I-1,PT5(I)
1570 DRAW I-1 , PT5(I)
```

```
1580 NEXT I
1590 NEXT J
1600 LORG 4
1610 MOVE NDP/2,-1.333
1620 CSIZE 3
1630 DEG
1640 LABEL "NDP" @ MOVE NDP/2+2,3.75 @ LABEL F$ @ CSIZE 4
.....MOVE NDP/2,-1.66 @ LABEL "PRESSURE CHANGE"
1650 MOVE -16,1
1660 LDIR 90 @ CSIZE 3
1670 LABEL "Pressure (kpa)"
1680 ALPA
1690 DISP "FILE NAME "
1700 INPUT F$
1710 CREATE F$,RC,256
1720 ASSIGN# 1 TO F$
1730 PRINT # 1 ; NDP, PT2(), PT3(), PT4(), PT5()
1740 ASSIGN# 1 TO *
1750 DISP "DO YOU WISH TO LABEL Y/N"
1760 INPUT R$
1770 IF R$ = "N" THEN GOTO 1960
1780 DEG
1790 DISP "INPUT DIR"
1800 INPUT D
1810 LDIR D
1820 DISP "SET LORG"
1830 INPUT LO
1840 LORG LO
1850 DISP "DISP ENTER LABEL COORDINATES X,Y"
1860 INPUT X,Y
1870 MOVE X,Y
1880 DISP "ENTER CSIZE"
1890 INPUT SIZ
1900 CSIZE SIZ
1910 DISP "ENTER LABEL"
1920 INPUT LAB$
1930 LABEL LAB$
1940 GOTO 1750
1950 RETURN
1960 END
1970 PT2(I) = -(MULTPLX(C1)*CAL2)+PT2(I) @ C1 = C1+1
1980 PT3(I) = -(MULTPLX(C1)*CAL3)+PT3(I) @ C1 = C1+1
1990 PT4(I) = -(MULTPLX(C1)*CAL4)+PT4(I) @ C1 = C1+1
2000 PT5(I) = -(MULTPLX(C1)*CAL5)+PT5(I) @ C1 = C1+1
2010 NEXT I
2020 GOTO 830
2030 DISP "FILE NAME ";
2050 INPUT F$
2060 CREATE F$,RC,256
2070 ASSIGN # 1 TO F$
2080 PRINT # 1 ; NDP, PT2(), PT3(), PT4(), PT5()
2090 ASSIGN# 1 TO *
2100 GOTO 2290
2110 DISP "FILE ALREADY EXISTS ....."
```

```
2120 DISP "TRY AGAIN ? Y/N "
2130 INPUT A$
2140 IF A$ = "Y" THEN 2040
2150 IF A$ = "N" THEN 2290
2170 END
2180 DISP "FILE NAME"
2190 INPUT F$
2200 ASSIGN# 1 TO F$
2210 READ# 1 ; NDP, PT2(), PT3(), PT4(), PT5()
2220 ASSIGN# 1 TO F$
2230 I = 1
2240 DISP PT2(I); PT3(I); PT4(I); PT5(I)
2280 GOSUB 1110
2290 END
```